Ollscoil na hÉireann, Corcaigh

National University of Ireland, Cork

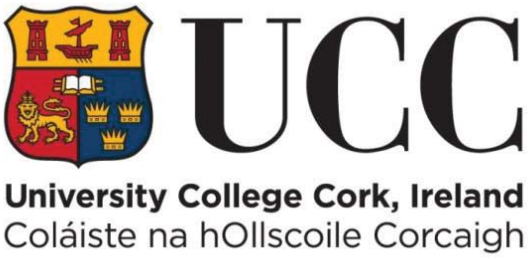

Contributions to the Modeling of the Incremental Optical Encoder and Speed Estimation Methods for Motion Control

Thesis presented by

Yeny Vázquez Gutiérrez

orcid.org/0000-0003-3122-9644

for the degree of

Doctor of Philosophy

University College Cork

School of Electrical and Electronic Engineering

Head of School: Dr. William Marnane

Supervisors: Dr. Richard C. Kavanagh, Dr. John G. Hayes

and Dr. Dara L. O'Sullivan

2019

DECLARATION

This is to certify that the work I am submitting is my own and has not been submitted for another degree, either at University College Cork or elsewhere. All external references and sources are clearly acknowledged and identified within the contents. I have read and understood the regulations of University College Cork concerning plagiarism.

Yeny Vázquez Gutiérrez

ABSTRACT

This work studies the incremental optical encoder sensor and its impact on motor motion. The small-signal model of the sensor combined with the chosen speed estimation method is derived, experimentally validated and compared with existing models. A novel experimental setup emulates the encoder behaviour. Therefore, the sensor is isolated from the rest of the system (motor and driver) that unavoidably biases the dynamic study. The small-signal model demonstrates that the phase lag of the encoder increases as the speed and the resolution decreases. This increment of the delay adversely reduces the phase margin of the motion control-loop.

In addition, a simple lead compensator is proposed and implemented on a DSP to recover correct performance of the motor (smooth rotation) previously degraded by the encoder. The coefficients of the proposed lead compensator adapt to the specific commanded speed automatically.

As part of this thesis an improvement of the elapsed time (ET) method, that expands the use of this method to all speed ranges, is proposed. The Improved-ET speed estimation method has a good balance between static error and dynamic behaviour.

ACKNOWLEDGEMENTS

The PhD is a four year long way. The enterprise is plagued with success and failures and failure is a better teacher than success. Success prizes patience, hard work and the strong belief of never ever quit the goal.

First, I would like to express my gratitude to my supervisors Dr. Richard Kavanagh, the academic supervisor, and Dr. Dara O'Sullivan, the enterprise supervisor, for their guidance during the thesis. I would like to thank also to Dr. John Hayes for nurturing the collaboration among UCC, Analog Devices and the Irish Research Center (IRC) that finally led to the this research. I also wish to extend my appreciation to the funding bodies: the IRC and Analog Devices. I would like to thank Dr. Gordon Ligthbody for his thorough observations on the content of the research work.

My sincere appreciation to the staff of the Electrical and Electronic School: Niahm O'Sullivan, Ralph O'Flaherty, Michel O'Shea, Timothy Power, Hilary Mansfield, Mary O'Leary, Claudia Cashman, Gerard Hooton and especially to James Griffiths for his valuable technical advice all these years.

I am indebted to Dr. Antonio Lázaro Blanco for his timely and useful comments.

It has been a privilege being part of the PERL lab and to share the last few years with Diarmaid Hogan, Brendan Barry, Adrian O'Sullivan, Conor O'Shea, Edward O'Dwyer, Oliwier Melon, Patrick Xie, Alex Jaeger, Robert Ryan, George O'Mahony, Brian Murphy, Alison O'Shea, Juan Pablo La Torre. I owe especial thanks to Kevin Davis and Oksana Semenova. I enjoyed and valued our chats!

I would like to acknowledge the support of my lifelong friends: Irene, Adrián, Beatriz, Itziar, Alina and Héctor Javier. I also extend the appreciation to those that I met in Cork and at the end became the Corkonian family: Lara, Héctor, Vero, Oscar, Andgelka, Juan, Laura, Dani, Fran, Elia, Blanca, Carlos, Elizabeth and Ana.

I would like to dedicate this thesis to my family. To my parents Ramón and María del Carmen for their devoted, selfless and unwavering support. They are a model to me. Also to my brother Ramón Alejandro, he is the most kind person I have ever known,

and to my grandparents. Last but not least, I would like to thank Virgilio for being an excellent life partner.

LIST OF PUBLICATIONS

Journal paper

1. Y. Vazquez-Gutierrez, D. L. O'Sullivan and R. C. Kavanagh, ‘Small-signal modeling of the incremental optical encoder for motor control', *IEEE Trans. Ind. Electron*., pp. 1-1, 2019. DOI 10.1109/TIE.2019.2916307.

2. Y. Vazquez-Gutierrez, D. L. O'Sullivan and R. C. Kavanagh, ‘Study of the impact of the incremental optical encoder sensor on the dynamic performance of velocity servosystems’, *J. Eng.*, Jan. 2019. DOI 10.1049/joe.2018.8255.

3. Y. Vazquez-Gutierrez, D. L. O'Sullivan and R. C. Kavanagh, ‘Evaluation of three optical-encoder-based speed estimation methods for motion control’, *J. Eng.*, Jan. 2019. DOI 10.1049/joe.2018.8058.

Papers 2 and 3 were also presented to the Power Electronics Machine and Drives (PEMD 2018) Conference that took place in Liverpool, United Kingdom.

TABLE OF CONTENTS

LIST OF ABBREVIATIONS AND SYMBOLS

ABBREVIATION	DEFINITION
ADC	Analog to Digital Converter.
ADSP	Advanced Digital Signal Processor.
CSDT	Constant Sampled Digital-time Tachometer speed estimation method.
CNT	General Purpose Counter.
DAC	Digital to Analog Converter.
DSP	Digital Signal Processor.
DTF	Discrete Fourier Transformed.
ET	Elapsed Time speed estimation method.
FIR	Finite Impulse Response.
FOC	Field Oriented Control.
FPGA	Field Programmable Gate Array.
GM	Gain Margin.
I-ET	Improved Elapsed Time speed estimation method.
I-ET-S	Improved Elapsed Time Simplified speed estimation method.
ISR	Interrupt Service Routine.
PC	Pulse Count speed estimation method.
PI	Proportional Integral.
PM	Phase Margin.
PID	Proportional Integral Derivative.
QPLL	Quadrature Phase-locked Loop.
SYSCLK	System Clock.
VCO	Voltage Controlled Oscillator.

SYMBOL	DEFINITION
R	Effective resolution of the encoder, one, two or four (termed quadrature detection) times the number of slits nominally evenly distributed around the disc; (pulses per revolution; ppr).
θ	The minimum rotated angle detected by the sensor. $\theta = 360°/R$; degrees.
T_s	Control-loop sample time in seconds (s).
T_e	Time elapsed between consecutive encoder transitions (or edges) $T_e = 60 / (\overline{n} \cdot R)$; (s).
$n(t)$	Actual motor speed in revolutions per minute (r/min).
$\overline{n}(t)$, $\overline{n}$	Estimated and average motor speed (r/min).
L	Number of encoder transitions (edges) per control sample time T_s.
l	Normalized speed as the number of encoder transitions per sample interval (tr./T_s).
N	Number so samples.
T_{Clock}	Fixed time duration of a cycle of the peripheral high-frequency clock.
m	Number of cycles of the high-frequency clock occurring over time T_e.
θ_{Clock}	Rotated angle during a T_e period of time, $\theta_{Clock} = \theta/m$ in degrees.
$\overline{x}$	Symbolizes the average value of a signal x.
$\tilde{x}$	Symbolizes small-signal disturbance superimposed to a signal x.
td	Time delay between two asynchronous signals.
f_{Enc}	Frequency of the signal of the encoder in Hz. Note that $f_{Enc} = n(t) \cdot 60 / R$.
f_{VCO}	Frequency at the output of the VCO.
f_o	Steady-state frequency that is modulated in the VCO; (Hz).
G	Gain of the VCO; (Hz/V).
$V_{in}(t)$	Modulator input of the VCO; (V).
k,i	Sample number indeces in the discrete domain.

LIST OF FIGURES

LIST OF TABLES

Chapter 1. Introduction

Motor drives play a key role in modern industry, with the performance of the intrinsically closed-loop system being greatly determined by the choice of the feedback sensor. Optical encoders are found in applications such as computer numerical control (CNC) machines, printers, paper production, food and beverage automation, elevator control, etc. One of the key design drivers in most of those applications is cost. A way of reducing cost is selecting an optical encoder with a low resolution. Nevertheless, this has an impact on the dynamic performance of the control loop, which brings challenges that are not addressed in the state of the art. The aim of this thesis is to address some of the challenges related to the utilization of incremental optical encoders with limited resolution.

In this chapter, the motivation and objectives of this thesis are outlined. An introduction to electrical machines and industrial applications in section 1.1 precede the overview of typical motor control architectures based on incremental optical encoder sensors in section 1.2. The problems associated to the encoder use are described. The review of the state of the art of prosed control solutions are addressed in section 1.3. It also describes the gaps found in the proposed state of the art to later enumerate the main contributions of this thesis. Finally, section 1.4 concludes describing the content of the rest of the chapters.

1.1 Overview of Electric Machines and its Applications

Since 1995 electric motors has experienced an increase of the sales. Many of the current research efforts are oriented to the improvement of the efficiency of this machine, motor drives and sensors [1].

A report release by [2] in 2011 quantifies the impact of the industry (64 %) in the global energy released consumption see Figure 1.1 – (a). Motors emerge as one of the biggest energy consumer (46 %) in the industry sector as can be seen in Figure 1.1 – (b).

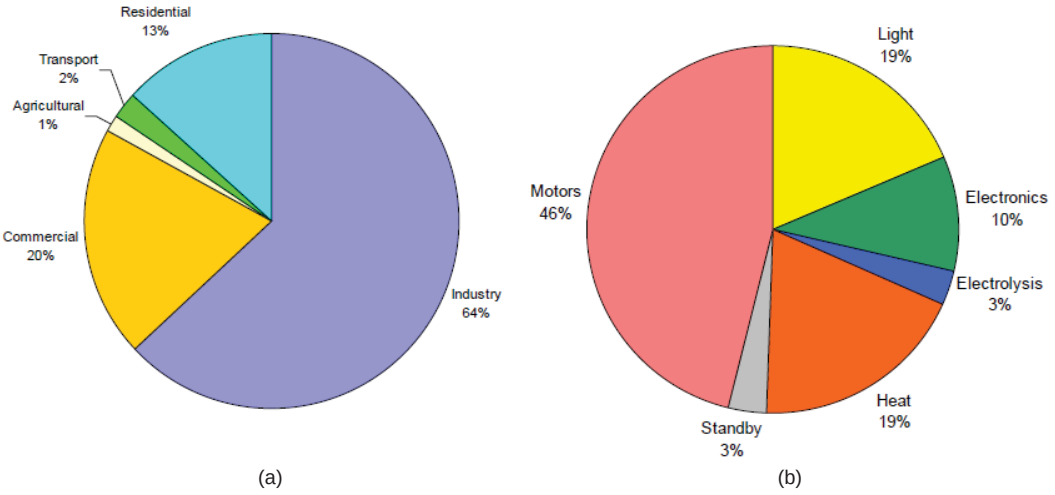

Figure 1.1 (a) Electricity demanded by sectors and (b) major energy consumers in industry [2].

Motors can be found in multiple applications and different power ranges, as shown in Figure 1.2.

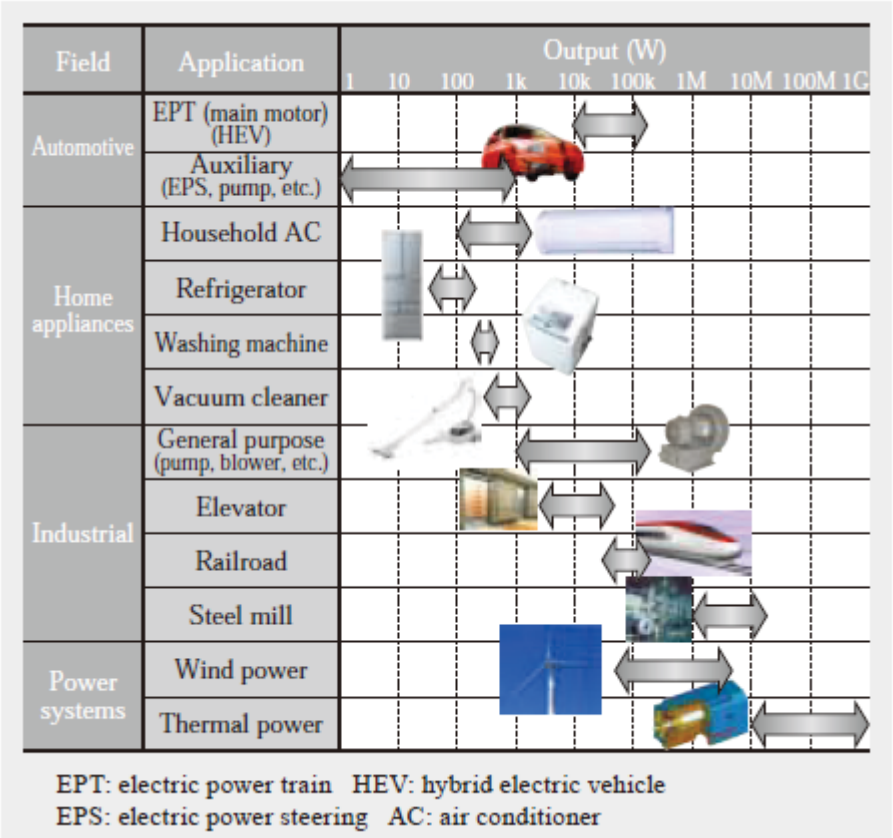

Figure 1.2 Examples of Hitachi Electric Motors found in [3].

The replacement of pneumatic actuators by electromechanical actuators has also fostered the use of these electric machines in the past. There are many types of motors and can be classified as in Figure 1.3.

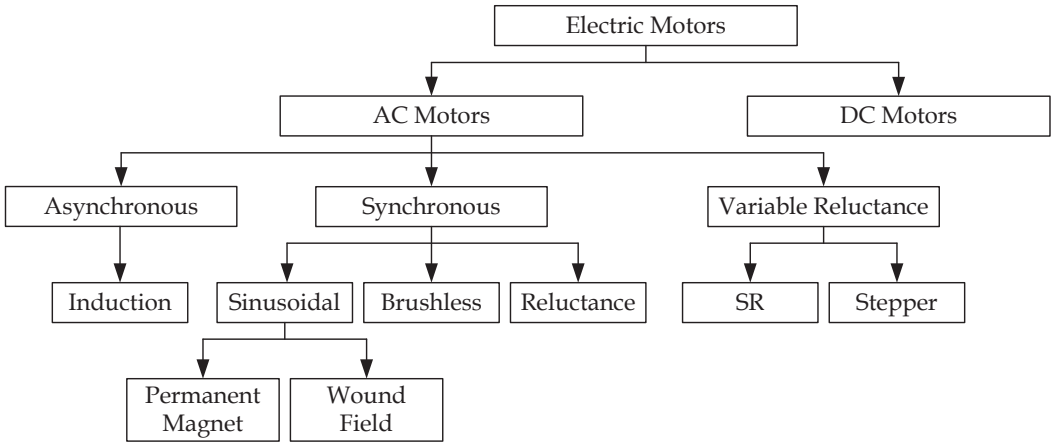

Figure 1.3 Types of electric motors.

Each motor type has different applications and faces different challenges such as: speed range, rated torque requirements, speed ripple, acceleration time, breakaway torque, environment, protection features and communication requirement among others, as listed in [4]. Prior to the 1950s most of the applications required the use of DC motors operating at a fixed speed, proportional to the voltage. It was after 1957 that the benefits of semiconductors proved their utility in variable frequency applications, with the first "silicon controlled rectifier" (SCR). This expanded the use of AC motors to many applications formerly covered by DC motors [4] and [5]. The evolution of motors is represented, in Figure 1.4. It can be seen that an improvement of the performance is closely linked to the evolution of motors (from DC motors to AC and induction motors), drivers (from thyristors to IGBTs) and the different control devices (from analog control to digital control). Digital controllers provided a platform to implement more sophisticated control techniques and advanced algorithms.

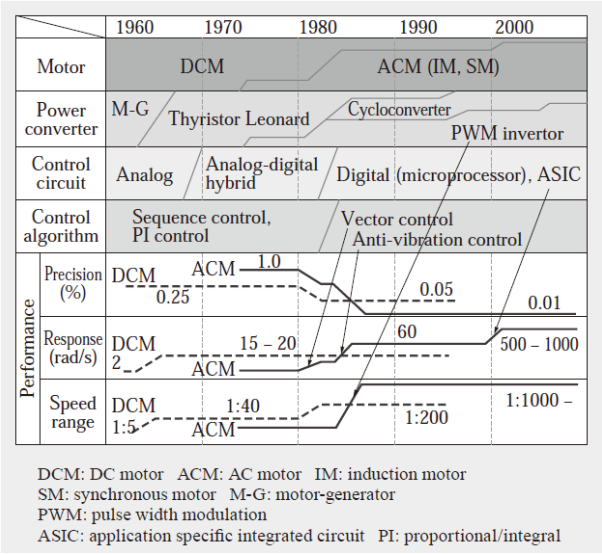

Figure 1.4 History and advances in Motor drive control [3].

The control is the brain of any application. From the controller perspective, zero steady-state error and fast transient conditions are key parameters defining its performance. The precision is defined as the difference between the measurement and the commanded speed value that must be almost zero. The transient response to step tests defines the capability of the system to track variations. Similarly, the sensors used in the feedback are defined by their bandwidth which affects the transient performance, together with the dynamics of the controller.

Although the first proportional-integral-derivative (PID) controller was presented in 1886, it was not until the 1940s that it was first used in motor controllers, originally implemented by analog means via operational amplifiers. More recently, during the last 40 years, the control migrated to a digital device with the advent of microcontrollers, digital signal processors (DSP), and field programmable gate arrays (FPGA). Digital control facilitates the implementation of classical control techniques such as scalar motion control, Figure 1.5.

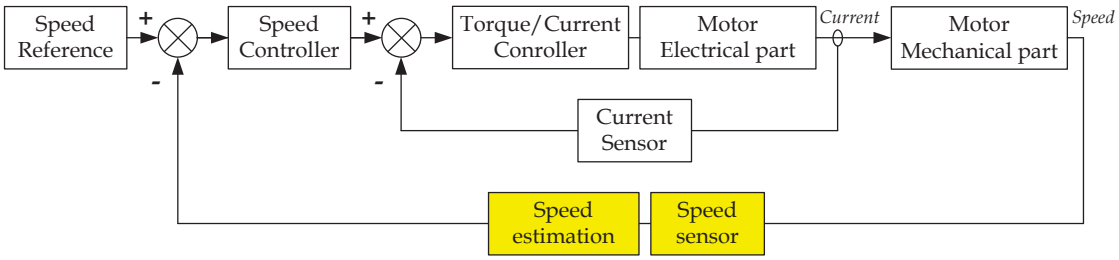

Figure 1.5 Simplified diagram of a scalar control with internal current loop and external speed loop.

A simple speed control, as in Figure 1.5, senses the speed of the rotor of the motor to correct any deviation from the reference speed (or target speed).

More advanced controllers like vector control, field oriented control (FOC), etc., can also improve the performance of the motor, as in Figure 1.6.

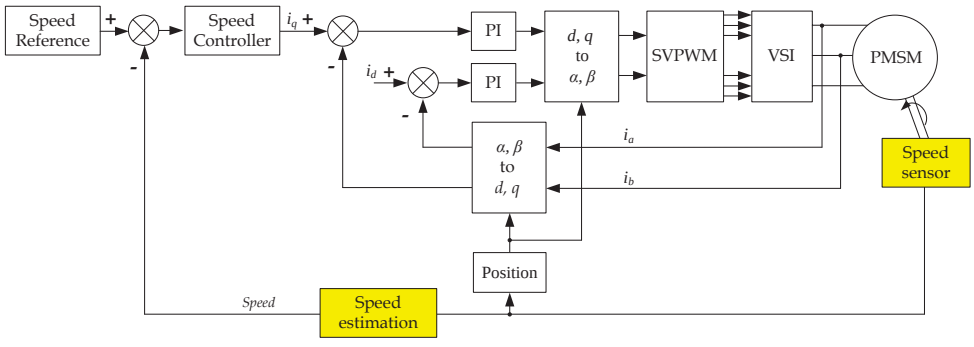

Figure 1.6 Simplified diagram of a vector control: FOC.

The FOC is used to control induction and permanent magnet motors. The FOC separately controls the torque and the magnetic flux achieving good static and dynamic performance. The required torque is determined by the specific application. By controlling the flux, the rotor can be oriented perpendicularly to the magnetic field guaranteeing that the resulting torque is maximum regardless of the rotation [6] and [7].

A thorough study of the literature shows that there are several variations of the FOC; however, in all the cases their performance is highly dependent on the quality of speed and position information. The information of the rotor position is used in the $\alpha\beta$ and dq decomposition to separate the sensed information i_a and i_b into information of the actual torque and flux. This feedback is used to orientate the motor shaft while keeping the commanded torque. Additionally, an external speed loop controls the speed.

In both type of controllers the optical encoder can be used in the feedback and the motion control because of the good balance between performance and cost.

1.2 Incremental Optical Encoder and Associated Problems

The sensors for motion control can be classified according to their different physical characteristics, prices, etc., depicted in Figure 1.7. These vary greatly in terms of both cost and performance.

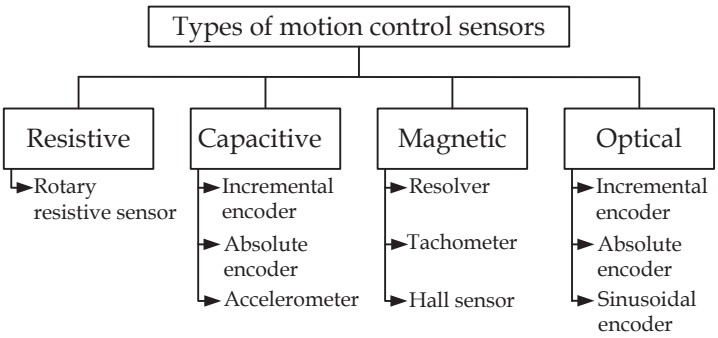

Figure 1.7 Types of speed sensor according to its physical principles.

The specific application dictates which sensor and technology must be chosen according to multiple criteria such as: cost, required accuracy, immunity to electromagnetic noise, light or duty classification (light, industrial, servo and heavy duty), high-temperature exposure, environmental humidity or dust, harsh environment such as shock or vibration, the type of interface with the control unit (TTL, analog interface, Ethernet etc…), to mention but a few.

As an example, resolvers are frequently used for critical applications like aerospace because these sensors are both robust and reliable. Optical encoders provide a good trade-off between performance and cost. The encoder includes a disc coupled to the shaft of the motor as in Figure 1.8.

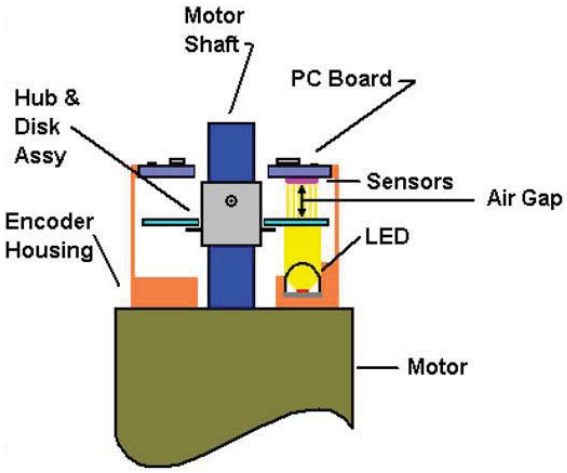

Figure 1.8 Optical encoder for motion control from [8].

The optical encoders are classified, according to the pattern printed in the border of the disc, as incremental and absolute encoders, as in Figure 1.9.

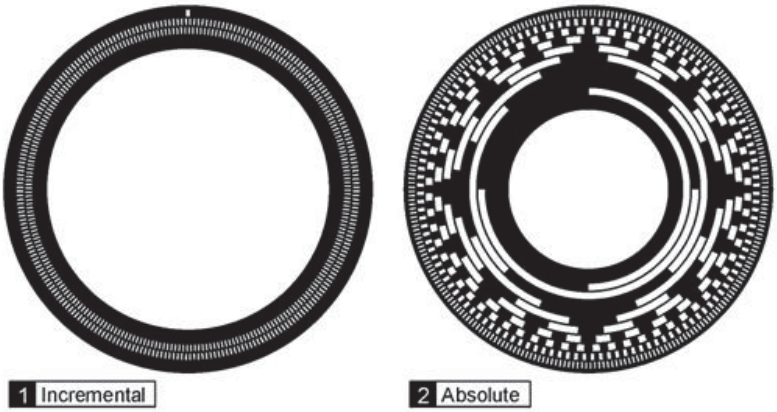

Figure 1.9 Patterns of the disc of the encoder [9].

An incremental encoder has a pattern of slits (line or band of slit), nominal evenly spaced, printed in the circumference of the disc. The total number of slits over the circumference is termed as *R'*. The slits distributed within the 360^{o} determine the resolution of the encoder. The resolution is the minimum increment of rotation θ that can be measured. The slit transmits the light of a photodiode placed on one side of the disc. The light beam is sensed by a photodetector on the other side of the disc. The photodiode produces a waveform with amplitude proportional to the received light,

which has an almost sinusoidal shape as in Figure 1.10. From this perspective, all optical encoders are pseudosinusoidal encoders in origin.

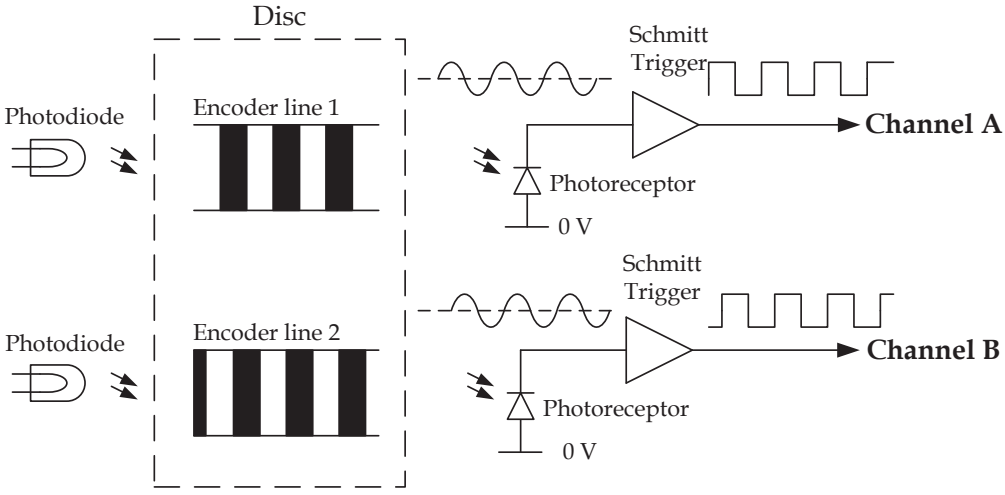

Figure 1.10 Representation of the incremental optical encoder.

As shown in Figure 1.10, the sinusoidal waveform is squared by using a Schmitt Trigger. The incremental encoder usually has two lines with slits shifted 90^o to each other. Consequently, the squared output signal, labelled as Channel A and Channel B, are also shifted 90^o, nominally. Alternatively, some incremental encoders have a single line and produce the two channels electronically. The encoders with two channels are known as quadrature encoders. The output of the two channels follows a Grey Code pattern. This pattern is used to detect the direction of the rotation. The motor moves in a clockwise direction if Channel A leads Channel B by 90^o, if the opposite occurs, then the motor spin direction is anticlockwise. The differences between ideal encoders and real encoders are discussed in subsequent sections.

Absolute encoders have several coded lines *n*-lines and also *n* photodiodes and photodetectors. The absolute encoder has *n* channels and the combination of those defines in a unique way every rotated angle. The resolution for this sensor is $\theta = 360^o / 2^n$. This sensor provides precise information of the position even after the system has been powered off. The manufacturing cost of this sensor is also higher than that of an incremental encoder. The price is determined by the cost of printing a complex mask on the disc. High accuracy requires a complex and expensive manufacturing process.

While the absolute encoder is used in applications where the precise knowledge of position is required such as in robots, the incremental optical encoder in particular is frequently found in applications like:

- CNC machines, printers
- Paper production
- Food and beverage automation (mixing, bottling, labelling),
- Elevators (in speed control, the motor commutation, elevator doors, vertical positioning and for elevator governor).

Recently, encoders have been incorporated to assess the health of rotating machinery [10]. This thesis focuses on the incremental optical encoder used in motion control. The main speed estimation methods used for this type of sensor are known as: pulse (or transition) count method (PC), and elapsed time method (ET). In the first case the speed is estimated as the count of encoder transitions during a fixed time interval, T_s. This method is applied at high speeds with several transitions per sampling interval. The ET method estimates the speed based on the time measurement between consecutive encoder transitions and is used for low speeds. Although this method can be used over the full speed range, empirical results show that is unpractical at high speeds because of the measurement errors as in (1.1). This is discussed in chapter 4.

$$\text{Total error} = \text{encoder error} + \text{electronic error} + \text{system interaction error} \quad (1.1)$$

The encoder errors could be due to one or several of the following reasons according to [11].

- Assembly error and manufacturing mechanical tolerance built-up.
- Mask or disc misalignment,
- Mechanical vibration,
- Temperature variations,
- Electrical noise,
- Faulty power supply regulation.

The quantized and sampled position measurement limits the performance of the system [12]. Some of the reported adverse effects are: vibration [12], torque ripple [13] and [14], or motor noise [15]. Specific studies on the field oriented control (FOC) for permanent magnet synchronous motors (PMSM) are found in [14] and [16]. The quantized nature of the sensor can induce limit cycling in the system, causing speed oscillations [17]. Speed oscillation in encoder-based systems is studied in [18] by means

of a harmonic approximation. The encoder also reduces the control bandwidth [15] and [19] , and causes the estimated motor speed to intrinsically lag the actual speed.

When the number of encoder transitions per control sample time (T_s) is higher than one, the simple solution of low-pass-filtering of the velocity estimate is not favoured due to bandwidth reduction, so alternative approaches are provided in [12] and [20] that reduce the phase lag.

When the number of encoder transitions per control sample interval is less than one, the measurement delay can become significant due to the infrequent encoder updating of the position information [21]. Under those circumstances, the frequency response of the motor drive control loop can be impacted by the dynamics of the encoder. The system can even become unstable due to the dynamics of the encoder, if it is not considered when tuning the speed loop compensator.

1.2.1 Hardware-based Solutions to Compensate the Limited Resolution of the Encoder

One of the possible hardware based solution is a gear-box in the coupling of the motor and the load (coupled system) as in Figure 1.11. The gearbox is typically used to increase the speed [11] and [22].

The disadvantages of this solution are reported in [22]:

- Backslash inherent to the gearbox, with looseness when motion is reversed;
- reduces the system efficiency;
- Increases of the volume and weight of the motor and the system in general;
- Increase of the cost;
- Increase of the audible noise.

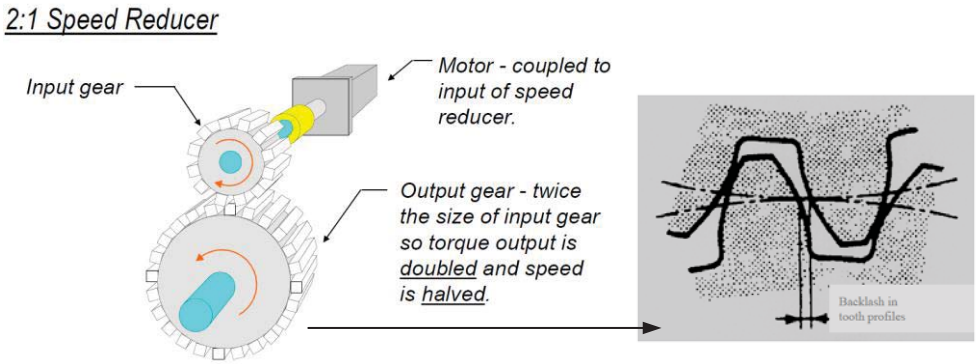

Figure 1.11 A gearbox in the coupling of the motor and the load [11].

The Quadrature-based Phase Locked-Loop (QPLL), found in [23] and shown in Figure 1.12, detects the frequency of the input signal and produces a square signal with frequency equal to the frequency of the input signal. This is particularly useful in electromagnetic encoders employed within a vehicle where electrical noisy signals may produce false triggers and induce incorrect speed estimations.

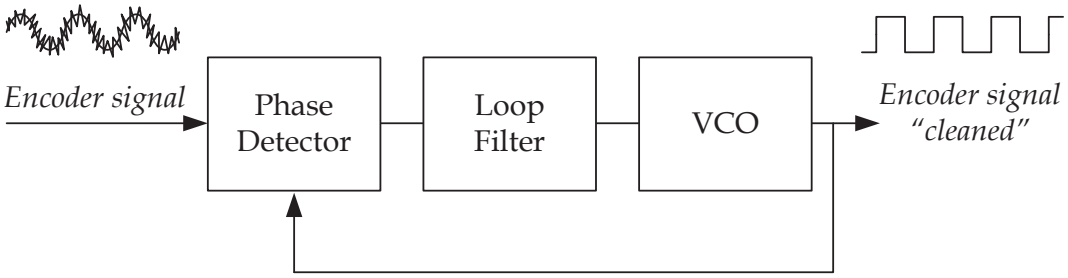

Figure 1.12 Structure of a QPLL implemented using a LM565 [23]

It was proven in [23] that the output signal of the QPLL can lose track of the input signal at constant and low speed. Additionally, there is a delay time for the PLL to track the correct frequency.

1.2.2 Software-based Solutions to Compensate the Limited Resolution of Encoders at Low Speeds

Several methodologies and algorithms are found in literature to reduce the impact of the quantization error on the control loop. It is observed that many papers address specific technological constraints. For instance, in the late 80s and 90s the pulse count was often implemented with an external counter so that the maximum count of pulses was 2^n-1 (where *n* is the resolution and bit size). This conveys at least two problems:

- How often should the *n* output of the counter be sampled?
- How to detect the count overflow (of the external counter) without losing information?

These type of problems were addressed in [24] computing in advance the bit size that corresponds to the transition count at each speed and sampling only that output. The bit size varies with speed and so the counter output sampling frequency. This section describes different software solutions found in literature to improve the speed estimation. These solutions address more general and methodological problems rather than technological issues.

The software-based solutions for the improvement of the speed estimation can be classified into non-model based method and model based method as proposed in. The non-model based methods refer to those methods focused on processing the encoder signal. The model based methods combine the information from the encoder and a mathematical model of the motor and the driver to improve the speed estimation especially at low speed. Figure 1.13 shows a list of relevant methods which are briefly mentioned in this section.

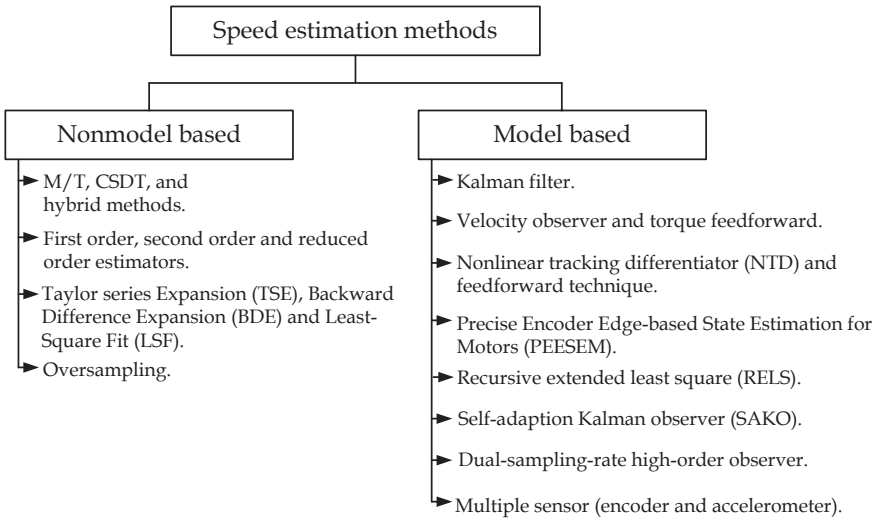

Figure 1.13 Some relevant speed estimation methods.

- Nonmodel based methods.

The M/T method was proposed in 1982 in [25]. This method combined the best of the existing pulse count method (M) and the elapsed time method (T). It also improved the detection time, which was particularly relevant for microprocessor-based speed estimation. Similarly, the constant sample-time digital tachometer (CSDT) was presented in 2000 in [26]. This method was implemented on a FPGA and targeted the reduction of the sensor sensitivity to nonidealities.

The delay between the actual motor speed and the estimation is reported in 1988 [12]. This paper proposed a higher order estimate (first order, second order and reduced order estimators) to reduce this delay. Following the same idea of the delay, [27] proposed a reconstruction of the velocity estimate based on a Taylor series expansion (TSE), a backward difference expansion (BDE) and a least square fit (LSF). An oversampling technique is also proposed in [28] to reduce the noise of the speed estimation based on optical encoders.

- Model based methods.

The low update rate of the information when using encoders at low speed is one of the key challenges inherent of this type of sensor. Many researchers have approached the problem by means of state observers. The observer predicts a future state of a signal based on a model of the plant to be controlled (the plant must be previously characterized) along with past measurements of the inputs and the outputs of the system.

Various types of observers are reviewed in [29] as well as their foundation and algorithms. The following text is quoted from this paper:

> *"One intuitive ideal to deal with this problem is to estimate the disturbance (or the influence of the disturbance) from measurable variables, and then, a control action can be taken, based on the disturbance estimate, to compensate for the influence of the disturbance."*

The observers then predicts the value of the unknown variable which cannot be measured. Another fragment of the same paper states:

> *"This basic idea can be intuitively extended to deal with uncertainties where the influence of the uncertainties or unmodeled dynamics could be considered as part of the disturbance. Consequently, in a similar fashion, the influence of the uncertainty can be suppressed and the system robustness can be improved".*
>
> The paper continues saying that *"this motivates the development and application of a wide variety of disturbance/uncertainty attenuation algorithm independently by researchers and practitioners working in different industrial sector. Although under different names and developed from different prospects, those algorithms/methods share a fundamental idea, i.e. an observation mechanism if designed to estimate disturbances or uncertainties (or both of them), and corresponding compensation is then generated by making use of the estimate"*

Observers are used when the mathematical equation of the system (i.e. the encoder) is "*unmodeled*". Many of recent works in this area are based on the original work of Kalman observers, also referred to as the Kalman filter. A paper published in 1961 [30] provides insight on this matter. Later, in 1971 Luenberger expanded the work in the field of observers for a deterministic setting in [31].

Modifications on the Kalman and Luenberger observer have been proposed to overcome the issues of encoders at low speed as in [32]. Also a velocity observer combined with a torque feedforward was proposed in [33] to improve the field orientation of ac servodrive. A nonlinear tracking differentiation (NTD) in [34] is combined with a velocity and acceleration feedforward to overcome the characteristic phase lag of the differentiation. Another algorithm, based on a Kalman filter, is the precise encoder edge-based state estimation for motors (PEESEM) proposed in [35]. A recursive extended least square method (RELS) is proposed in [36] for a wide-speed range. The RELS identifies variations in the parameter of the plant to adjust the gain of the speed controller automatically for a good dynamic response. A self-adaptive Kalman observer (SAKO) is described in [37] that updates the gain matrix by calculating the actual noise - more likely the noise covariance at every control sample interval in order to accurately observe the speed when data is not available at low speed. The dual-sampling-rate high order observer in [20] updates the sampling time to the rotational speed to guarantee that encoder data is always available, this method also considers the relation of the estimation and the error correction periods. More recently, researchers proposed a combination of multiples sensors like encoders and accelerometers as in [38] and [39].

The uncertainty in the plant model or parameters can limit the performance of observer. The algorithm itself increases the computational burden [40] of the control algorithm, or possibly necessitate the application of system identification techniques, [36], [37] to update the motor parameters of observers.

The slightest variation of the model of the plant (like inertia or load) or the point of operation affects the performance of the observer. Online identification algorithms have been developed to update the plant model. However, the computational burden narrows their applications. The advantages and disadvantages of the observers are described and discussed in [19].

Alternatively, this thesis proposes the study and derivation of small-signals models of the encoder and speed estimation algorithms to easily quantify the impact of the sensor on the control loop and to propose a simple compensation.

The first model of the dynamics of the encoder is found in [41] where the dynamics of the sensor and the speed estimation method are represented by a delay.

$$H_{Enc}(s) = e^{-s\cdot\frac{T_s}{2}} \tag{1.2}$$

The same paper proposes an approximation for the low speeds; with T_e being the time between consecutive encoder transitions.

$$H_{Enc}(s) = e^{-s\cdot T_e} \tag{1.3}$$

Alternatively, [42] proposes the following equation to model the dynamics of the encoder at low speed:

$$H_{Enc}(s) = \frac{1-e^{-s\cdot T_e}}{s\cdot T_e} \tag{1.4}$$

The previously mentioned models do not fit the phase and the magnitude simultaneously in all conditions as it will be demonstrated later on in this thesis.

1.3 Purpose of the Thesis and Contributions

At least two problems can be identified in the area of study of the incremental optical encoder for motion control:

1. There is not a precise and validated transfer function for the incremental optical encoder sensor. Therefore, the designer assumes an ideal encoder, i.e. no attenuation and no phase lag at the operating frequency, for the motion control design. It indirectly increases the cost of the design, since such conditions are only achievable with a very high resolution encoder.
2. There is not a simple and unique and smooth speed estimation method that can be used for all speed intervals, particularly in quadrature configuration [43]. Moreover, those speed estimation methods that have a good dynamic performance presents a bad static error and vice versa. A mix of speed estimation methods are used in applications involving variable frequencies.

The defined problem in 1 is also acknowledged by the manufacturing companies of encoders such as Heidenhain Corp. This company listed five challenges and opportunities for encoders in [44] that are: *increasing precision while lowering ownerships cost*, *speed at nanometre level resolution*, *choosing the right motion*

feedback solution, conquering the functional safety issues and security customized solutions. For the first point, the report details:

> *"(...) high accuracy and high stiffness are achievable, but at a cost that is sometimes prohibitive"*

Similarly, ENCODER PRODUCTS COMPANY, a manufacturer of motion sensor and controllers, list five tips when specifying incremental optical encoders in [45]:

1. Integrating the encoder into the equipment.
2. Determining the desired resolution.
3. Selecting the output type.
4. Environmental considerations.
5. Use a 3D model.
6. Consider a programmable encoder.

Particularly for point 2 it says:

> *"This key metric is more difficult to specify than it might appear, because if the resolution is too high, encoder cost will increase unnecessarily and will exceed the output frequencies of the controller. The encoder should remain within the specifications of the controller. It's also important to consider that many applications do not require extremely high resolution, so there's no need to over-specify it. Conversely, resolution that is too low will likely limit the system's ability to accurately control speed or position."*

In order to address and solve the first problem of this thesis has:

1. Developed and validated the small-signal models of the incremental optical encoder and different speed estimation methods. Those methods are: the Pulse Count (PC) method, the elapsed time (ET) method and the Constant Sample-time Digital Tachometer (CSDT) method.
2. Designed of a novel system set up used to experimentally validate the small-signal models.
3. Implemented a lead compensator in a digital control of a DC motor that operates at low speed with a low resolution encoder in the feedback loop. The lead compensator is designed based on the developed small-signal model. The lead

compensator improves significantly the performance and stability of the motor in the described conditions.

The second defined problem is solved by introducing improvements on an existing speed estimation method.

1. The method is named the Improved-ET and has a good balance between static error and dynamic performance. This method is experimentally compared to the existing methods in a closed-loop configuration using a DC motor.

A sequenced methodological approach applied to this thesis:

I. Definition of the problem.
II. Study of the state of the art related to the topic.
III. Theoretical study of the problem by simulation and/or mathematically.
IV. Experimental validation of the concept.
V. Practical example of application of the concept in a real system.

The small-signal model has a positive impact in many different areas.

1. Cost of the project. The designer can select in an early design stage the correct resolution for the encoder without oversizing the sensor.
2. For low speed application a correct simple compensator can be implemented to compensate a low resolution encoder. The proposed simple compensator can be implemented in a non-high performance device. In addition, the simplicity of the compensator facilitates long-term maintenance and lowers failure probabilities, against the use of complex algorithms.
3. The study developed here for incremental encoders can be easily expanded to other sensors like magnetics encoders, see Figure 1.14. One of the advantages of magnetic sensor is that these sensors are not affected by environmental dust.

Figure 1.14 Similarities between magnetic encoders for railway applications (a) and (b) and incremental optical encoders (c).

1.4 Thesis Outline

This thesis is structured in six chapters. The first chapter corresponds to the introduction. The second chapter presents the characterization and the implementation of the three speed estimation methods under analysis on the ADSP signal processor. In the third chapter the small-signal models of the encoder in combination with three different speed estimation methods are derived and experimentally tested in a novel set up. The fourth chapter corresponds to the study of the improved elapsed time method. The fifth chapter considers the practical application for the small-signal model of the incremental optical encoder and the improved elapsed time. Chapter sixth is the conclusion of the present thesis and the proposal of ideas for future works.

Chapter 2. Analysis and Implementation of the Speed Estimation Methods

The static performance and the steady-state error, *e*, of the three speed estimation methodologies: pulse count (PC), elapsed time (ET) and constant sample-time digital tachometer (CSDT) methods are discussed and implemented on a specialized DSP (CM403f) from Analog Devices. This DSP includes dedicated hardware for interfacing with quadrature encoders that facilitates the implementation of advanced speed estimation methods, such as the CSDT, by minimizing the delay resulting from software intervention. In addition, the three methods are used to sense speed in the motion control loop of the DC motor.

2.1 Introduction

Quadrature optical encoders are frequently used in motion control for servo-systems, industrial automation and robotics. In previous literature, incremental optical encoders are also listed as digital tachometers. Speed and position can be estimated by counting the number of encoder pulses during a given time interval (sampling interval, T_s). Inaccurate or delayed estimation of the speed impacts on the stability and performance of the system, potentially reducing quality and throughput in automation/robotic applications, and increasing acoustic noise and vibrations [15].

The resolution of the encoder, defined as the detectable angle of rotation θ', is determined as (2.1) in degrees and depicted in Figure 2.1.

$$\theta' = \frac{360}{R'} \tag{2.1}$$

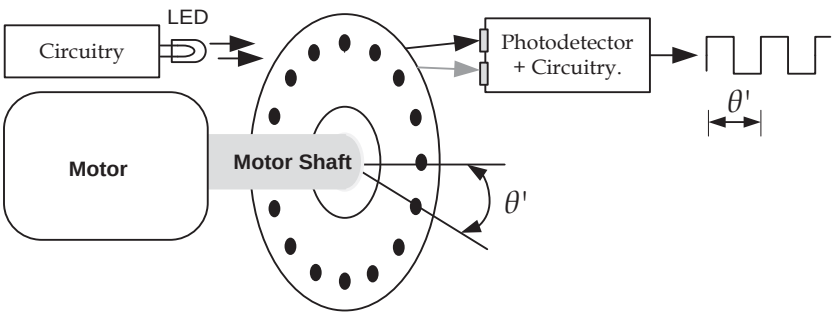

Figure 2.1 Minimum rotated angle.

where: R' is the encoder resolution in pulse per revolution (ppr) that can be increased by a factor γ (γ can be 1, 2 and 4) according to the encoder peripheral configuration. The optical incremental encoder has two channels (Channel A and Channel B) with one nominally shifted 90°, as shown in Figure 2.2. The term θ represents the effective rotated angle once the resolution is electronically increased.

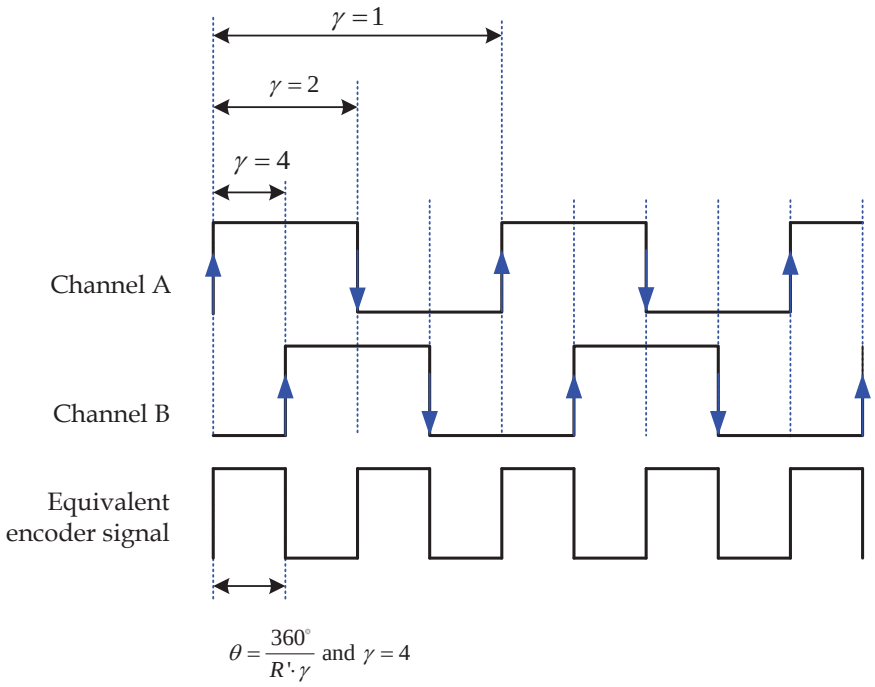

Figure 2.2 Different encoder configurations with electronically increased resolution.

For γ = 1 only the rising edge or falling edge of a single channel is counted. For γ = 2, both rising and falling edge of a single channel are considered; and for γ = 4 the rising and falling edges of both Channel A and Channel B are used, this configuration is commonly known as the quadrature configuration mode. The quadrature configuration of the encoder facilitates the detection of the direction of the rotation by the relative phasing of the two channels. The effective encoder resolution, R, is defined as $R = R' \cdot \gamma$.

The speed estimation errors can be divided in two main categories: steady-state error and dynamic error, corresponding to the accuracy of the speed measurement and the capability of the system to track a variable signal, i.e. accelerations. This chapter is focused on a comparative study of the steady-state error of the PC, CSDT and ET methods.

Several factors can affect the accuracy of the measurement over one transition (the ideal location of encoder edge and actual location) as shown in Figure 2.3.

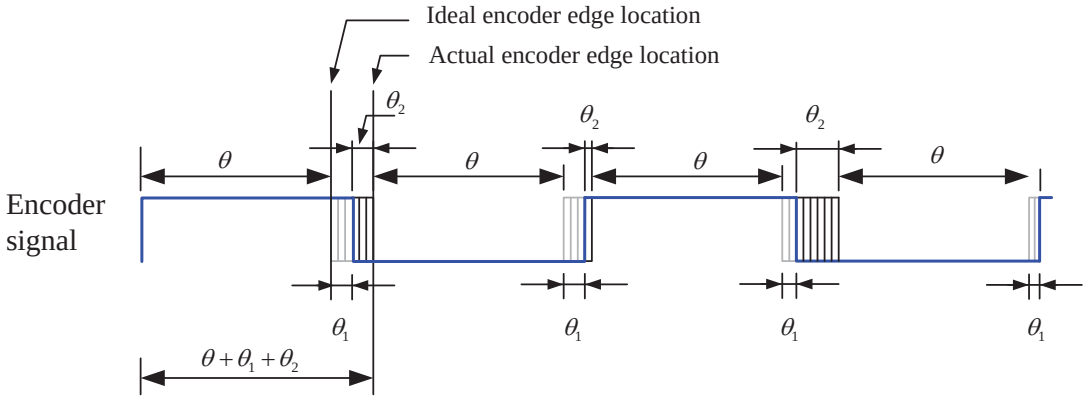

Figure 2.3 Representation of the errors in the speed measurement between consecutive intervals.

The accuracy of the speed estimation depends on the term θ in Figure 2.3. This term represents the position of the expected ideal transition, and can vary due its physical and electrical nonidealities represented by θ_1 and motor and control nonidealities represented by θ_2.

The term θ_1 represents the error in the location of the transition due to: incorrect assembly, manufacturing tolerances, the electric circuit that is used to condition and square the optical signal [46] from the photodetector. These errors are periodic and their impact is often significant on the speed estimation, especially in a quadrature configuration at high speed. Filters or averaging techniques can be used to minimize the impact of those errors on the measurement. However, filtering or averaging adversely affects the dynamic performance of the system because of the phase lag inherent to those processing techniques.

The term θ_2 represents variations on the location of the actual encoder transition. This variation is produced by motor accelerations, e.g. due to motor friction and unbalances. The effect of θ_2 in the speed measurement can be reduced with a properly tuned controller.

Additionally, the general purpose counter (CNT) peripheral of the DSP introduces some measurement errors because it is a digital device with quantized peripherals.

2.2 The Speed Estimation Methods

2.2.1 The Pulse Count Method

The Pulse Count (PC) is a well-known method [25] for the speed estimation. It is also named as *M*-method in the same paper. The method is based on the encoder edge (pulse) count over T_s, a fixed time interval, and the used unit is revolutions per minute (r/min).

The angular speed is

$$\bar{\omega}_{PC} = \frac{\theta_{Total}}{T_s} \qquad \text{(deg/s)} \tag{2.2}$$

where θ_{Total} is the total rotated angle during the sample time T_s. This can also be expressed as a function of the encoder effective resolution θ by counting the number of total encoder transitions (L) occurred during T_s.

$$\bar{\omega}_{PC} = \frac{L \cdot \theta}{T_s} \qquad \text{(deg/s)} \tag{2.3}$$

This can be expressed in radians per second (rad/s).

$$\bar{\omega}_{PC} = \frac{L \cdot \theta}{Ts} \cdot \frac{2\pi\, rad}{360} \qquad \text{(rad/s)} \tag{2.4}$$

and with units of revolutions per minute (r/min):

$$\bar{n}_{PC} = \frac{L \cdot \theta}{T_s} \cdot \frac{2\pi\, rad}{360} \cdot \frac{1 rev.}{2\pi\, rad} \cdot \frac{60}{1} \qquad \text{(r/min)} \tag{2.5}$$

$$\bar{n}_{PC} = \frac{L \cdot \theta}{T_s} \cdot \frac{60}{360} \qquad \text{(r/min)} \tag{2.6}$$

Simplifying equation (2.6) with (2.1)

$$\bar{n}_{PC} = \frac{L}{T_s} \cdot \frac{60}{R} \qquad \text{(r/min)} \tag{2.7}$$

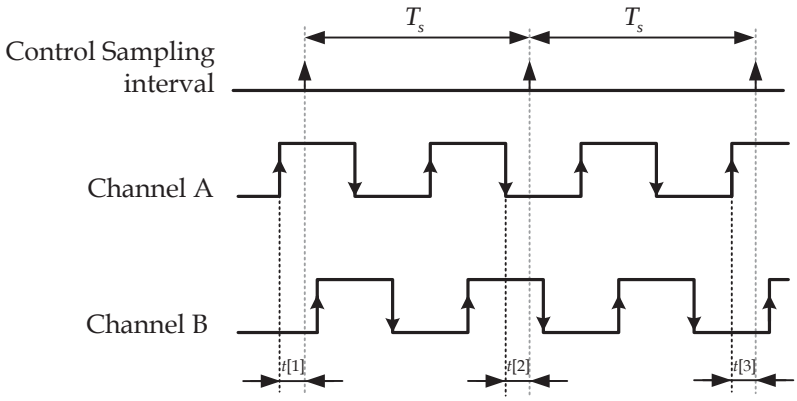

Figure 2.4 Diagram showing relevant signals of the encoder in the PC method.

The time $t[1]$ and $t[2]$ are not considered in the computation of the PC-based speed estimation method. This leads to an inaccurate result because the fractional part of the transition at the beginning and the end are not considered[1]. This quantization error is more relevant at medium speed as will be analysed later.

The speed interval can be classified as low, medium and high speed. The average speed, $\bar{n}$ with units of r/min, can also be expressed as normalized speed (l) in units of encoder transition per control sample time (tr./T_s).

$$l = \frac{\bar{n} \cdot \frac{R}{60}}{T_s} \tag{2.8}$$

According to (2.8) the speed is classified as:

- Low speed for $l < 1$ tr./T_s, i.e. less than one encoder transition per sample time.
- The authors consider medium speed for 1 tr./$T_s \leq l <$ 20 tr./T_s. In general, the criterion to delimit medium and high speed is not unique and will be application-dependent.
- High speed is hence defined for $l >$ 20 tr./T_s.

The PC method can be used, in theory, for any speed such that $l \geq 1$ tr./T_s. However, in practice it is used at high speed to avoid the negative the impact of the quantization error in the control loop. For example, 20 tr./T_s implies a 5% percentage error in the PC based speed estimation. In a high-inertia load the PC would not cause a major inconvenience because the mechanical pole filters the noise produced by the estimation error.

[1] The DSP counter counts an integer number of encoder transitions.

2.2.2 The CSDT method

The error of the PC method is corrected by including the extra time (t[1] and t[2]), leading to the constant-sample digital tachometer (CSDT) method. This method estimates the speed of the motor based on the number of completed encoder transitions, as shown in Figure 2.5.

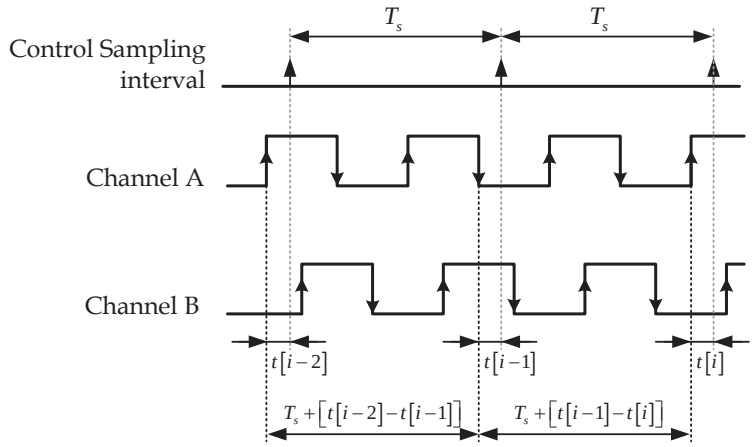

Figure 2.5 Diagram showing relevant signals of the encoder of the CSDT method.

The expression of this method is:

$$\bar{n}_{CSDT} = \frac{L}{T_s + \Delta t_{Auxiliary}} \cdot \frac{60}{R} \qquad \text{(r/min)} \qquad (2.9)$$

where $\Delta t_{auxiliary} = t[i\text{-}1] - t[i]$ and i is the subscript for a sample instant.

The use of this auxiliary time greatly improves the accuracy of the speed estimation. Previous works in [26] and [47] present experimental and theoretical analysis of the performance of this method. The implementation of the CSDT, on a single chip, using a new targeted Analog Devices Advanced Digital Signal Processor (ADSP), is a novel contribution of this work.

The CSDT method is used in medium and high speeds (>1tr./T_s) and the PC method is used at high speeds generally.

2.2.3 The Elapsed Time Method

This method estimates the speed based on the time elapsed between the latest two encoder transitions, T_e, at low speed $T_e > T_s$. This method is also named as T-method in [25]. The time T_e is obtained by counting pulses (m) of a high-frequency clock, with period T_{SYSCLK}, which is part of the peripheral. A representation of this method is found

in Figure 2.6. The information provided by the ET method is the most recent speed estimation of the motor system.

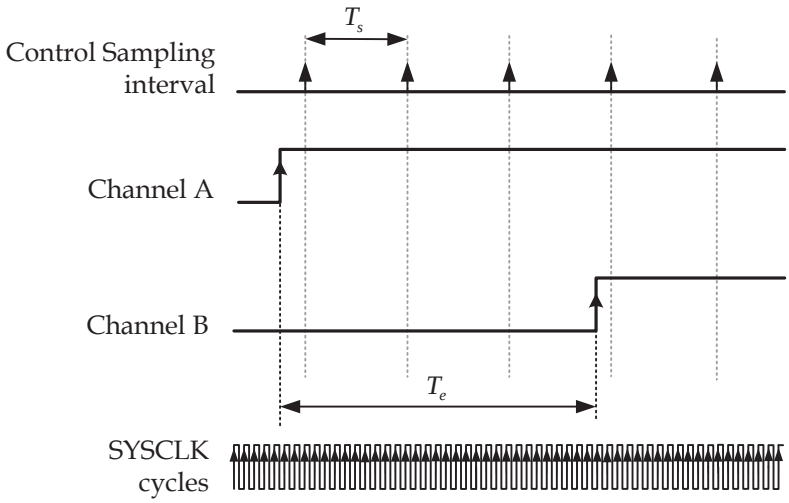

Figure 2.6 Diagram showing relevant signals of the encoder the Elapsed Time method.

The expression of the method is

$$\bar{n}_{ET} = \frac{1}{T_e} \cdot \frac{60}{R} \qquad \text{(r/min)} \tag{2.10}$$

where $T_e = m \cdot T_{SYSCLK}$

2.3 Analysis of the Steady-State Error of the Speed Estimation Methods

The steady-state error of the measurement, *e*, is defined as:

$$e = \frac{\left|\bar{n}_{Estimation} - n_{Actual}\right|}{n_{Actual}} \cdot 100\% \tag{2.11}$$

For the PC method, the error is produced by the ± 1 pulse count. For instance, assume a target speed of 225 r/min, an encoder with resolution 500 ppr, quadrature configuration and sample time of 1 ms, then L = 7.3 tr./T_s. However, the DSP only counts entire number of transitions, that is, the number of transition will vary between 7 and 8 transitions.

Assume δL ($0 \leq \delta L$ <1) as the non-desired count and replace in (2.6) and (2.11). The worst case errors are computed as the addition of the different errors.

$$e_{PC} = \frac{\left| \frac{L+\delta L}{T_S} \cdot \frac{60}{R} - \frac{L}{T_S} \cdot \frac{60}{R} \right|}{\frac{L}{T_S} \cdot \frac{60}{R}} \cdot 100\% \tag{2.12}$$

$$e_{PC} = \frac{|L+\delta L - L|}{L} \cdot 100\% = \frac{\delta L}{L} \cdot 100\% \tag{2.13}$$

Similarly, for the ET method, as the encoder signal is not synchronous with the DSP clock, the error is determined by the ± 1 T_{SYSCLK} clock count symbolized as δm ($0 \leq \delta m <1$). The error of this method is:

$$e_{ET} = \frac{\left| \frac{1}{(m+\delta m) \cdot T_{SYSCLK}} \cdot \frac{60}{R} - \frac{1}{m \cdot T_{SYSCLK}} \cdot \frac{60}{R} \right|}{\frac{1}{m \cdot T_{SYSCLK}} \cdot \frac{60}{R}} \cdot 100\% \tag{2.14}$$

$$\frac{\left| \frac{1}{(m+\delta m)} - \frac{1}{m} \right|}{\frac{1}{m}} \cdot 100\% \tag{2.15}$$

$$\frac{\delta m}{m+\delta m} \cdot 100\% \tag{2.16}$$

If $\delta m = 1$, then $m \gg \delta m$, and (2.16) is simplified to

$$e_{ET} = \frac{\delta m}{m} \cdot 100\% \tag{2.17}$$

The third method under study is the CSDT method. This method, thanks to the inclusion of the $\Delta t_{auxiliary}$ eliminates the error due to quantization of the PC method. A small error remains due to the lack of synchrony between the encoder signal and the high frequency clock that is the time base of the DSP. The expression of the error is as follows:

$$e_{CSDT} = \frac{\left| \frac{L}{T_s + (m[i-1] - m[i] + \delta m) \cdot T_{SYSCLK}} \cdot \frac{60}{R} - \frac{L}{T_s + (m[i-1] - m[i]_i) \cdot T_{SYSCLK}} \cdot \frac{60}{R} \right|}{\frac{L}{T_s + (m[i-1] - m[i]) \cdot T_{SYSCLK}} \cdot \frac{60}{R}} \cdot 100\% \tag{2.18}$$

$$\frac{\left|\frac{1}{T_s+\left(m[i-1]-m[i]+\delta m\right)\cdot T_{SYSCLK}}-\frac{1}{T_s+\left(m[i-1]-m[i]\right)\cdot T_{SYSCLK}}\right|}{\frac{1}{T_s+\left(m[i-1]-m[i]\right)\cdot T_{SYSCLK}}}\cdot 100\% \quad (2.19)$$

$$\frac{\left|\frac{T_s+\left(m[i-1]-m[i]\right)\cdot T_{SYSCLK}-\left(T_s+\left(m[i-1]-m[i]+\delta m\right)\cdot T_{SYSCLK}\right)}{\left(T_s+\left(m[i-1]-m[i]+\delta m\right)\cdot T_{SYSCLK}\right)\cdot\left(T_s+\left(m[i-1]-m[i]\right)\cdot T_{SYSCLK}\right)}\right|}{\frac{1}{T_s+\left(m[i-1]-m[i]\right)\cdot T_{SYSCLK}}}\cdot 100\% \quad (2.20)$$

$$\frac{T_s+\left(m[i-1]-m[i]\right)\cdot T_{SYSCLK}-\left(T_s+\left(m[i-1]-m[i]+\delta m\right)\cdot T_{SYSCLK}\right)}{T_s+\left(m[i-1]-m[i]+\delta m\right)\cdot T_{SYSCLK}}\cdot 100\% \quad (2.21)$$

$$e_{CSDT}=\frac{\delta m\cdot T_{SYSCLK}}{T_s+\left(m[i-1]-m[i]+\delta m\right)\cdot T_{SYSCLK}}\cdot 100\% \quad (2.22)$$

The plot of the steady-state error for the three expressions in (2.13), (2.17) and (2.22) is found in Figure 2.7.

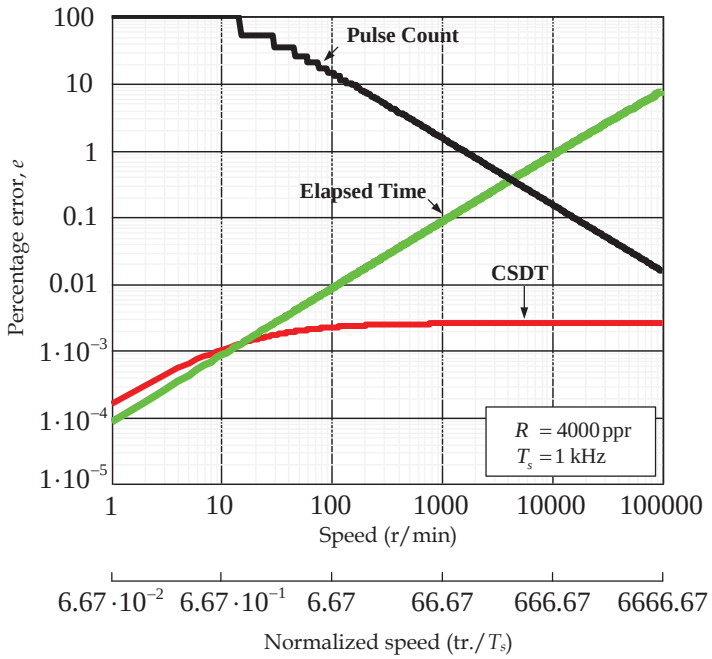

Figure 2.7 Comparative of the steady-state error of the different speed estimation methods.

As can be seen in Figure 2.7, the percentage error of the PC diminishes as the speed increases. Conversely, the error of the ET method increases when the speed increases and the error of the CSDT is almost constant in all speed range.

At low speed (up to 10 r/min), the error of the CSDT method is low and increases similar to the error of the ET method. As the speed increases the error is still small and effectively constant.

2.4 Model of the Incremental Optical Encoder for Simulations

The lack of a simulation model in some software tools for the incremental optical encoder and the speed estimation method was presented as a problem at the beginning of this work. In order to facilitate the understanding of this sensor, the author presents a simulation model that can be implemented in any simulation tool. The model is represented in Figure 2.8.

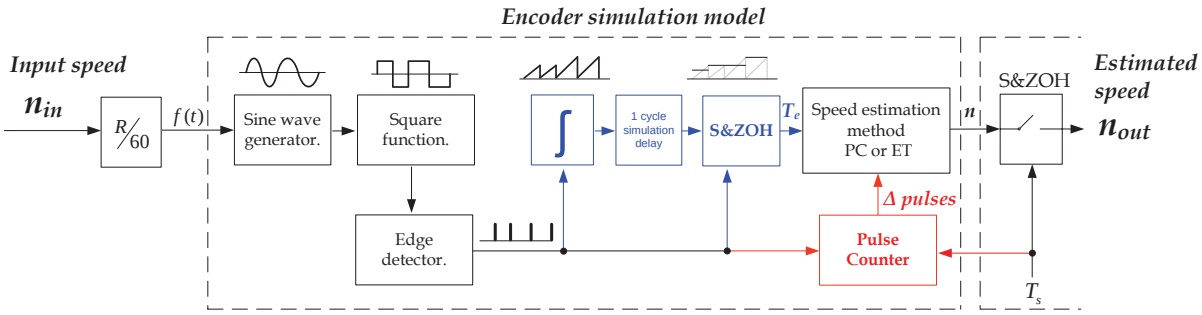

Figure 2.8 Simulation model of the incremental optical encoder.

Figure 2.8 represents a simulation model of the optical incremental encoder, where a sinusoidal block creates a waveform with a frequency equivalent to the rotor speed.

$$f(t) = \frac{R}{60} \cdot \bar{n}_{in} \tag{2.23}$$

The sinusoidal signal is squared by a sign-detector[2] block to create the square signal of the encoder channel. The edge detector is implemented with a derivative function. Every incoming edge resets the timer (an integral function). The time between pulses T_e, is held with a resettable-sample and zero-order-hold (ZOH). Later, the number of pulses, from the pulse counter, can be used to compute the PC-based speed. Alternatively, the time T_e can be used to compute the ET-based speed. The sample and hold block represents the sampling effect of the digital control with a frequency of T_s. Figure 2.9 shows the performance of the simulation model for the ET and PC methods when reproducing a sinusoidal speed profile at the input.

[2] The sign-detector block detects if the input signal is higher (positive) or lower (negative) than cero i.e. a zero crossing detector

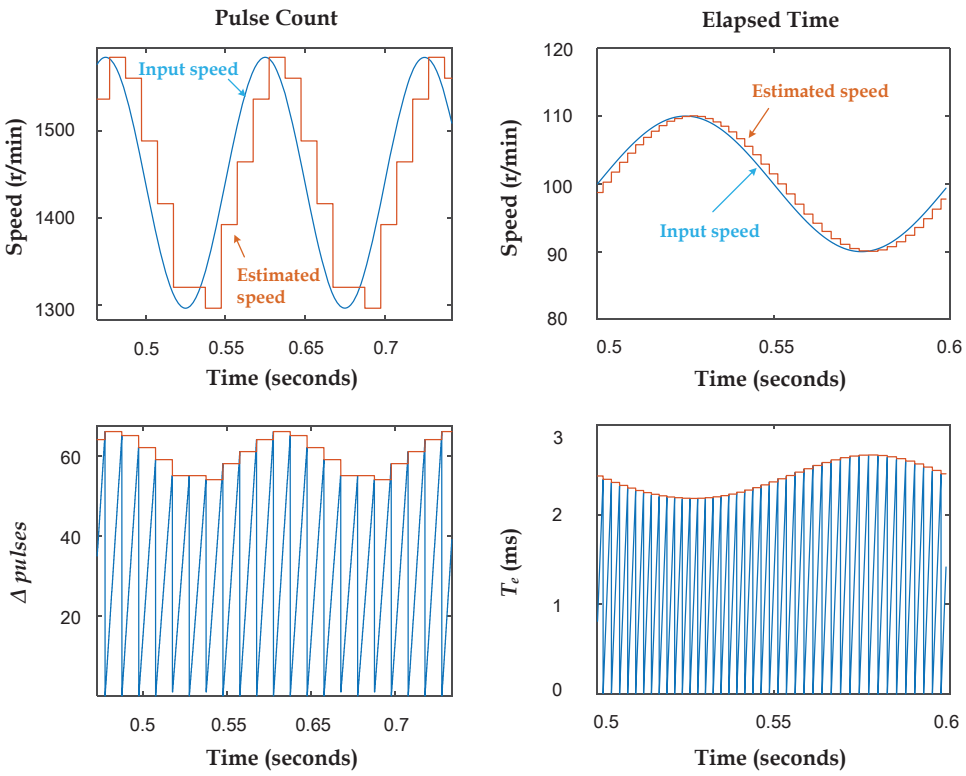

Figure 2.9 Results of the simulation model for the PC and ET methods (encoder R = 250 ppr).

2.5 Implementation of the Methods on the DSP

The three speed estimation methods are implemented on a ADSP CM403f, which is a mixed-signal control processor with ARM Cortex-M4 architecture. It includes a floating-point unit, a twenty-four channel analog front end (AFE) with twenty-four sixteen-bit Analog to Digital Converters (ADCs) and two twelve-bit digital to analog converters (DACs). The core clock frequency is 240 MHz. A counter unit (CNT) provides dedicated counting/timing circuitry that facilitates processing of the encoder output, unaffected by other control software. The CNT on-chip circuitry, combined with the General-Purpose Timer (TIMER), allows several speed estimation methods to be implemented.

The implementation of the three speed estimation algorithms requires the following capabilities:

- Counting encoder pulses.
- Counting time between pulses.
- Counting the auxiliary time required to implement the CSDT.

The fulfilment of these requirements leads to a configuration of the following peripherals: CNT, in "Capturing Time interval between successive Counter Events" mode, the timer (timer 6 or timer 7) and the trigger routing unit (TRU). The time diagram is depicted in Figure 2.10.

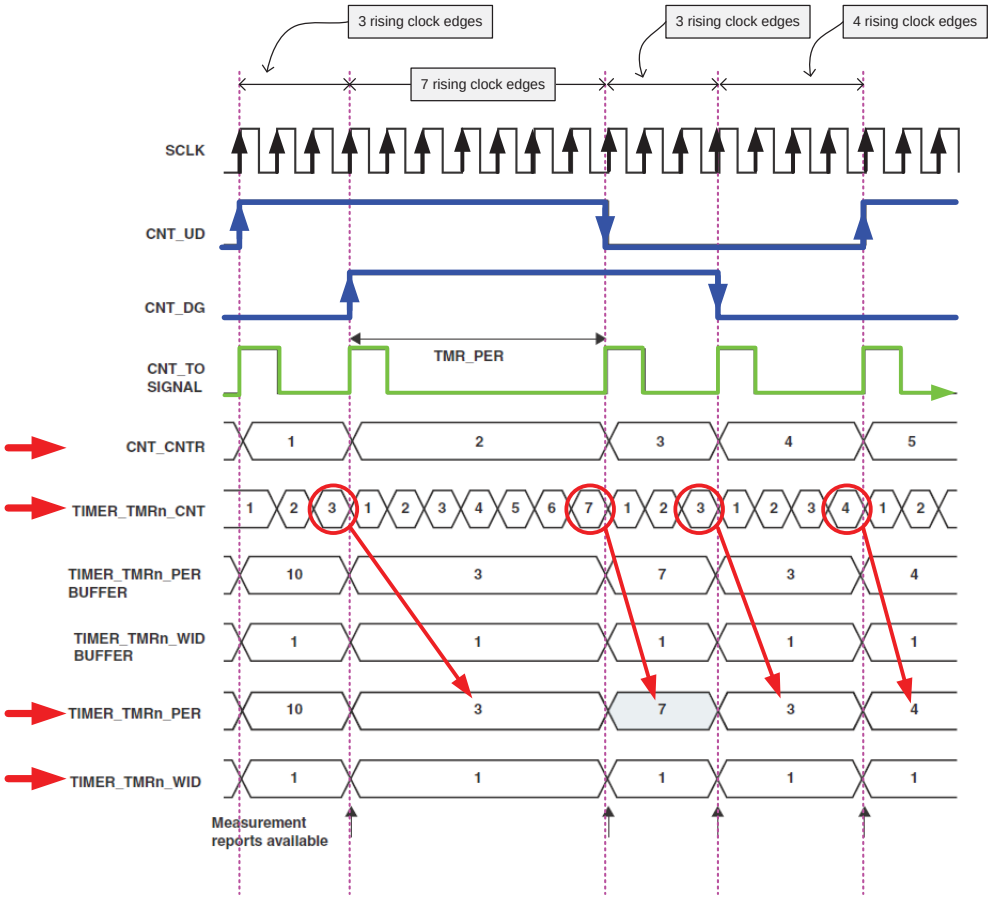

Figure 2.10 Time domain diagram of the peripheral CNT from the datasheet [48].

The three main registers that will provide the information for the speed estimation are:

- The CNT_CNTR register. This register is a read register and increments with every encoder transition (L), until it reaches the maximum count corresponding to 2^{32} - 1.
- The TIMER_TMRn_PER register. This register contains the number of SCLK cycles (m) during two consecutive encoder transitions.
- The TIMER_TMRn_CNT register. This register contains the instantaneous count of the high frequency clock cycles (m) that occurred during two transitions. It resets by hardware with every incoming encoder transition. The register TIMER_TMRn_PER latches the last count of this register during the next transition.

The SCLK is a high-frequency clock used to synchronize the peripheral tasks; it is also used as a time base. The frequency of the SCLK, also named as system clock (SYSCLK), is 80 MHz for this thesis. This frequency is achieved by means of a PLL.

Figure 2.10 shows a diagram of the relevant registers for the motion control of the ADSP, where the SYSCLK is an 80MHz free-running clock used by the CNT peripheral for time measurement. Simultaneously, a different timer generates an interrupt at a user-defined sample interval T_s, which is the control interval at which the CNT peripheral is sampled. Channel A and Channel B represent the quadrature encoder signals. Relevant registers of the CNT for motion control are represented in Figure 2.11.

Figure 2.11 shows the SYSCLK signal. This is the time base for all the CNT peripheral processes in the DSP. The signal T_s represents the regular time intervals for the speed estimation. Channel A and Channel B are the encoder signals. The signals TIMER_TMRn_CNT, TIMER_TMRn_PER and CNT_CNTR are the relevant CNT registers. The TIMER_TMRn_CNT is a real time counter of the time between encoder transitions T_e. Every incoming encoder transition reset this register. The TIMER_TMRn_PER register latches and hold the last count of the TIMER_TMRn_CNT before the reset. The CNT_CNTR register increments with every incoming transition L.

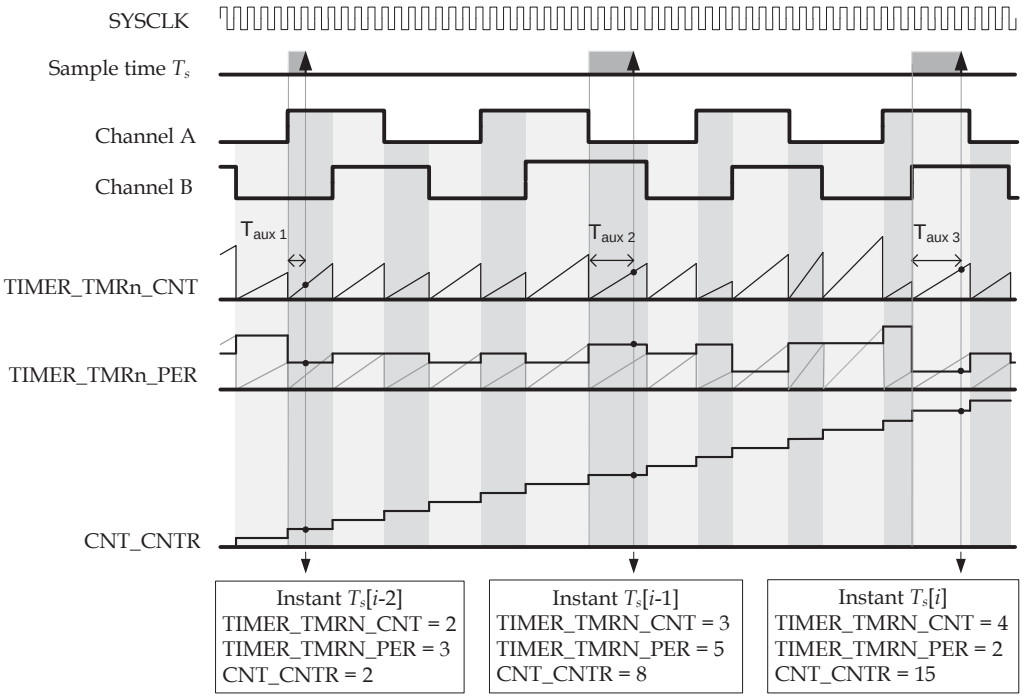

Figure 2.11 Time domain diagram of the CNT peripheral and its relevant registers, assuming a non-uniform speed.

For instance, at sample instant *i*, the estimated speed according to the different methods is as follows:

- Pulse Count method

$$\bar{n}_{PC} = \frac{\text{CNT\_CNTR}[i] - \text{CNT\_CNTR}[i-1]}{T_s} \cdot \frac{60}{R} \tag{2.24}$$

- CSDT method

$$\bar{n}_{CSDT} = \frac{\text{CNT\_CNTR}[i] - \text{CNT\_CNTR}[i-1]}{T_s - \left(\text{Timer\_TMRn\_CNT}[i] + \text{Timer\_TMRn\_CNT}[i-1]\right) \cdot T_{SYSCLK}} \cdot \frac{60}{R} \tag{2.25}$$

- Elapsed time method

$$\bar{n}_{ET} = \frac{1}{\text{TIMER\_TMRn\_PER}[i] \cdot T_{SYSCLK}} \cdot \frac{60}{R} \tag{2.26}$$

None of the existing speed estimation methods provide the true value of the actual speed. The PC and the CSDT methods average the speed of L transitions occurring within T_s. Conversely, the ET method provides the most recently updated speed estimate, based on the last encoder transition.

2.6 Experimental Validation

The diagram of the implementation of the speed estimation methods on the DSP is in Figure 2.12.

2.6.1 Open-Loop Tests

The processor performance is analysed for the PC, ET and CSDT methods. This can be done by emulating the encoder using a signal generator (TTi 50MHz Dual Function/Arb/Pulse Generator TG5012A) to produce the encoder signals. The emulated speed is set at 1038 r/min in quadrature configuration mode, R = 4000, and a sampling control interval of T_s = 1 ms. Results are depicted in Figure 2.13.

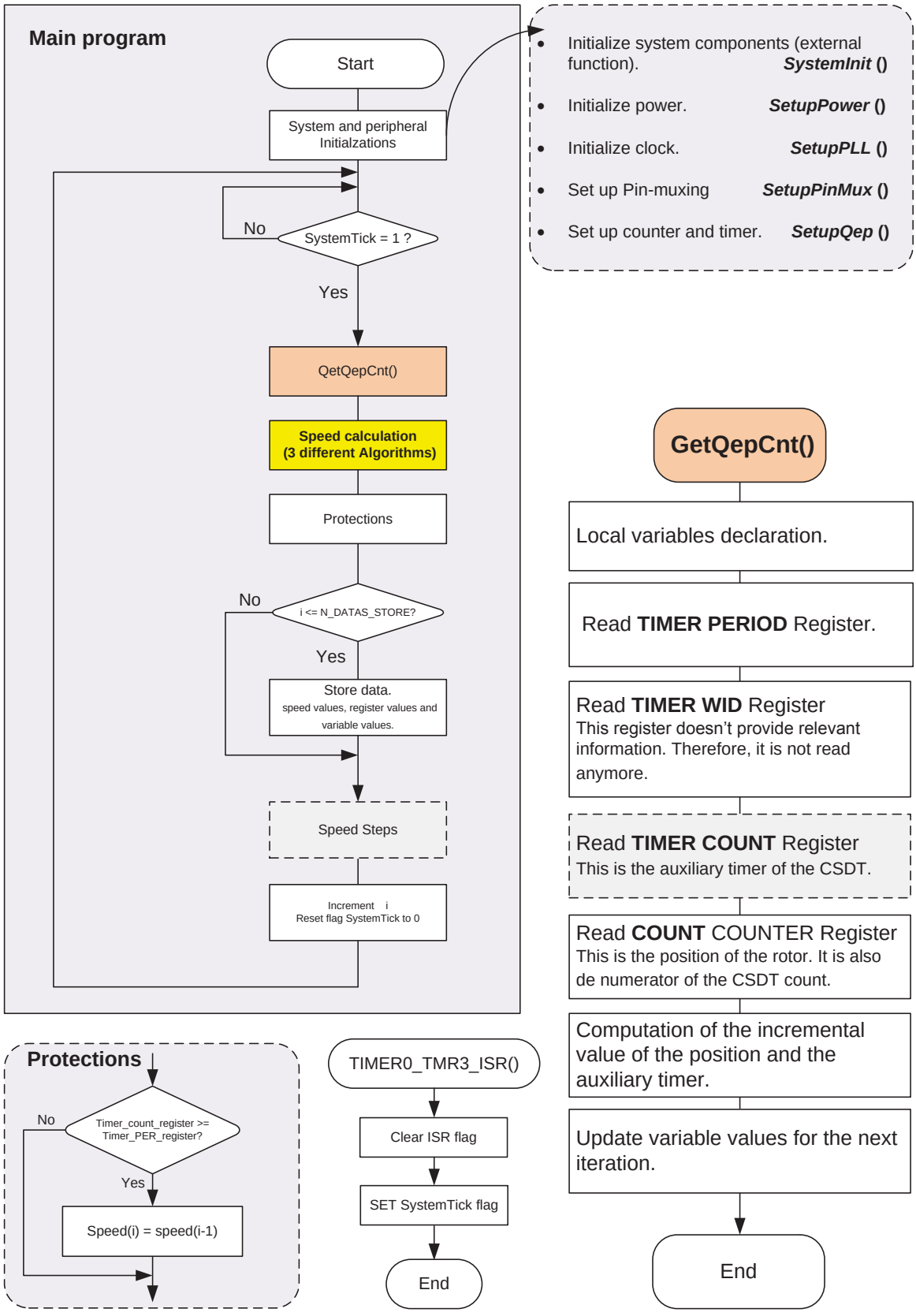

Figure 2.12 Flowchart of the algorithm implemented on the ADSP for the speed estimation.

Figure 2.13 (a) PC has the highest percent speed error of 1.1561%. Speed measurement is affected by a variable number of transitions per T_s (69 to 70), as can be seen in (b). The ET method indicates a speed error of 0.1793 %, this corresponds to a minimum theoretical count error ± 2 counts, twice that of the theoretical minimum (±1 counts). As can be seen in (c), the maximum count error is ± 2 counts because the timer register is incremental and is reset with every incoming transition. Finally, the CSDT presents the lowest speed error of 0.0048 %, through the use of the auxiliary time ΔT, see (d).

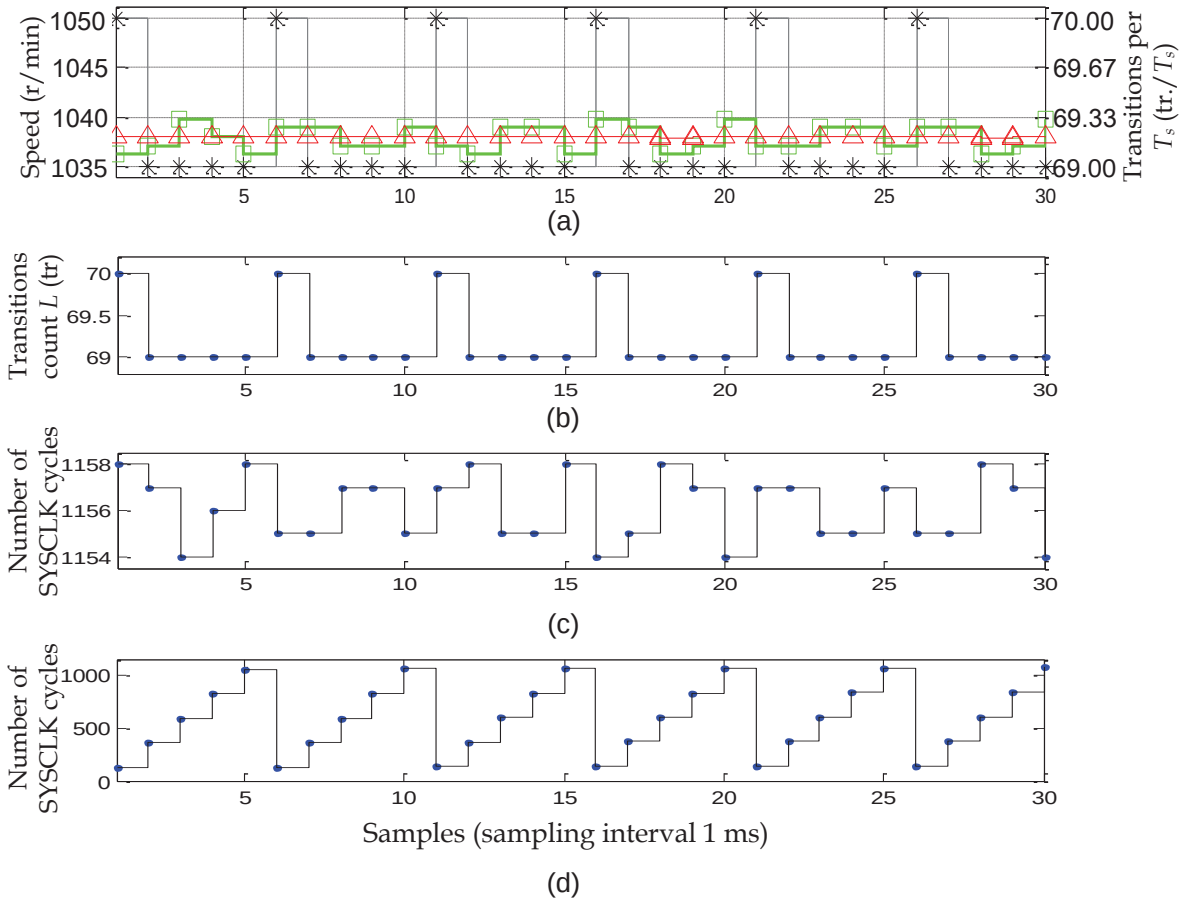

Figure 2.13 Experimental results of open-loop testing. In (a) estimated speed symbols are: '*' is PC, '□' is ET and 'Δ' is CSDT, theoretical speed is 1380 r/min. In this figure (b) is the number of transitions per T_s, (c) represents the time elapsed between preceding transitions and (d) is the auxiliary time Δt.

In terms of implementation, the PC method is the simplest method because it only requires a single peripheral to detect edges or transitions. The ET method is implemented by combining a timer and an edge or transition detector. The implementation of the CSDT involves a more sophisticated peripheral configuration, as already explained.

2.6.2 Closed-Loop Tests

In this section, each methodology is tested with a real optical incremental encoder coupled to the shaft of the encoder. The DC motor is controlled by a digital proportional and integral (PI) regulator, as in Figure 2.14.

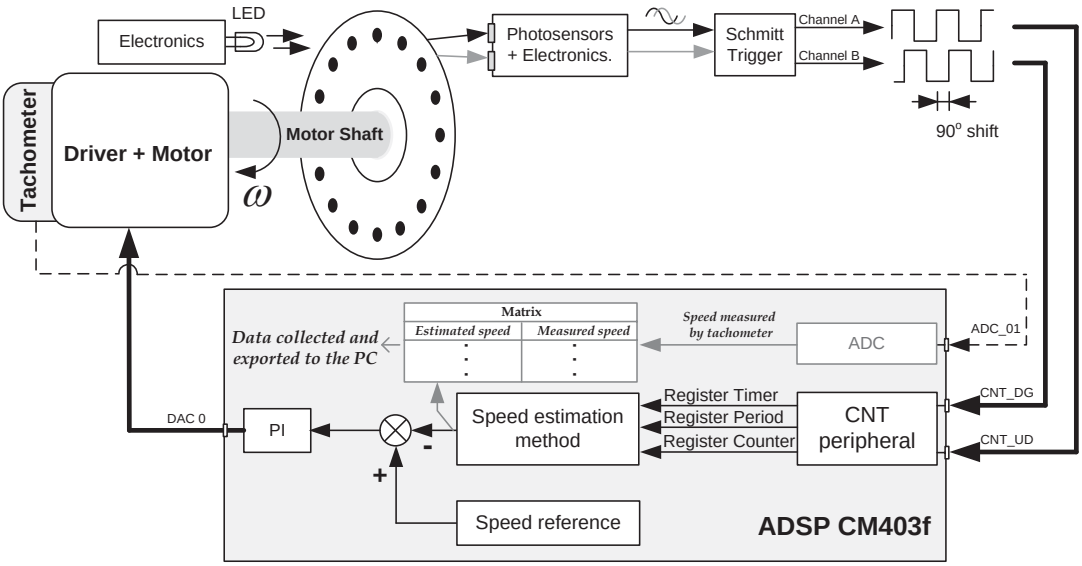

Figure 2.14 Diagram of the DC motor in a closed-loop setup.

The system is composed of the following devices:

- DC motor;
- A driver that includes torque/current control-loop;
- A tachometer coupled to the shaft of the motor;
- An encoder coupled to the shaft of the motor;
- A DSP for the digital control;

The driver has a current loop that is tuned by means of potentiometers. The motion control loop is programmed in the DSP. The following peripherals of the DSP have been configured: the TIMER, the ADC, the DAC and the CNT, along with related support peripherals.

In order to evaluate the performance of the three implemented speed estimation methods, under similar conditions, the speed reference was configured to track a sinusoidal speed profile. Simultaneously, the DSP estimates the speed based on the information provided by the CNT peripheral. The estimate is saved in a vector that is later exported to the PC. Results are depicted in Figure 2.15.

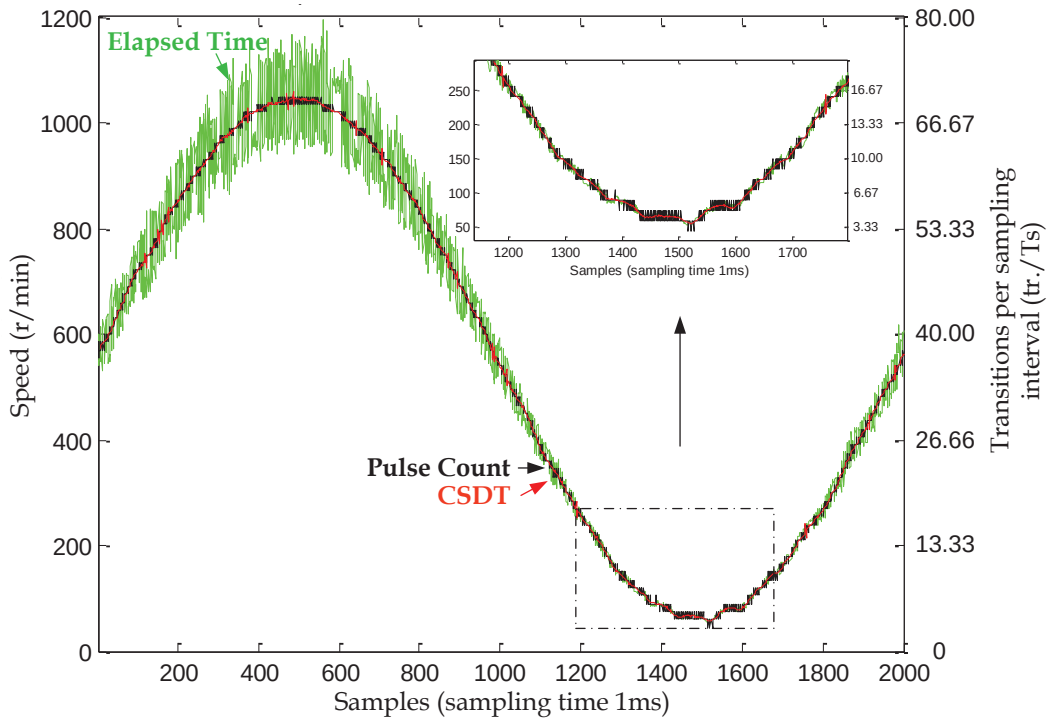

Figure 2.15 Comparison of the three algorithms estimating the speed based on the information of a real encoder coupled to the shaft of the DC motor. The encoder resolution is 4000 ppr.

Experimental results in Figure 2.15 validate the theoretical study in Figure 2.7. The error inherent in the PC method is smaller at high speed, while the error associated with the ET method is increased. The error can be treated as high-frequency noise. At low speed, the ET method has smaller error compared to the PC method and the CSDT shows consistently small error over the full speed range studied.

A speed step response is used to evaluate the closed-loop performance of the speed estimation methods implemented on the DSP. Here the incremental optical encoder is used to sense the motor rotation. This information is processed by the CNT peripheral, and later used to estimate the speed and close the loop. Simultaneously, the speed is sensed by the tachometer, whose signal is digitalized by the ADC. This value is later stored in the memory of the DSP. The stored tachometer measurement is used to evaluate the actual performance of the motor when the different speed estimation methods are used to feedback the motion control loop.

The flow chart of the motion control loop implemented on the DSP is in Figure 2.16.

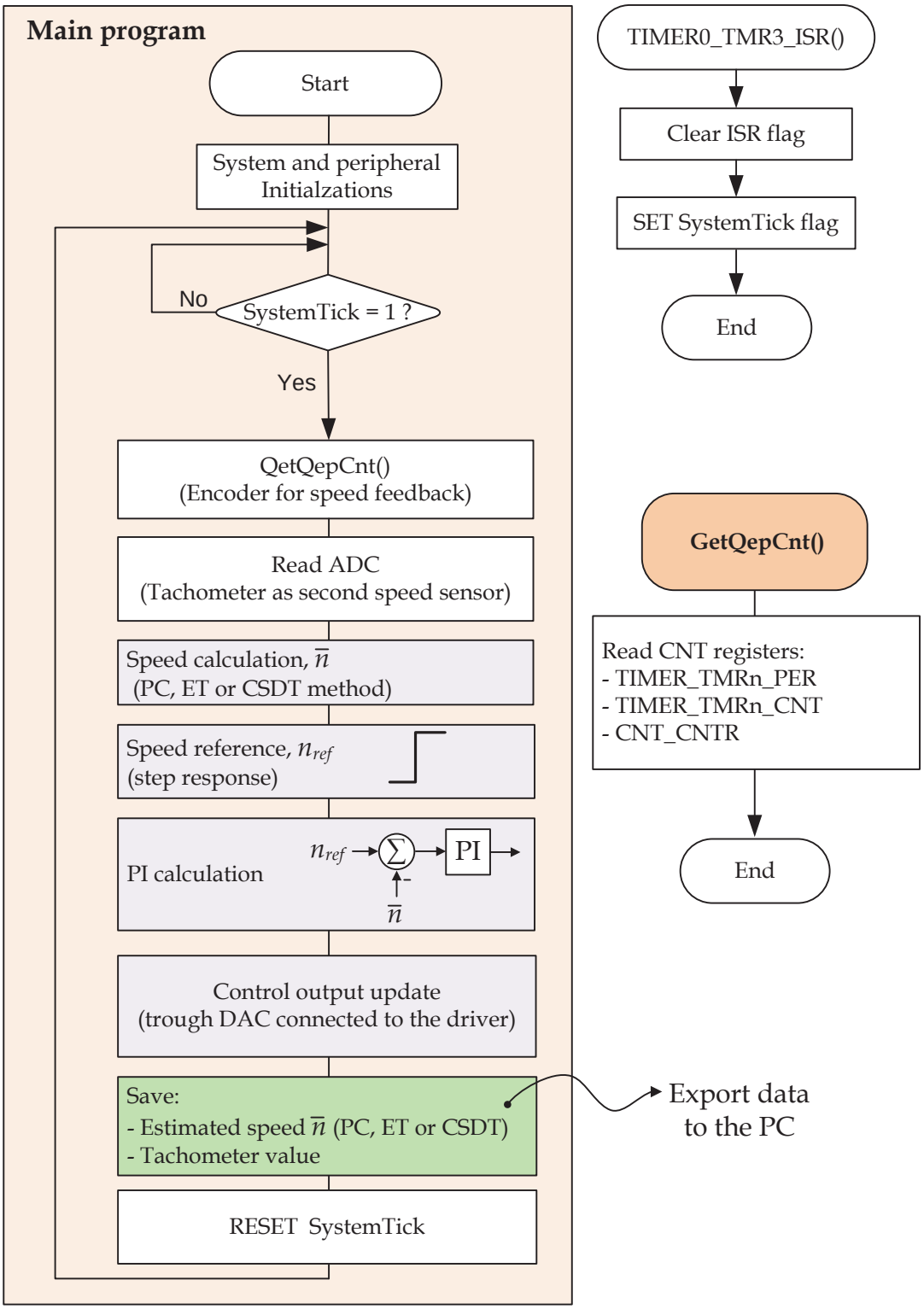

Figure 2.16 Motion control loop flow chart.

The ET method is used to estimate the speed at low speed (L < 1 tr./T_s). Figure 2.17 shows the speed reference step from 60 r/min (0.1 tr./T_s) to 540 r/min (0.9 tr./T_s). Figure 2.17 shows also that the characteristic error of the ET is smaller at low speed and increases as the speed increases. As the speed reduces, the system becomes unstable as a consequence of the reduction of the phase margin. To cope with this problem, the gain of the digital PI regulator is reduced.

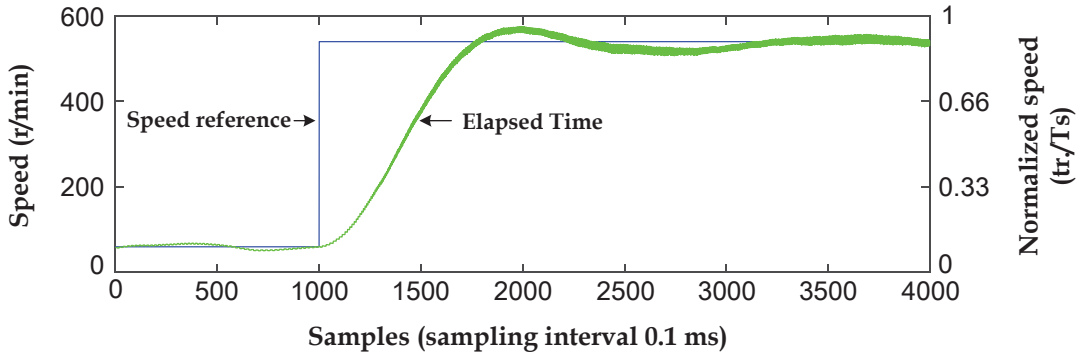

Figure 2.17 Speed reference step test from 60 r/min (0.1 tr./T_s) to 540 r/min (0.9 tr./T_s). Speed estimation based on the ET method. R = 1000 ppr.

Figure 2.18 - (a) shows the response of the closed-loop system to a speed reference step from 600 r/min to 1100 r/min. The encoder resolution is R = 4000 ppr (encoder in quadrature configuration) and the control sampling interval is 0.1 ms. Three tests are performed with PC, TE and CSDT methods as the feedback signal.

The PC, the ET and CSDT methods are used at medium and high speeds ($L \geq 1$ tr./T_s). As can be seen in Figure 2.18 - (a), the accuracy of the PC method improves at higher motor speeds due to an increased number of transitions per T_s. Conversely, the accuracy of ET diminishes as the motor speed increases, because the number of SYSCLK cycles between transitions is lower at high speed, thereby increasing the effect of a spurious count of SYSCLK cycles. In addition, the impact of errors described previously is more noticeable in the measurement of the ET, at high speed. As previously stated, the CSDT method estimation is by far the most accurate, as a consequence of including the auxiliary time ΔT.

The error of the speed estimation based on the PC method is produced by the ± 1 pulse count error in the transition counter. As the number of encoder transitions increases the impact of such error diminishes. On the other hand the error in the ET and CSDT methods is produced by the ± 1 cycle count (m) of the SYSCLK. As the speed increases, T_e and the number of m diminishes and the impact of ± 1 cycle count is more

significant. It was experimentally checked that this error produces audible noise in a control technique with an inner current loop.

Additionally, the speed step test response of each method demonstrates a similar dynamic performance of each speed estimation method at high speed.

Figure 2.18 - (b) shows the result of the speed measured simultaneously by a tachometer (resolution 3 V/krpm) when using each one of the speed estimation methods to close the loop. The tachometer was not used for feedback purposes but only as a second sensor, whose result is not biased by the speed estimation method under study.

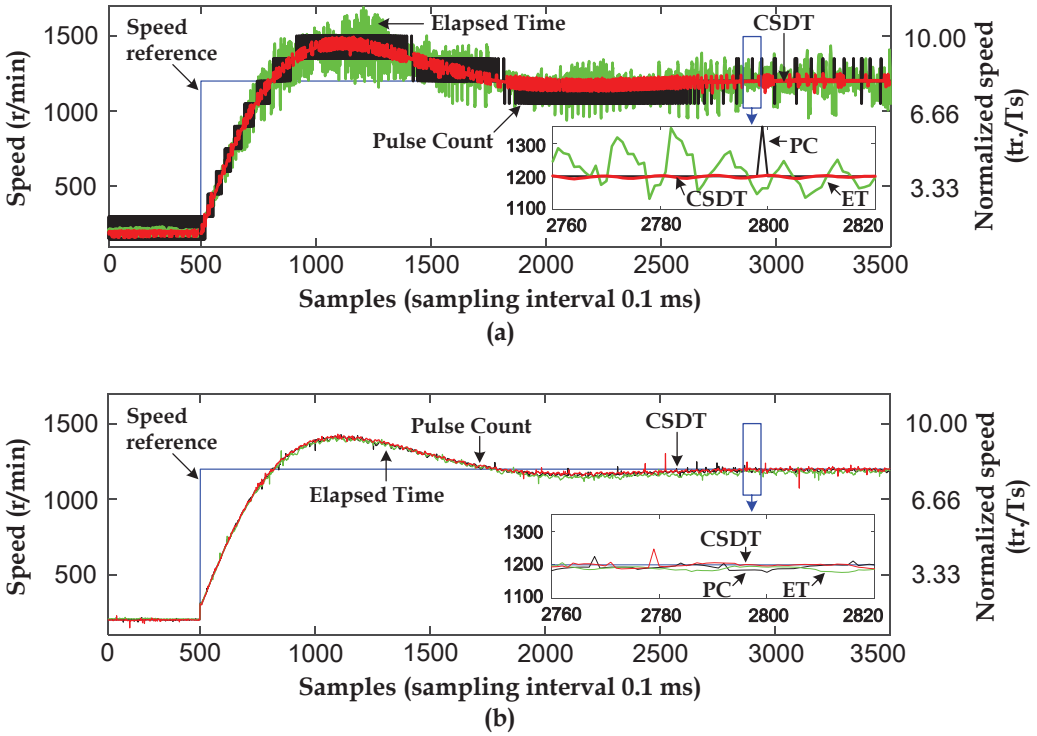

Figure 2.18 (a) Speed reference step test from 200 r/min (1.33 tr./T_s) to 1200 r/min (8 tr./T_s). R = 4000 ppr. The green line is the speed estimated when the ET is used to close the loop; the black line is the PC and the red line corresponds to the speed when the CSDT closes the loop. (b) is the signal measured with the tachometer. Note that the tachometer is used for display purposes only, and not for the feedback. The green line is ET, the black line is PC and the red line is the CSDT method.

By comparing Figure 2.18- (a) and Figure 2.18 - (b) it can be seen that the motor, the driver and the digital PI controller filter the noise that can be seen in the speed estimated signal used to feedback the speed control loop. From the motion control loop perspective and regardless of the accuracy of the methodology used, all the methodologies perform similarly due to the natural filter of the mechanical motor pole and the PI that filter the noise.

However, in motor applications with a double control loop (an inner current loop and outer speed loop) the current loop has a wide bandwidth (BW) so that the noise affects the current loop, as shown in Figure 2.19.

A current clamp was used to sense the current[3] while the motor was spinning at constant speed. Samples were taken at the speed of 1.33 tr./T_s and 8 tr./T_s for each one of the methods. Data were later processed in Matlab by means of a standard DFT algorithm.

The armature current spectra of the ET 1.33 tr./T_s is similar in magnitude to the current spectra of the PC and the CSDT methods (see Figure 2.19 (a)). On the contrary, at a higher speed of 8 tr./T_s, the magnitude of the ET armature current spectra is higher as a consequence of the ET corresponding error (see Figure 2.19 - (b))

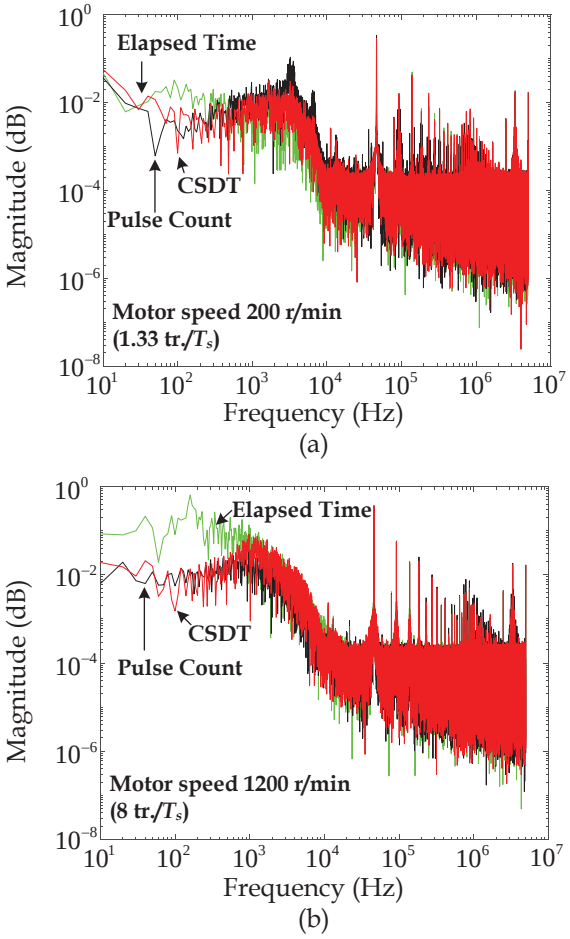

Figure 2.19 Armature current spectra when the ET (green), the PC (black) and the CSDT (red) are used as feedback the control loop. Plot (a) shows the test at the speed of 1.33 tr./T_s and plot (b) at the speed of 8 tr./T_s.

A thorough study of the impact of the speed estimation error on the current control loop, the noise, torque ripple, etc. is required; however, this is out of the scope of this thesis.

[3] The current clamp was placed between the output of the DSP and the input of the motor driver.

2.6.2.1 Oversampling

In order to filter the noise, an oversampling technique is applied to the ET signal [28], which effectively averages the estimated speed and smooths the signal. It is based on oversampling the TIMER_TMRn_PER$_k$ register at a higher rate than T_s. To do that, a timer interrupt service routine (ISR) is set, and a circular buffer of length p stores the last p samples of the time elapsed between consecutive transitions. The average ET between transitions is obtained from the circular buffer, as in (2.27).

$$\bar{n}_{ET\_Over.} = \frac{1}{\sum_{i=0}^{p-1} T_e[p] \cdot T_{SYSCLK}} \cdot \frac{60}{R} \tag{2.27}$$

A speed reference step test form 600 r/min to 1100 r/min is presented. The over oversampling technique is evaluated at the frequency of 100 kHz and (p = 100). Figure 2.20 shows the resulting reduction of the errors at both low and high speeds.

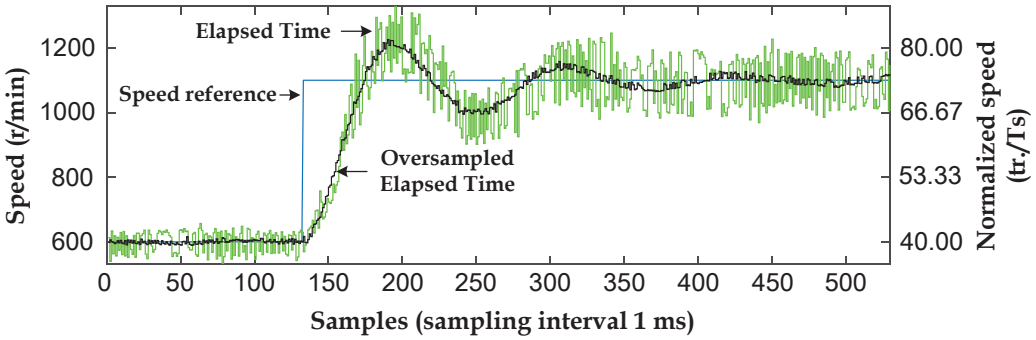

Figure 2.20 Oversampling technique applied to the ET to filter the inherent noise of this technique at high speed.

2.7 Conclusions

Three speed estimation methods: PC, ET and CSDT methods are successfully implemented on the Analog Devices DSP CM403f and tested in closed-loop configuration. The ET method exhibits increasing speed error as the speed increases. In contrast the PC method has lower percentage speed error at higher speed. The CSDT has consistently the lowest speed error. The speed error does not affect the speed control loop because the mechanical pole of the motor and the PI controller filter the signal, it does affect the current loop. To reduce the noise of the ET at high speed, an oversampling technique is implemented. In terms of implementation requirements, the PC method can be implemented by means of an edge detector and counter. The ET

method, which is based on the inverse proportionality of the speed and the elapsed time between consecutive pulses, requires a timer; the higher the frequency of the timer, the lower the error will be. Conversely, the CSDT requires a peripheral that combines pulse count and time count. The integrated and targeted functionality of the DSP device minimizes the latency involved in the speed estimation, which can improve the overall servosystem control. In summary, the ET method has a better performance at low speed, the CSDT is a useful method for medium and high speed, and the PC method is more suitable for very high speeds, as depicted in Figure 2.21.

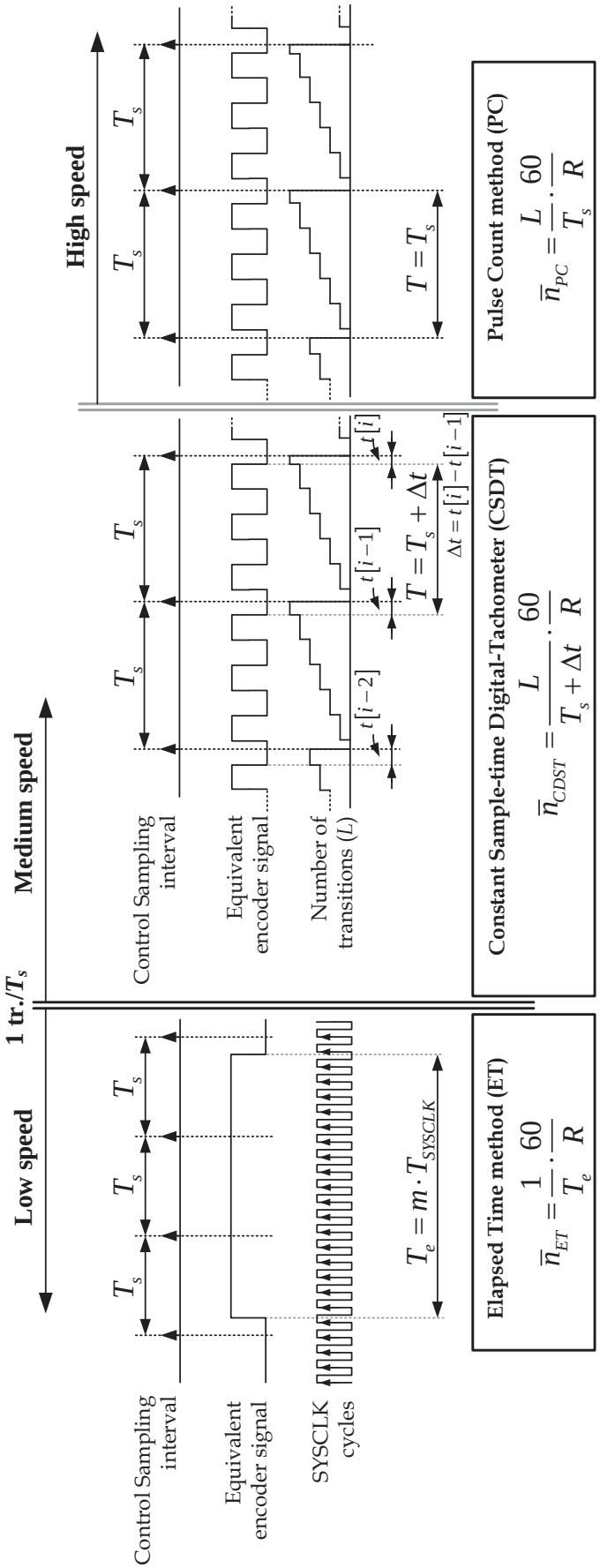

Figure 2.21 Summary of the principal signals and calculations for the speed methods studied.

Chapter 3. Small-Signal Modeling of the Incremental Optical Encoder

The main goal of this chapter is to explain the physical reason for the poor performance of low-resolution encoders at low speed. To do so, the small-signal model of the incremental optical encoder, for low and high speed, is derived. The small-signal model is composed of the sensor and the speed methodology that process the sensor signal to estimate the speed. Additionally, a physical setup is proposed to experimentally validate the mathematics of the derived small-signal model.

3.1 Introduction

It is well reported in literature that square incremental optical encoders perform poorly in low-speed applications; particularly those sensors with low resolution. On the other hand, these are more affordable in terms of cost.

As reported in previous papers, a phase lag between the actual speed and the estimated speed is found if see Figure 3.1 in paper [25].

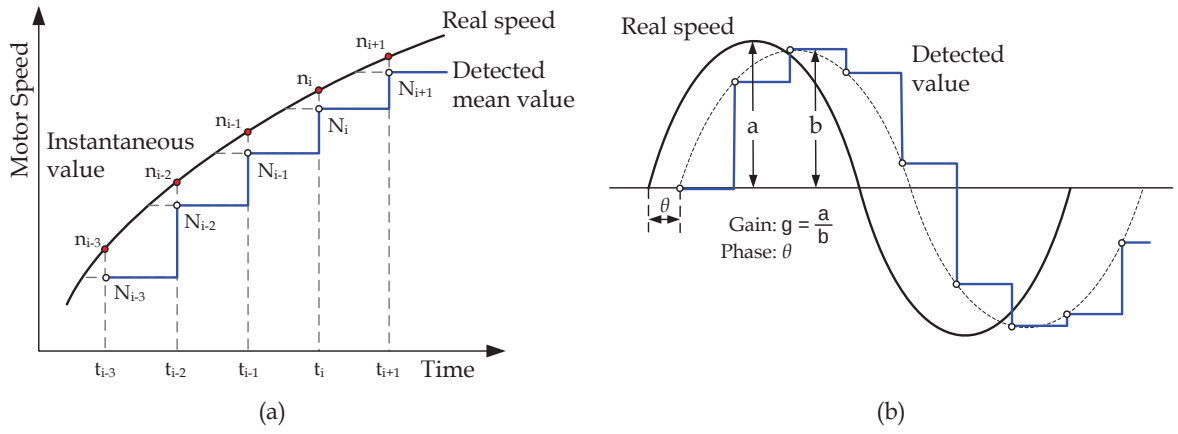

Figure 3.1 (a) Relation between instantaneous value and detected mean value of motor speed, and (b) Definition of gain and phase characteristics of speed detection.

Many algorithms have been developed to minimize such phase lag by developing higher order estimators [27]. A higher order estimator will provide a better speed estimate. However, to achieve this several speed estimation samples are averaged to obtain the current speed estimate. Then, this is an averaging process with an inherent delay. The calculation delay adds to the inherent encoder delay. At low speed, with low resolution encoders, such techniques perform poorly.

The majority of the work related to the encoder was focused on the study of characterization of the static errors, as mentioned in the previous chapter. Other papers focus on the mathematical description and prediction of the error due to the quantized nature of the sensor [49]. This paper also states that the speed estimation algorithm must achieve a smooth speed estimate and a high-bandwidth and these are opposite goals.

As will be demonstrated in this chapter, the bandwidth is a paramount parameter due to its relationship with the phase lag.

Encoders have usually been included in control loop diagrams as a non-linear element and as a position sensor [50] and [15], see Figure 3.2.

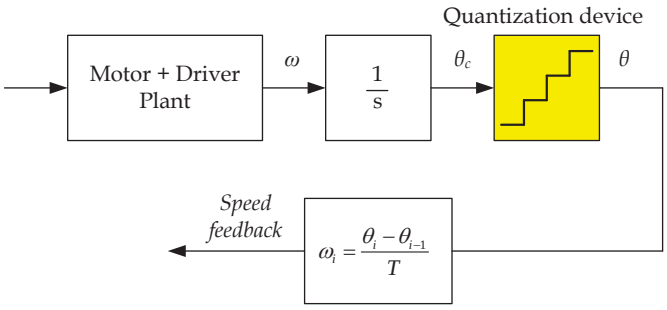

Figure 3.2 Simplified schematic of the motion control loop and the traditional representation of the encoder.

Following this approach to the differentiated position, the system is non-linear. The nonlinearity is produced by the quantization device. The quantization noise of the encoder and its characteristics have been thoroughly studied in [51].

The nonlinear quantization device difficult the derivation of an encoder dynamic model and a speed estimation transfer function. However, the speed (n or ω) is a linear variable since it has linear properties:

- Homogeneous property. If the speed of the shaft increases, the speed estimation will increase in the same proportion.

- Additive property. No matter the type of speed profile in the speed reference, the motor and hence the speed estimation will match the speed reference.

Therefore, the dynamics of the encoders can be studied and the system can be linearized. The precise knowledge of the encoder transfer function is paramount for two reasons:

1. The adequate and optimal tuning of the controller.
2. The adequate selection of the encoder resolution at an early design stage. This allows the optimization of the costs of the project.

The first attempt to approach the problem through the derivation of the speed transfer function is found in [41] where two expressions are proposed to model the dynamic behaviour of the encoder for high and low speed, at high speed, the sample time is higher than the time between transitions ($T_s > T_e$), and then the author proposes to model the system as a delay:

$$H(s) = e^{-s\cdot\frac{T_s}{2}} \tag{3.1}$$

At low speed, the time between encoder transitions is higher than the control sample time ($T_e > T_s$), and the expression of the encoder dynamics for this condition is:

$$H(s) = e^{-s\cdot T_e} \tag{3.2}$$

More recently, a new expression was found in [42] where the idea is that the encoder at low speed is inherently modeled by a sample and hold with sampling frequency proportional to the time between encoder transitions T_e.

$$H(s) = \frac{1-e^{-s\cdot T_e}}{s\cdot T_e} \tag{3.3}$$

where T_e is

$$T_e = \frac{60}{n\cdot R} \tag{3.4}$$

The following ideas derive from previous equations:

- The delay, at low speed, depends of the speed ($\bar{n}$) and the resolution (R).

- The delay can be modelled as a delay with no impact on the magnitude of the signal, as in (3.1) and (3.2), or as a delay that also impacts in the magnitude as the ideal sampler and zero order hold reflects in (3.3).

None of those models are experimentally validated, or are found to accurately match a real system. Therefore, in this chapter an accurate small-signal model of the incremental optical encoder, including the speed estimation methods for low and high speeds, are derived and experimentally validated. Due to technical limitation in the validation process of the model, a novel setup is proposed to emulate the encoder dynamic behaviour apart from the stability and dynamic problems that arise in a real motor control.

3.2 Review of Basic Concepts

The background of the derived small-signal models of the studied speed estimation methods: PC, ET and CSDT, are explained in this section. These include the dynamic difference between a delay and sample and zero order hold, the mathematical difference between a sampler and zero order hold, and a zero order hold, and finally the delay between two signals that are asynchronous. The last concept can explain the delay between asynchronous signals found in the encoder and speed estimation system.

3.2.1 Delay and Sample and Zero-Order-Hold

The expression of the delay has been already presented in (3.2), and that for the sample and zero order hold is presented in (3.3). Given the same value for T, the bode plot of the two expressions is as depicted in Figure 3.3.

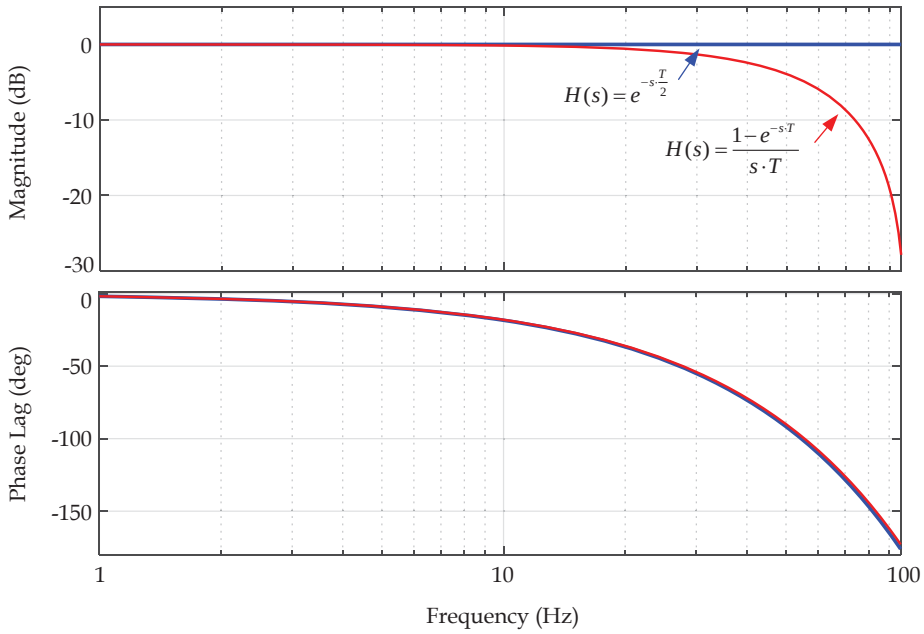

Figure 3.3 Bode plot of the delay and the sampler and zero-order-hold.

As can be seen, both mathematical expressions have the same phase lag. However, the pure delay does not impact in the magnitude, having a constant gain over all frequencies. Conversely, the zero-order-hold does impact on the magnitude of the signal. The zero-order-hold is composed of an ideal sampler and a zero-order-hold, as in Figure 3.4.

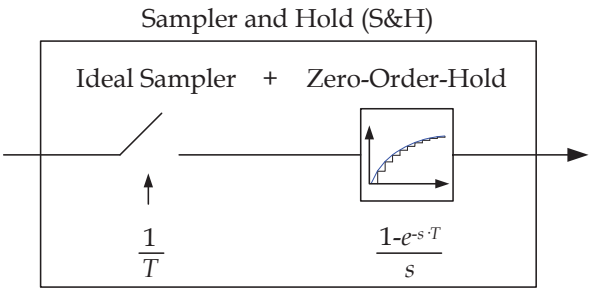

Figure 3.4 Representation of the sampler and hold.

The combined transfer function that leads to the transfer function of the sampler and zero-order-hold (S&H) is:

$$H_{S\&H}(s)=\frac{1-e^{-s\cdot T}}{s\cdot T} \tag{3.5}$$

In the time domain, the S&H hold the value of the input signal that is sampled at a rate of *T*, as depicted in Figure 3.5.

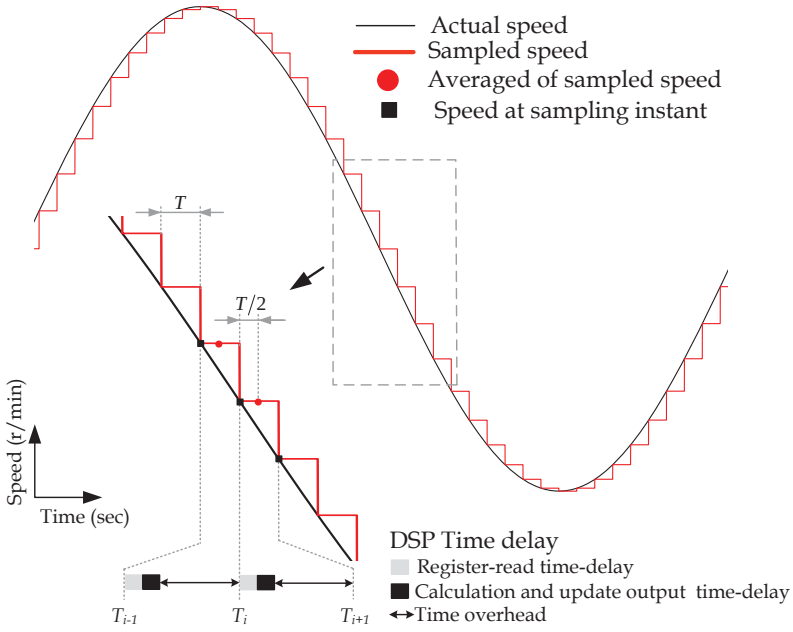

Figure 3.5 Time-domain representation of a sinusoidal signal (black) and the same signal sampled by a S&H (red).

The black line in Figure 3.5 represents the actual speed signal that is sampled at a rate $1/T$. The red line is the resulting sampled signal. The black-squared marker indicates the instantaneous speed at the sampling instant; this value is held by the S&H during time-interval T. The averaged sampled speed is indicated with a red dot. The signal of the estimated speed can be obtained by joining the red dots. The principal harmonic of this reconstructed signal has the same amplitude and phase lag of $T/2$. The time consumed in the encoder signal processing and the speed estimation is less than 10 % of the control sample time, providing enough time overhead for other processing.

However, experimental test with the encoder and speed estimation algorithms shows an additional delay not modelled by an S&H, as in Figure 3.6.

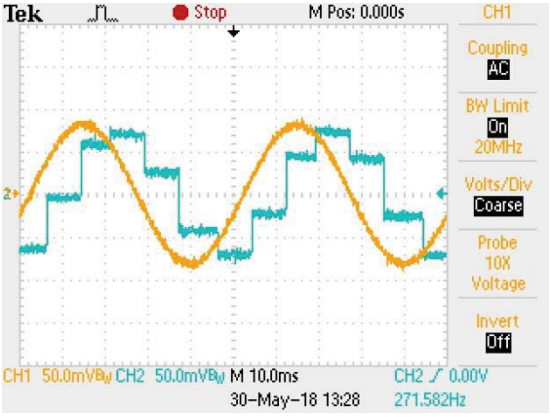

Figure 3.6 Experimental results with an encoder-based speed estimation (Ch2 in green) of a sinusoidal speed profile (Ch1 in yellow).

3.2.2 Uniform Distribution of the Delay Between Two Asynchronous Signals

Two asynchronous signals at different frequencies are considered. The parameter t_d is defined as the time elapsed between the last encoder transition or edge and the next control sample transition, or edge of the low frequency signal, as depicted in Figure 3.7. This figure represents the edge produced on every encoder transition, with period T_e, and the edge produced by every control sample instant with period T_s. In this particular case, the encoder transitions are less frequent than the control sample interval. Therefore, Figure 3.7 represents a low speed condition.

The DSP gathers information from one encoder transition to the next. For high speed, this information is the number of encoder transitions or pulses over a fixed control interval. As for the low speed the DSP counts the number of cycles of a high frequency clock during consecutive encoder transitions.

The gathered information is not transmitted to the control, for speed feedback purposes, until the next control sample instant. This produces a delay in the information, t_d, producing no impact on the magnitude but altering the phase. The term t_d is the time between the encoder transition and the control sample instant. Therefore this delay can be mathematically modelled as:

$$H_D(s) = e^{-s \cdot t_d} \tag{3.6}$$

The periodic variation in time of t_d between two signals of different frequencies is shown in Figure 3.7.

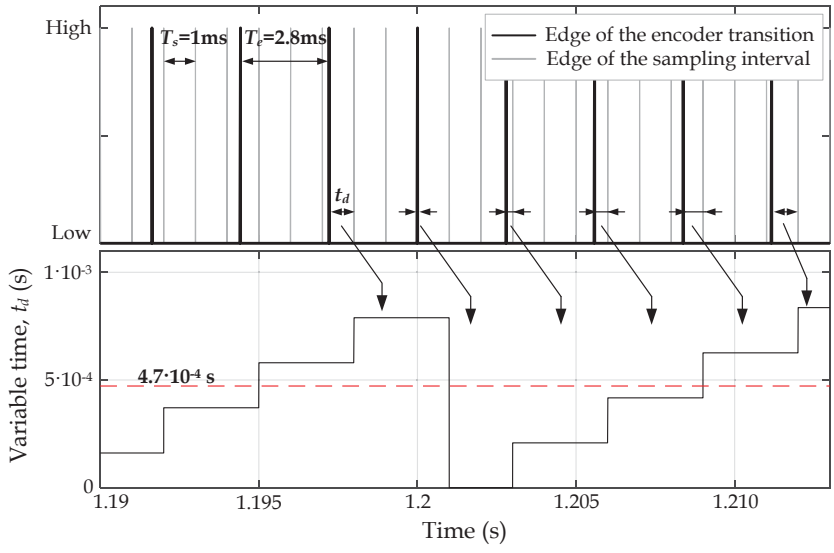

Figure 3.7 Time-domain representation of the encoder transitions and the control sample interval.

The time t_d is a consequence of the two signals that are asynchronous (different frequencies) and consequently drift. It is statistically proven that the distribution of t_d is almost periodic at constant speed and follows a uniform distribution, as in Figure 3.8.

Simulation results are depicted in Figure 3.8 that show the instantaneous encoder transition with speed of 0.347 tr./T_s and instantaneous control sampling interval of 1 ms. The total number of samples is 44.

At low speed, the value of the time delay t_d is within the range $0 < t_d < T_s$ and on average the value of the delay is $t_d \approx T_s/2$.

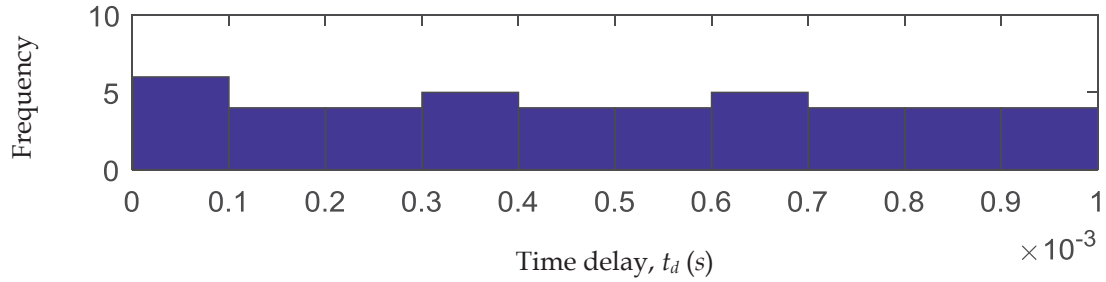

Figure 3.8 Histogram of the variable t_d.

Experimental results are similar at high speed. For these experiments, the total number of samples to be analysed is 8000.

In this test, time delay is expressed as the number of cycles of the high-frequency clock counted; the equivalence between these two parameters is:

$$t_d = \text{Number of clock cycles} \cdot \frac{1}{80 \cdot 10^6\, Hz} \tag{3.7}$$

In Figure 3.9, the results of the tests are presented. This corresponds to a speed of 2.3 tr./T_s, with a sample interval of 1 ms. The total number of cycles of one encoder period T_e is 28673 cycles and the average time delay is 14337 cycles, as the red line depicts in Figure 3.9.

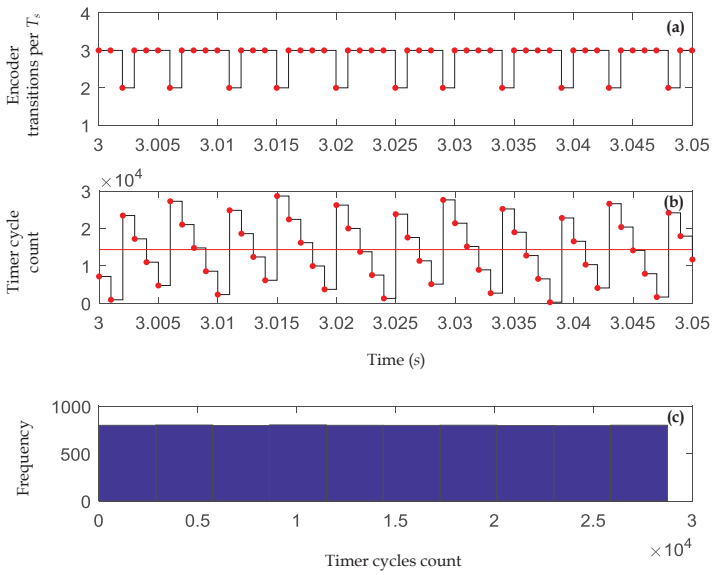

Figure 3.9 The speed represented in (a) is 2.7 tr./T_s and with a control sample intervals of 1 ms. The time delay t_d of the encoder and the control sample interval are depicted in (b) and the corresponding histogram is represented in (c).

In Figure 3.10, results corresponding to a speed of 10 tr./T_s with sample interval of 1 ms are shown. The total number of cycles of one encoder period is 8000 cycles, and the average time delay is 4000 cycles, as depicted in Figure 3.10-(b).

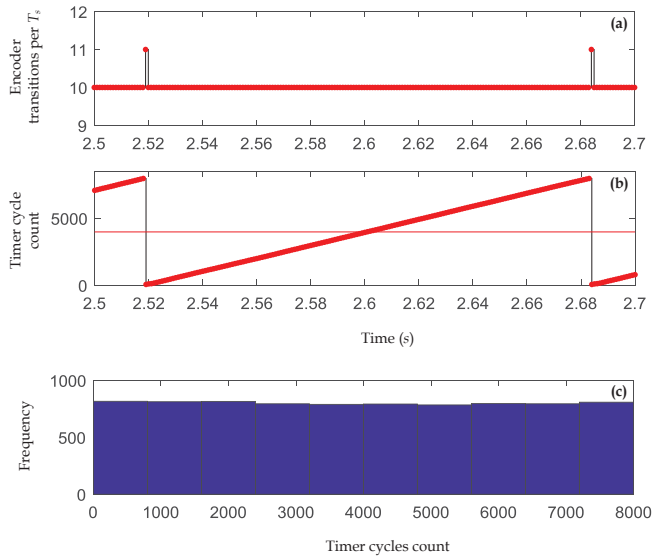

Figure 3.10 The speed represented in (a) is 10 tr./T_s and with control sample intervals of 1 ms. The time delay t_d of the encoder and the control sample interval are depicted in (b) and the corresponding histogram is represented in (c).

In Figure 3.11 the results of the tests are presented that correspond to a speed of 34.36 tr./T_s, with sample interval of 1 ms. The total number of cycles of one encoder period is 2928 cycles and the average time delay is 1164 cycles, as depicted in Figure 3.11-(b).

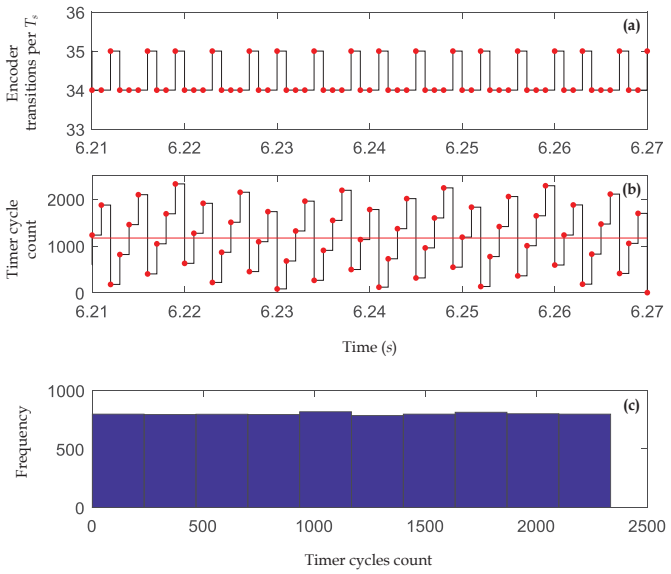

Figure 3.11 The speed represented in (a) is 34.5 tr./T_s and with control sample intervals of 1 ms. The time delay t_d of the encoder and the control sample interval are depicted in (b) and the corresponding histogram is represented in (c).

Then, it is clear from the tests that the time delay follows an uniform distribution. Therefore, the delay between the encoder transition and the control sample instant, at low speed, can be modelled as:

$$H_D(s) = e^{-s\frac{Ts}{2}} \tag{3.8}$$

with T_s being the sample frequency, and at high speed the delay between the encoder transition and the control sample time is modeled as:

$$H_D(s) = e^{-s\frac{Te}{2}} \tag{3.9}$$

where

$$T_e = \frac{T_s}{L} \tag{3.10}$$

and L is the number of transitions per sample interval at high speed.

3.3 Derivation of the Small-signal Model of the Incremental Optical Encoder

Although the output of the encoder is square and seems to be nonlinear, the speed is indeed linear. The encoder "codes" the speed of the rotor. This is later decoded by counting pulses during a fixed time interval in the PC method, or by timing the time

elapsed between encoder transitions, based on counting pulses of a high frequency clock associated with the CNT peripheral, when using the ET method.

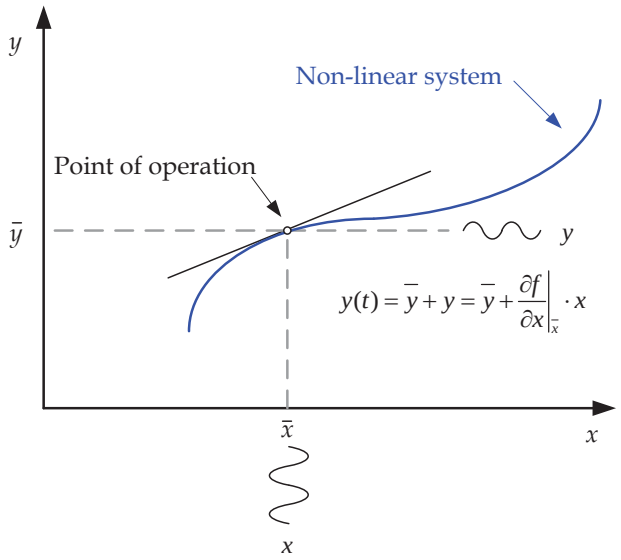

Figure 3.12 Small-signal modeling technique.

For the derivation of the small signal model of the encoder and the speed estimation method, the small signal technique is applied. This modeling technique is widely used in power converters [52]. A nonlinear system can be linearized around a steady-state operating point *X*. The system will be considered to be linear in the vicinity of *X*. The linear input and output relation is defined by the slope of the curve around the point, as depicted in Figure 3.12.

The difference between the linearized curve and the real curve is defined and depicted in Figure 3.12 as "error". The amplitude of the disturbance signal $\tilde{x}(t)$ must be small enough so the error due to non-linearities can be neglected. By comparing the injected disturbance and the output of the system in this condition, the frequency response of a non-linear system can be obtained.

Before continuing with the small-signal derivation, it is defined that:

- The output of the system is expressed as:

$$x(t) = X + \tilde{x}(t) \tag{3.11}$$

- The amplitude of the injected disturbance is much smaller than the operating point. A 10 % of the operating point could be small enough to avoid the excitation of the nonlinearities.

$$|X| \gg |\tilde{x}(t)| \tag{3.12}$$

3.3.1 Small-signal Modeling of the PC Method

The closed-loop motion control loop, using the PC method is depicted in Figure 3.13.

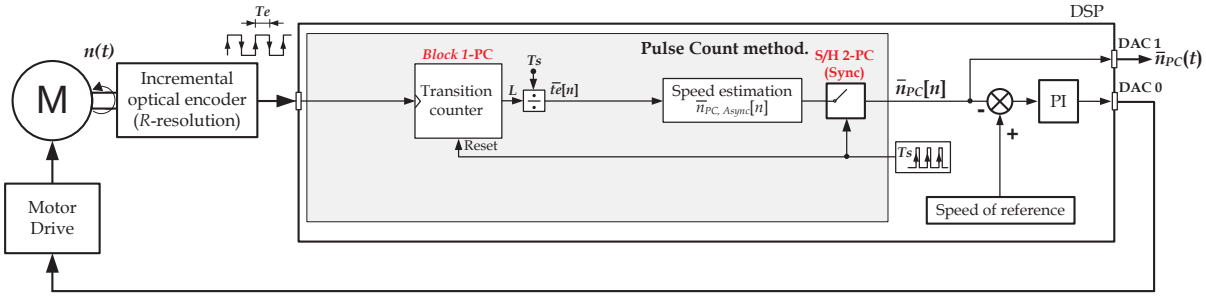

Figure 3.13 Symbolic and simplified block diagram of the motion control-loop implemented using the PC method at high speed.

The motion control loop is composed of the speed estimation method in the feedback signal as well as the controller. The TIMER peripheral produces an interrupt service routine (ISR) at the regular time interval of T_s. This control sample time is dynamically modelled as a sampler and zero-order-hold (S/H-T_s). At the beginning of the control sample interval, the data from the CNT peripheral is processed to estimate the actual speed of the motor, to later compare this value with the target speed and produce the adequate compensation by means of a PI controller. The remaining time overhead guarantees the adequate performance of the digital controller and the system in general avoiding overflows.

The transfer function of the PC method is composed of "Block 1-PC", which is the encoder transition counter (L) and the "S/H 1 - PC" corresponding to the control sampling interval. The encoder signal and the control sampling interval are asynchronous processes. Therefore, the transfer function must be completed with a delay $H_D(s)$, as explained previously. Then the overall transfer function is:

$$H_{Enc\,PC}(s) = \frac{\bar{n}_{PC}(s)}{n(s)} = H_{Mov\ Avg-L}(s) \cdot H_{S/H-Ts}(s) \tag{3.13}$$

The speed of the rotating shaft is considered the input $n(t)$ and the estimated average speed is the output $\bar{n}_{PC}(t)$.

The relevant signals of the PC method are represented in Figure 3.14. An ideal encoder, without mechanical or electronic nonidealities, is assumed.

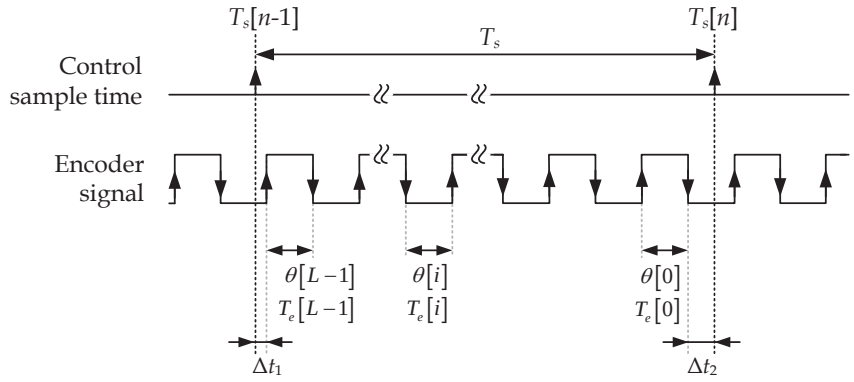

Figure 3.14 Control sample time and encoder signals in the PC method.

The speed $\bar{n}_{PC}$ is updated at regular T_s. The number of encoder transitions, L, per sample, varies in proportion to the speed. The rotated angle θ during T_e remains constant and proportional to the encoder resolution $\theta = 360^{\circ}/R$. The average estimate speed in r/min, over interval T_s, is

$$\bar{n}_{PC} = \frac{L \cdot \theta}{T_s} \cdot \frac{60}{360} = \frac{L}{T_s} \cdot \frac{60}{R} \tag{3.14}$$

The fixed control sampling time T_s in (3.14) can be alternatively expressed as:

$$T_s \approx T_e[0] + T_e[1] + ... + T_e[i] + ... + T_e[L-1] \tag{3.15}$$

The resulting expression is:

$$\bar{n}_{PC-Asynch.}[n] = \frac{1}{\dfrac{T_e[0] + T_e[1] + ... + T_e[i] + ... + T_e[L-1]}{L}} \cdot \frac{60}{R} \tag{3.16}$$

where the speed is inversely proportional to the average time between consecutive encoder transitions $\bar{T}_e[n]$.

$$\bar{T}_e[n] = \sum_{n=0}^{L-1} \frac{T_e[n]}{L} \tag{3.17}$$

This can be expressed in the discrete domain as

$$\bar{T}_e[z] = \sum_{k=0}^{L-1} \frac{T_e[z]}{L} \cdot z^{-k} \tag{3.18}$$

It has been reported in [49] that any pulse counter can be modeled as a FIR filter.

$$\frac{\bar{T}_e[z]}{T_e[z]} = \frac{1}{L} \cdot \sum_{k=0}^{L-1} z^{-k} = \frac{1}{L} \cdot \frac{1 - z^{-L}}{1 - z^{-1}} \tag{3.19}$$

The discrete control theory is developed mainly for time-driven sampled systems, where continuous-time signal (i.e. the motor speed) is represented by its time equidistant sampled values. However, the motor speed is actually sampled by the encoder edge, at the frequency rate ($1/T_e$) that is proportional to the motor speed and therefore, it is not equidistant. Then, the encoder constitutes a type of event-driven system.

Nevertheless, it is demonstrated next that although the encoder is inherently an event-driven system (with the transition being the events), the classical digital control theory can be applied to its analysis to obtain its small-signal model.

3.3.1.1 Event-driven Sampling Interval

In order to apply the classical digital control theory, it is stated that the encoder sample rate is almost constant and proportional to the average speed at steady state if the disturbance applied to the speed has a sufficient small value to avoid the excitation of nonlinearities.

$$\left|\bar{n}\right| \gg \left|\tilde{n}(t)\right| \Leftrightarrow \left|\bar{T}_e\right| \gg \left|\tilde{T}_e(t)\right| \tag{3.20}$$

The instantaneous speed is expressed as:

$$n(t) = \bar{n} + \tilde{n}(t) = \frac{1}{T_e(t)} \cdot \frac{60}{R} = \frac{1}{\bar{T}_e + \tilde{T}_e(t)} \cdot \frac{60}{R} \tag{3.21}$$

The variable term in (3.21) is expanded as a Maclaurin series:

$$\frac{1}{\bar{T}_e + \tilde{T}_e(t)} = \frac{1}{\bar{T}_e} - \frac{\tilde{T}_e(t)}{\bar{T}_e^{\,2}} + \frac{\tilde{T}_e(t)^2}{\bar{T}_e^{\,3}} - \frac{\tilde{T}_e(t)^3}{\bar{T}_e^{\,4}} + ... \approx \frac{1}{\bar{T}_e} - \frac{\tilde{T}_e(t)}{\bar{T}_e^{\,2}} \tag{3.22}$$

Considering that$|\ \bar{T}_e\ | \gg |\ \tilde{T}_e\ |$ the quadratic and higher order terms in (3.22) can be neglected and the speed expressed as:

$$n(t) = \bar{n} + \tilde{n}(t) = \left(\frac{1}{\bar{T}_e} - \frac{\tilde{T}_e(t)}{\bar{T}_e^{\,2}} \right) \cdot \frac{60}{R} \tag{3.23}$$

where $\bar{n} = 60/\left(R \cdot \bar{T}_e\right)$ and $\tilde{n}(t) = -\left(60/R\right) \cdot \tilde{T}_e(t)/\bar{T}_e^2$. Finally,

$$\frac{\left|\tilde{n}(t)\right|}{\left|\bar{n}\right|} = \frac{\left|-\frac{\tilde{T}_e(t)}{T_e^2} \cdot \frac{60}{R}\right|}{\left|\frac{1}{T_e} \cdot \frac{60}{R}\right|} = \frac{\left|\tilde{T}_e(t)\right|}{\left|\bar{T}_e\right|} \tag{3.24}$$

The ratio between the average speed, $\bar{n}$, and the amplitude of the superimposed disturbance, $n(t)$, is the same than the ratio between $\bar{T}_e$ and T_e. The amplitude $n(t)$ is chosen to be small enough to comply with small-signal technique requirements. Hence, it is demonstrated that the time between transitions $T_e[i]$ equals to $\bar{T}_e$. This implies that the encoder, which is an event-driven sampler, can be treated as an almost-constant sampled system and the classical digital control theory can be employed to derive the small-signal model of the incremental optical encoder.

In order to continue with the derivation of the small-signal model, expression (3.19) can be mapped to the *s*-domain using the mapping factor: $z = e^{s \cdot Te}$ where $\bar{T}_e = T_s / L$.

$$H_{Mov\,Avg-PC}(s) = \frac{\bar{T}_e(s)}{T_e(s)} = \frac{1}{L} \cdot \frac{1 - \left(e^{s \cdot \frac{T_s}{L}}\right)^{-L}}{1 - \left(e^{s \cdot \frac{T_s}{L}}\right)^{-1}} \tag{3.25}$$

The expression (3.25) corresponds to the "Block 1-PC" in Figure 3.14.

This transfer function constitutes can be a contradiction because it is initially derived from the term in the denominator of (3.16). However, it is finally located in the numerator of the overall encoder transfer function in (3.13). This is equivalent to invert the input signal. Figure 3.15 shows that the estimated speed and the time between encoder transitions is T_e are inverted.

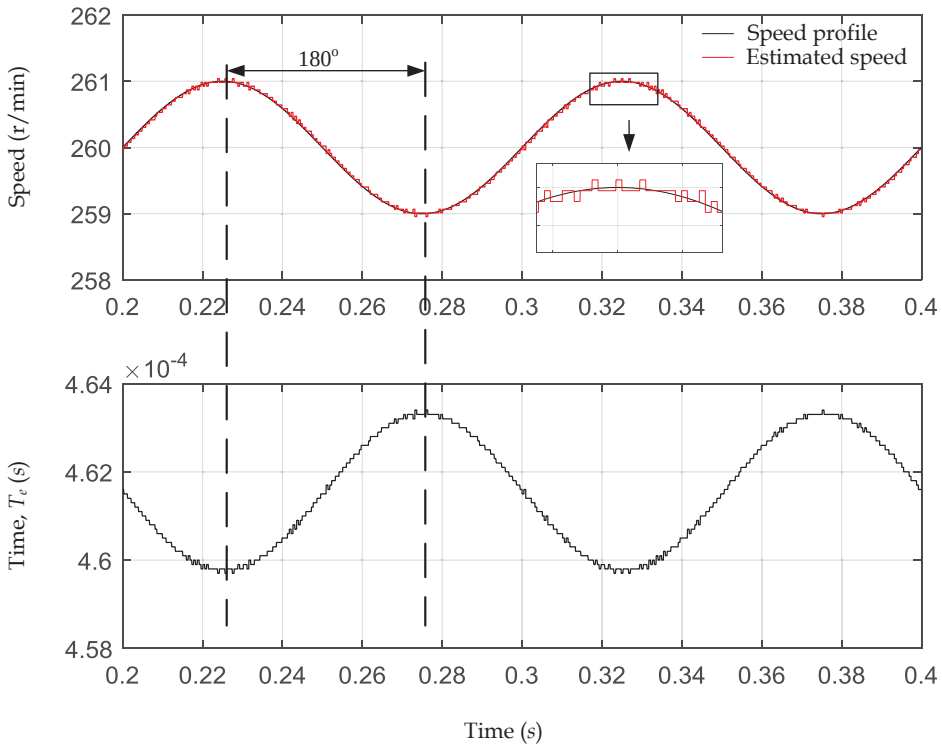

Figure 3.15 Phase relationship between the speed and the time T_e.

This can also be demonstrated by deriving the transfer function of the encoder at the instant *i*:

$$n[i] = \frac{\theta[i]}{T_e[i]} \cdot \frac{60}{360} \tag{3.26}$$

The expression of the disturbed speed in the Laplace domain is:

$$\tilde{n}(s) = -\frac{60/R}{T_e^{\,2}} \cdot \tilde{T}_e(s) \tag{3.27}$$

Similarly, the small-signal (3.26) of the disturbed averaged speed is:

$$\tilde{\bar{n}}_{PC}(s) = -\frac{60/R}{\bar{T}_e^{\,2}} \cdot \tilde{\bar{T}}_e(s) \tag{3.28}$$

Then, with $\bar{T}_e(s)$ being the average time between encoder transitions and $\tilde{\bar{T}}_e(s)$ the disturbed averaged time between consecutive encoder transitions it is demonstrated that:

$$\frac{\tilde{\bar{n}}_{PC}(s)}{\tilde{n}(s)} = \frac{-\frac{60/R}{\bar{T}_e^{\,2}} \cdot \tilde{\bar{T}}_e(s)}{-\frac{60/R}{T_e^{\,2}} \cdot \tilde{T}_e(s)} = \frac{\tilde{\bar{T}}_e(s)}{\tilde{T}_e(s)} = H_{Mov\,Avg}(s) \tag{3.29}$$

Consequently, the expression $H_{Mov\,Avg}(s)$, originally found in the denominator of (3.16), leads to a small-signal model with dynamic impact in the numerator of the encoder small signal model.

In steady state conditions, the varying times Δt_1 and Δt_2, from Figure 3.14, cause an error in the speed measurement. In the particular case of Δt_2 it produces an additional time delay that must be added to $H_{Mov\,Avg}(s)$ in (3.25) to correct for the effects of the asynchrony between the encoder transitions and the control sample time. The phase lag due to Δt_2 varies with a triangular almost-periodic shape and is modeled as $e^{-T_s/(2L)}$ as demonstrated in section 3.2.2. The encoder transfer function of the PC method is corrected by including this delay.

$$H_{Enc\,PC}(s) = \underbrace{\frac{1}{L}\cdot\frac{1-\left(e^{s\cdot\frac{T_s}{L}}\right)^{-L}}{1-\left(e^{s\cdot\frac{T_s}{L}}\right)^{-1}}}_{H_{Mov\,Avg-L}(s)}\cdot\underbrace{e^{-s\cdot\frac{T_s}{2L}}}_{H_D(s)}\cdot\underbrace{\frac{1-e^{-s\cdot T_s}}{s\cdot T_s}}_{H_{S/H\,\text{-}\,Ts}(s)} \tag{3.30}$$

In practice, expression (3.30) can be simplified by taking the limit as L tends to ∞.

$$H_{Mov\,Avg-L}(s) = \lim_{L\to\infty}\frac{1}{L}\cdot\frac{1-\left(e^{s\cdot\frac{T_s}{L}}\right)^{-L}}{1-\left(e^{s\cdot\frac{T_s}{L}}\right)^{-1}}\cdot e^{-s\cdot\frac{T_s}{2L}} \tag{3.31}$$

Consider the denominator:

$$1-\left(e^{s\cdot\frac{T_s}{L}}\right)^{-1} = 1-e^{-s\cdot\frac{T_s}{L}} \tag{3.32}$$

This can be expanded as the power series.

$$1-e^{-s\cdot\frac{T_s}{L}} \approx 1-\left(1-\frac{T_s\cdot s}{L}+\frac{T_s^2\cdot s^2}{2!\cdot L^2}-\frac{T_s^3\cdot s^3}{3!\cdot L^3}+\ldots\right) \tag{3.33}$$

Neglecting quadratic and higher terms, this expression can be simplified to:

$$1-e^{-s\cdot\frac{T_s}{L}} \approx 1-1+\frac{T_s\cdot s}{L}=\frac{T_s\cdot s}{L} \tag{3.34}$$

Then,

$$H_{Mov\,Avg-L}(s)=\lim_{L\to\infty}\frac{1}{L}\cdot\frac{1-\left(e^{s\cdot\frac{T_s}{L}}\right)^{-L}}{\frac{s\cdot T_s}{L}}\cdot e^{-s\cdot\frac{T_s}{2L}}=\lim_{L\to\infty}\frac{1-e^{-s\cdot T_s}}{s\cdot T_s}\cdot e^{-s\cdot\frac{T_s}{2L}}=\frac{1-e^{-s\cdot T_s}}{s\cdot T_s}\cdot 1 \tag{3.35}$$

This transfer function is shown to be valid for any $L \geq 10$. However, the use of (3.35) can even be extended to $L \geq 1$.

Even at a constant velocity, where the average value of L over several samples is the real number $\bar{L}$, the integer number of transitions will vary by one from cycle to cycle, in an almost periodic sequence. The output will be $\lfloor \bar{L} \rfloor$, where $\lfloor \bullet \rfloor$ is the floor function of $\bar{L}$, with probability $1-\langle \bar{L} \rangle$, and $\lceil \bar{L} \rceil = \lfloor \bar{L} \rfloor + 1$, (the 'ceiling function'), with probability $\langle \bar{L} \rangle$. Note that the fractional part of $\bar{L}$ is $\langle \bullet \rangle$. The PC method implicitly differentiates the quantized shaft position estimate, with considerable mean-squared error, but zero average error, even when the encoder is not ideal [53]. Note that $\bar{L} = \lceil \bar{L} \rceil \cdot \langle \bar{L} \rangle + \lfloor \bar{L} \rfloor \cdot \left(1-\langle \bar{L} \rangle\right)$, indicating zero average velocity error in steady state. If the actual real velocity in steady-state is $\bar{L}$ tr./T_s, the distinction between those samples for which the PC output gives estimates of $\lfloor \bar{L} \rfloor$ and $\lceil \bar{L} \rceil$ is dependent on the time delay from the encoder transition just before the sampling instant. This delay, shown in Figure 3.14, exhibits almost periodic variation; thereby, introducing a delay-type noise into the system, on a sample-by-sample basis. Explicitly, those samples for which the velocity estimate is $\lceil \bar{L} \rceil$ occurs when $0 \leq \Delta t_2 < \langle \bar{L} \rangle \cdot T_s / \bar{L}$. This is governed by a uniform distribution and has a probability of $\langle \bar{L} \rangle$, with an average delay of $\langle \bar{L} \rangle T_s / 2\bar{L}$. The corresponding average delay of the most delayed edge, delayed by a further $\lfloor \bar{L} \rfloor$ transition, is $\left(\langle \bar{L} \rangle / (2\bar{L}) + \lfloor \bar{L} \rfloor / \bar{L}\right) \cdot T_s$, giving an average delay in this case of $\left(\langle \bar{L} \rangle / (2\bar{L}) + \left(\lfloor \bar{L} \rfloor / 2\right) / \bar{L}\right) \cdot T_s = T_s / 2$ to the transition instants. However, the fact that

the speed estimate is constant over $T_s / \bar{L}$ implies a total average delay of $T_s/2 + T_s/(2\bar{L})$. Similarly, when the velocity estimate is $\lfloor \bar{L} \rfloor$, which occurs when $\langle \bar{L} \rangle T_s / \bar{L} \le \Delta t_2 < T_s / \bar{L}$, the average delay can again be shown to be $T_s/2 + T_s/(2\bar{L})$. Therefore, the statistical analysis shows that the average delay of the PC method is $T_s/2 + T_s/(2\bar{L})$. Combined with the delay of the 'S/H-1PC', this gives an overall delay of $T_s + T_s/(2\bar{L})$. The variation of the sample-by-sample delays clearly indicates that use of the small-signal model is suitable for the analysis of the encoder-based system, and that the actual system will contain increasingly significant noise as L decreases in the PC method, due to the quantized nature of the sensor.

Finally, the small signal of the incremental optical encoder introduced in (3.13) is:

$$H_{Enc\,PC-Simplified}(s) = \underbrace{\frac{1-e^{-s\cdot T_s}}{s\cdot T_s}}_{H_{Mov\ Avg-L}(s)} \cdot \underbrace{\frac{1-e^{-s\cdot T_s}}{s\cdot T_s}}_{H_{S/H-Ts}(s)} \tag{3.36}$$

On the other hand, the same conclusion as in (3.36) is achieved by comparing and analysing the delay graphically for a small-signal sinusoidal disturbance, as in Figure 3.16.

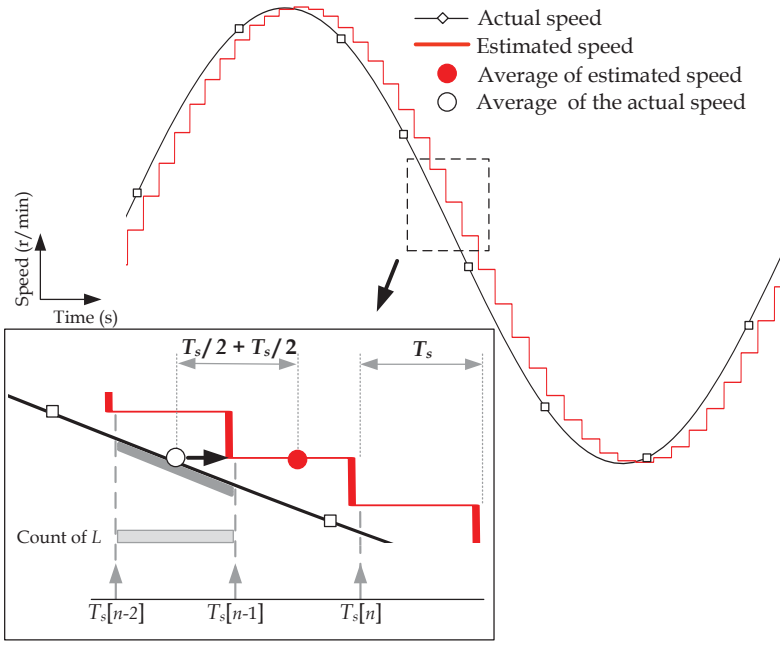

Figure 3.16 Graphical analysis of the delay for the PC method.

During the first control sample interval (between $T_s[n\text{-}2]$ and $T_s[n\text{-}1]$), the DSP peripheral counts encoder transitions, L. During the subsequent control interval, the speed is calculated and held until new measured data is available, giving a total average delay of T_s.

As can be seen in Figure 3.16, the described delay characteristic of the PC method is T_s, in contrast with the one reported in [41].

$$H_{Enc\,PC\,Literature}(s) = e^{-s\cdot\frac{T_s}{2}} \tag{3.37}$$

where the average delay is $T_s/2$.

3.3.2 Small-signal Modeling of the ET Method

The closed motion control loop, using the ET method is depicted in Figure 3.17.

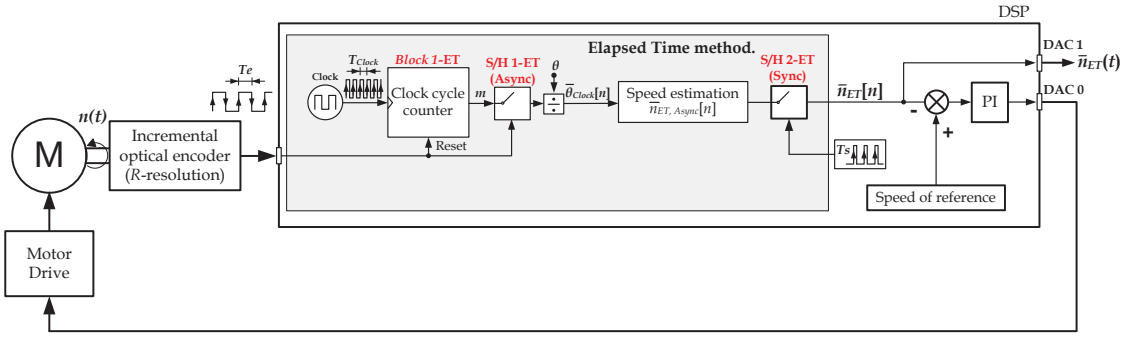

Figure 3.17 Symbolic and simplified block diagram of the motion control-loop implemented using the ET method at low speed.

The ET method, based on the time elapsed between encoder transitions, uses a high frequency clock to measure the time. This clock is connected to the CNT peripheral. It is represented in the Figure 3.17 as "Block 1-ET" which counts the number of clock cycles (m). The count of clock cycles in this block is reset with every incoming edge. The final value of the register, before being reset, is held in another register until new updated information is available. Then, the second block is a sampler and hold "S/H1-ET" inherently produced by the peripheral to provide the last value of m. The third block is "S/H1-ET". This block represents the sample and hold of the control sample interval. In this system, two sets of asynchronous signals are relevant:

- The signal of the encoder and the signal of the high frequency clock, used as a time base for the elapsed time, are asynchronous to each other

- The second block S/H1- ET with frequency corresponding to the encoder and the third block S/H2-ET corresponding to the sample control frequency.

For each one of the mentioned asynchronous signals, the correction in the form of a delay must be applied to derive the small-signal model. The overall transfer function for the ET method is defined as

$$H_{Enc\,ET}(s) = \frac{\bar{n}_{ET}(s)}{n(s)} = H_{Mov\,Avg-m}(s) \cdot H_{S/H-Te}(s) \cdot H_{S/H-Ts}(s) \tag{3.38}$$

where $n(t)$ is the input of the system and defines the actual rotor speed and the $\bar{n}_{ET}(t)$ is the estimated speed, as depicted in Figure 3.17.

Figure 3.18 shows a diagram of the ET method which is based on counting high-frequency clock cycles (T_{Clock}) during the time interval T_e. The rotated angle during an entire clock cycle is θ_{Clock}. The time Δt_1 corresponds to the time between an encoder transition and the next clock cycle. The time Δt_2 corresponds to the time between the last clock cycle and the encoder transition that resets the m-counter with rising and falling edges, while that between the last encoder transition and the next sampling control instant is t_d. The clock is asynchronous with the encoder signal and with the control sampling interval.

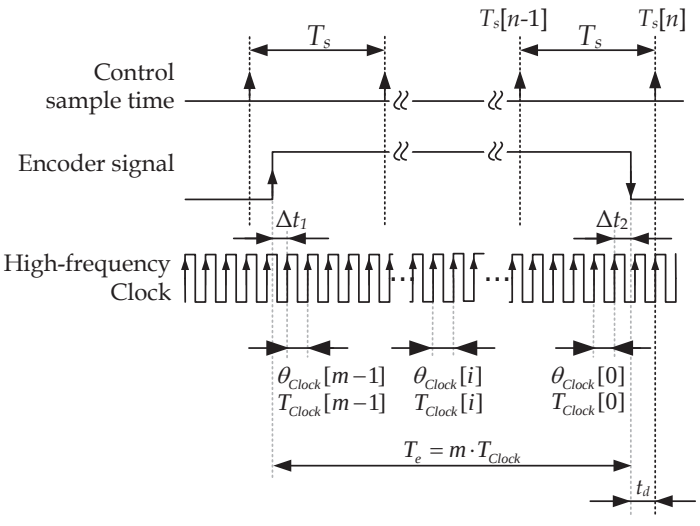

Figure 3.18 Control sample time and encoder signals in the ET method.

The average speed over the time T_e is expressed as:

$$\bar{n}_{ET} = \frac{\theta}{T_e} \cdot \frac{60}{360} \tag{3.39}$$

where θ is the effective rotated angle in the encoder measured in degrees. The time duration of the transition T_e is expressed as:

$$T_e = \sum_{i=0}^{m-1} T_{Clock}\left[i\right] = m \cdot T_{Clock} \tag{3.40}$$

The asynchronous process leads to an error of ± 1 cycle count that in practice has little impact, given the high clock frequencies of modern DSPs. The rotated angle θ during T_e can be obtained by considering the rotated angle over T_{Clock}

$$\theta = \theta_{Clock}[0] + ... + \theta_{Clock}[i] + ... + \theta_{Clock}[m-1] \tag{3.41}$$

Then, the average speed can be expressed as

$$\bar{n}_{ET}[n] = \frac{\theta_{Clock}[0] + ... + \theta_{Clock}[i] + ... + \theta_{Clock}[m-1]}{m \cdot T_{Clock}} \cdot \frac{60}{360^o} \tag{3.42}$$

and simplified to

$$\bar{n}_{ET} = \bar{\theta}_{Clock} \cdot \frac{60}{T_{Clock} \cdot 360^o} \tag{3.43}$$

where $\bar{\theta}_{Clock}$ is the average value of the rotated angle during T_{Clock}. This leads to:

$$\frac{\bar{\theta}_{Clock}[z]}{\theta_{Clock}[z]} = \frac{1}{m} \cdot \sum_{k=0}^{m-1} z^{-k} = \frac{1}{m} \cdot \frac{1 - z^{-m}}{1 - z^{-1}} \tag{3.44}$$

Expression (3.44) can be mapped into the s-plane by defining: $z = e^{s \cdot T_{Clock}}$ and $T_{Clock} = T_e / m$. A similar correction to the moving average in the PC method is applied to the ET method because of the delay between the consecutive transitions T_e and T_{Clock}, represented as Δt_2 in Figure 3.18. Since m is sufficiently large over the full speed range, the overall expression is simplified as a limit.

$$H_{Mov\,Avg-m}(s) = \lim_{m \to \infty} \left(\frac{1}{m} \cdot \frac{1 - \left(e^{s \cdot \frac{T_e}{m}} \right)^{-m}}{1 - \left(e^{s \cdot \frac{T_e}{m}} \right)^{-1}} \cdot e^{-s \cdot \frac{T_e}{2m}} \right) = \frac{1 - e^{-s \cdot T_e}}{s \cdot T_e} \tag{3.45}$$

Because the encoder transitions and the control sampling interval are asynchronous processes, the signals drift from each other. The time *td* between the events produced by such signals is almost periodic. The delay t_d varies quasi-uniformly over the period with an average delay of $T_s/2$, as demonstrated in section 3.2.2.

Then, the small-signal model for the encoder and the ET method in (3.38) is

$$H_{Enc\,ET-Simp.}(s)=\underbrace{\frac{1-e^{-s\cdot T_e}}{s\cdot T_e}}_{H_{MovAvg-m}(s)}\cdot\underbrace{\frac{1-e^{-s\cdot T_e}}{s\cdot T_e}}_{H_{S/H-Te}(s)}\cdot\underbrace{\frac{1-e^{-s\cdot Ts}}{s\cdot Ts}}_{H_{S/H-Ts}(s)} \tag{3.46}$$

where $T_e = 60/(\overline{n}_{ET}\cdot R)$. Therefore, the encoder transfer function depends on both: the resolution and the operating speed. The total average delay presented in (3.46) is $T_e + T_s/2$.

The conclusion presented in this paper regarding the average delay can be verified if the problem is graphically analysed, as in Figure 3.19.

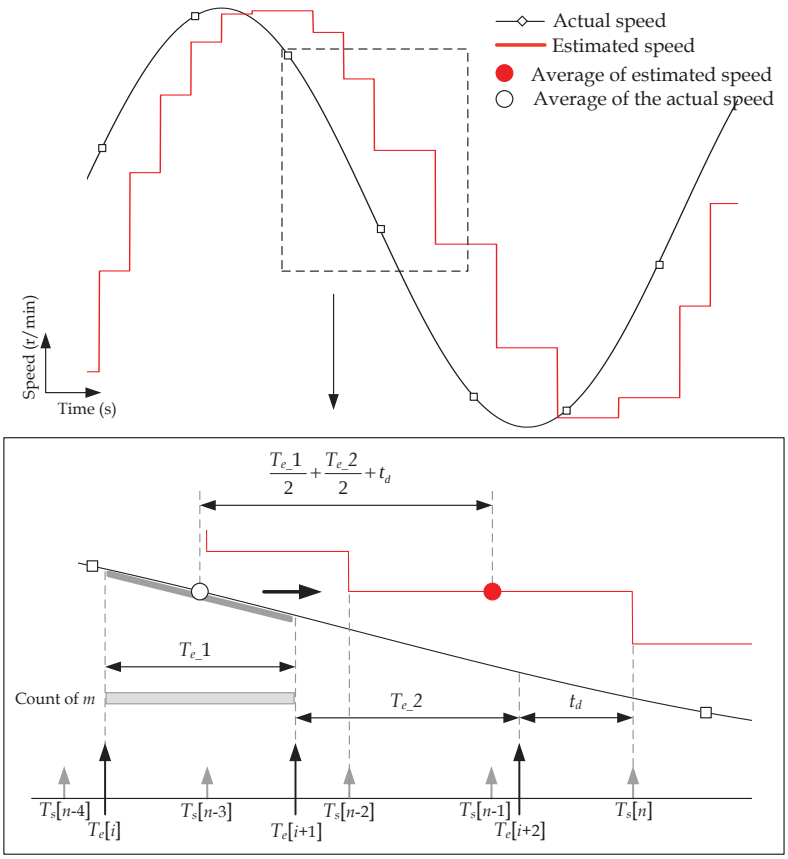

Figure 3.19 Graphical analysis of the delay for the ET method.

Because of the small-signal analysis, it is assumed that $T_e\_1 \approx T_e\_2 \approx \overline{T}_e$, as shown in Figure 3.19. The first delay corresponds to the process of counting the clock cycles

during T_e_1. The second delay, from Figure 3.17, models the 'S/H-1 ET'. This corresponds to the time interval over which the DSP register holds the value *m*. Finally, the third variable delay corresponds to the time between the encoder transition and the most immediate sampling instant that updates the value of the speed $\overline{n}_{ET}(t)$.

Previously, the encoder dynamics were approximated by the expressions:

$$H_{Enc\,ET\,Literature1}(s) = e^{-s \cdot T_e} \tag{3.47}$$

$$H_{Enc\,PC\,Literature}(s) = \frac{1 - e^{-s \cdot T_e}}{s \cdot T_e} \tag{3.48}$$

found in [41] and [42] respectively.

In the first case, the equation models a dynamic system that is purely a delay, with no impact on the magnitude. The equation (3.47) predicts the phase lag of T_e. As for equation (3.48), it models half of the total average delay (T_e/2).

3.3.3 Small-signal Modeling of the CSDT Method

The CSDT method is dynamically similar to the PC method, which on the other hand is reasonable. The CSDT method has proven to be very useful at medium speeds (more than 1 tr./T_s and lower than 20 tr./T_s). This occurs as a consequence of the inclusion of the auxiliary time that eliminates the quantization error characteristic of the PC method. It is obvious that this method can be used at very high speed. However, in those conditions, the simple PC method performs sufficiently well for most closed-loop systems and at the same time is less complex to implement. The relevant signals of the CSDT method are presented in Figure 3.20.

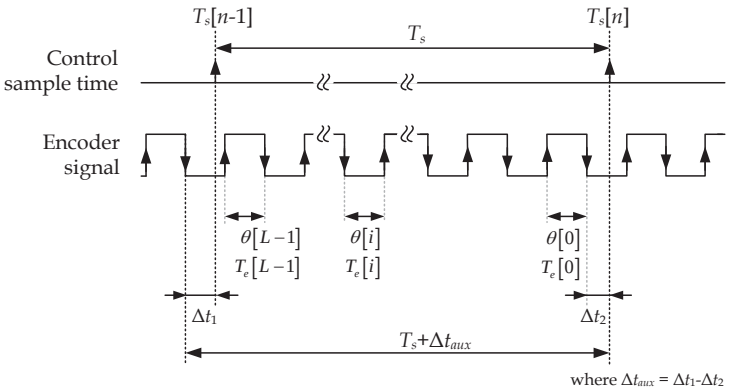

Figure 3.20 Control sample time and encoder signals in the CSDT method.

The expression used for the CSDT method is

$$\bar{n}_{CSDT} = \frac{L \cdot \theta}{T_s + \Delta t_{aux}} \cdot \frac{60}{360} = \frac{L}{T_s + \Delta t_{aux}} \cdot \frac{60}{R} \tag{3.49}$$

where the auxiliary time is defined by $\Delta t_{aux} = \Delta t_1 - \Delta t_2$. The fixed control sampling time T_s in (3.49) can be expressed as:

$$T_s + \Delta t_1 - \Delta t_2 = T_e[0] + T_e[1] + \ldots + T_e[i] + \ldots + T_e[L-1] \tag{3.50}$$

The resulting expression is:

$$\bar{n}_{CSDT}[n] = \frac{1}{\frac{T_e[0] + T_e[1] + \ldots + T_e[i] + \ldots + T_e[L-1]}{L}} \cdot \frac{60}{R} \tag{3.51}$$

where the speed is inversely proportional to the average $\bar{T}_e[n]$.

$$\bar{T}_e[n] = \sum_{n=0}^{L-1} \frac{T_e[n]}{L} \tag{3.52}$$

$$\bar{T}_e[z] = \sum_{k=0}^{L-1} \frac{T_e[z]}{L} \cdot z^{-k} \tag{3.53}$$

$$\frac{\bar{T}_e[z]}{T_e[z]} = \frac{1}{L} \cdot \sum_{k=0}^{L-1} z^{-k} = \frac{1}{L} \cdot \frac{1 - z^{-L}}{1 - z^{-1}} \tag{3.54}$$

Similarly to the PC method, the complete expression is:

$$H_{Enc\ CSDT}(s) = \underbrace{\frac{1}{L} \cdot \frac{1 - \left(e^{s \cdot \frac{T_s}{L}} \right)^{-L}}{1 - \left(e^{s \cdot \frac{T_s}{L}} \right)^{-1}} \cdot e^{-s \cdot \frac{T_s}{2L}}}_{H_{Mov\ Avg-L}(s)} \cdot \underbrace{\frac{1 - e^{-s \cdot T_s}}{s \cdot T_s}}_{H_{S/H \leftarrow Ts}(s)} \tag{3.55}$$

It can be simplified to:

$$H_{Enc\ CSDT}(s) = \left(\frac{1 - e^{-s \cdot T_s}}{s \cdot T_s} \right)^2 \tag{3.56}$$

As can be seen, this expression is equal to (3.36), the small-signal model of the PC method.

3.4 Experimental Validation Setup

The proposed small-signal models are experimentally validated in the setup depicted in Figure 3.21. This setup emulates the encoder behaviour and consequently can be used to evaluate speed estimation algorithms and their dynamics with the knowledge that other factors (motor dynamics, frictions, driver dynamics etc.) will not affect or bias the measurement and conclusions.

The Analog Discovery is used as a Network Analyzer [54] to measure the frequency response function of the incremental optical encoder and the different speed estimation algorithms. The network analyzer generates sinusoidal waveform of several tones, $A \cdot sin(2\pi f)$. The amplitude of the signal (A) can be configured. The signal is superimposed to a constant speed (point of operation) at the input of the system under analysis. Each tone (f) excites the system under analysis. The Network Analyzer is connected to the input and the output of the system. The device processes the input (injected signal) and the output of the system, so that a discrete Fourier transformed (DFT) provides the amplitude ($|H(2\pi f)|$) and phase ($\angle H(2\pi f)$) of the relevant harmonics of this signal. The network analyzer processes and averages three set of samples per tones. More advanced equipment averages more tones for a more precise result. The set of several tones results in the frequency response function of the system under analysis.

The most intuitive idea to experimentally validate the proposed small-signal models would be to do it with the encoder coupled to the motor shaft. Theoretically, a gradual reduction of the phase margin as the speed reduces would be expected. However, this is not possible in practice, for the following reasons:

For tests at high speed.

1. If the test is performed in a closed-loop system, the dynamics of the motor, the driver or the controller affect the final result. A second incremental optical encoder of much higher resolution (more than 5000 ppr) is required to control

the loop while the low-resolution encoder is simultaneously measured. Even with two encoders, results can be biased by the dynamics of components other than the encoder.

2. If the test is performed in open-loop, a DC motor is required. Generally, a DC motor in open-loop configuration has a very small bandwidth, e.g. 10 Hz, principally determined by the mechanical pole. At high speed, the bandwidth of the encoder is determined by the control sample frequency. Then, the motor will always attenuate any injected disturbance at any frequency higher than the system bandwidth.

For tests at low speed.

3. These tests are particularly complex at very low speed because the phase lag introduced by the encoder reduces dramatically the phase margin. At best, the system exhibits oscillations and in the worst case will become unstable and a reliable measurement will not be possible. Given the non-linear nature of the sensor, the phase lag is proportional to the speed, once the resolution is fixed. Due to the nonlinear nature of the system the reduction of the phase margin can occur suddenly and not gradually, as in other systems. In addition, the system may experience periods of stable speed and unstable speed when attempting to track a low speed. This will produce oscillations and non-acceptable behaviour of the system. This situation is further analysed in chapter 5.
4. The amplitude of the disturbance is proportional to the steady state point (as a rule of thumb, a maximum amplitude disturbance of 10% of the point of work[4]) in order to be considered small-signal. The first issue is that the motor and the driver may not be sensitive to such a small-amplitude signal and will attenuate the injected disturbance. In addition, the DSP must estimate the speed, including the superimposed disturbance. The estimated-digital speed is transformed into an analog value by a DAC connected to the Network Analyzer. A result of the analysis at many different tones established the frequency response functions of the incremental optical encoder.

The system depicted in Figure 3.21 emulates the encoder behaviour and at the same time avoids all the issues described before.

[4] This is a rule derived from experimental experience.

The encoder is experimentally simulated with a voltage-controlled-oscillator (VCO). The VCO was previously used in PLL-based speed estimation techniques because it mimics the encoder [55]. The VCO of a TG550 Function Generator modulates the frequency in proportion to the input voltage. Likewise the encoder modifies the frequency of its signal in proportion to variations in the motor speed.

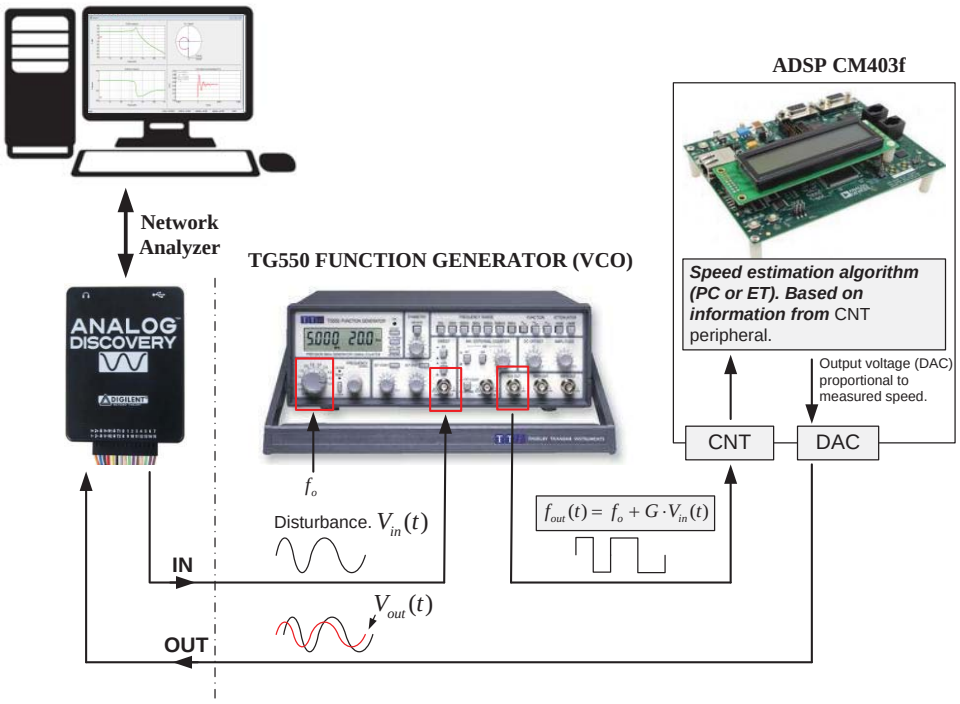

Figure 3.21 Proposed experimental setup.

The output frequency of the encoder coupled to the shaft of the motor is:

$$f_{Enc}(t) = \frac{R}{60} \cdot \left(\bar{n} + \tilde{n}(t) \right) \tag{3.57}$$

and similarly the frequency of the VCO is:

$$f_{VCO}(t) = f_o + G \cdot V_{in}(t) \tag{3.58}$$

with G being the gain (Hz/V) of the VCO. Then the following equalities can be established from (3.57) and (3.58). For the steady-state speed:

$$f_o = \frac{R}{60} \cdot \bar{n} \tag{3.59}$$

and for the disturbance:

$$G \cdot V_{in}(t) = \frac{R}{60} \cdot \tilde{n}(t) \tag{3.60}$$

In Figure 3.21, the Analog Discovery, as network analyzer, introduces a disturbance of small amplitude $V_{in}(t)$. The VCO produces a square wave of variable frequency, as in (3.57). The DSP peripheral, that processes the encoder signal, is the general purpose counter (CNT). The peripheral provides information about the number of transitions (L) and the time between pulses (T_e) for estimating the speed. The speed is digitally computed and transformed into an analog signal by a digital to analog converter (DAC) with a high update frequency that does not affect the experiment. It is later measured by the Analog Discovery unit that compares the input and the output to measure the frequency response of the encoder.

It is important to check that the configuration of the peripherals does not introduce additional unknown delays in the measurement. This validation can be done by measuring the frequency response of a sample and hold, whose transfer function is well known (3.5).

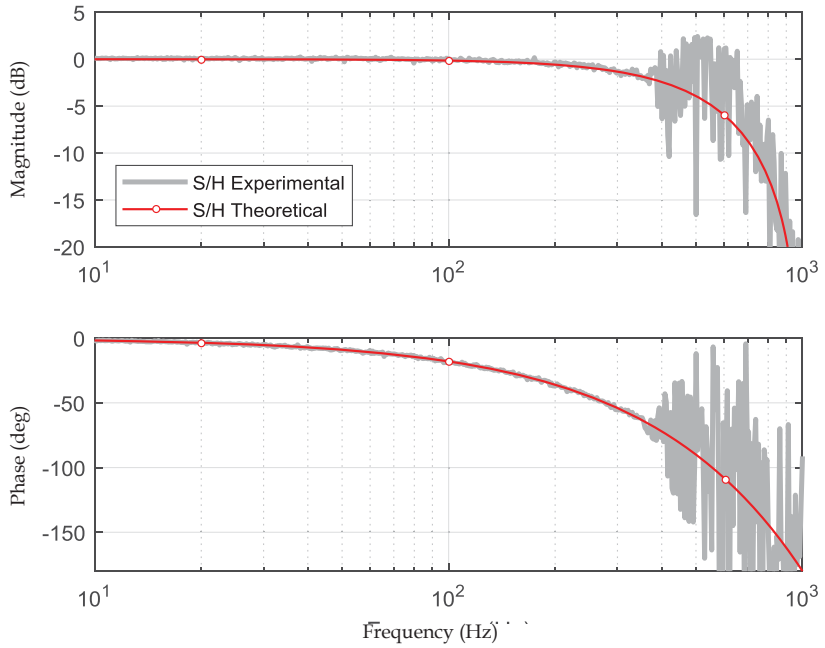

Figure 3.22 Comparison of the experimental and theoretical S/H implemented on the DSP.

In this test, the ADC of the DSP will convert the input analog signal generated by the Network Analyzer into a digital value at a fixed sample interval T_s of 1 ms (f_s = 1 kHz) and next the DAC will transform the digital value into an analog value again so the Network Analyzer can process the generated disturbance and that output. The

experimental results of Figure 3.22 show the effect of aliasing above the Shannon frequency (f_s / 2 = 500 Hz).

3.5 Experimental Validation of the Small-signal Models

The proposed small-signal models of the incremental optical encoder for the PC, ET and CSDT speed estimation methods are validated in this section. The proposed simulation model of the incremental optical encoder in chapter 2 is also validated. Table 3.1 contains a summary of the proposed small-signal model for each of the speed estimation methods and the existing small-signal models from the literature.

Table 3.1 Summary of the derived and used expressions.

Speed method	Proposed small-signal model	Literature model	Ref.
PC	$H_{Enc\,PC-Simplified}(s)=\left(\frac{1-e^{-s\cdot T_s}}{s\cdot T_s}\right)^2$	$H_{Enc\,PC-Literature}(s)=e^{-s\cdot\frac{T_s}{2}}$	[41]
ET	$H_{Enc\,ET-Simp.}(s)=\left(\frac{1-e^{-s\cdot T_e}}{s\cdot T_e}\right)^2\cdot\frac{1-e^{-s\cdot T_s}}{s\cdot T_s}$	$H_{Enc\,ET\,Literature\,-1}(s)=e^{-s\cdot T_e}$	[41]
		$H_{Enc\,PC\,Literature\,-2}(s)=\frac{1-e^{-s\cdot T_e}}{s\cdot T_e}$	[42]
CSDT	$H_{Enc\,CSDT}(s)=\left(\frac{1-e^{-s\cdot T_s}}{s\cdot T_s}\right)^2$	-	-

3.5.1 Validation of the Proposed Simulation Model

In this section, the frequency response of the proposed simulation model in chapter 2 is validated with the experimental results and the developed small-signal models. The simulation tool (e.g. Matlab, PSIM etc) does not perform the frequency response analysis of the encoder simulator and the speed estimation methods automatically. Consequently, the test must be done manually, introducing a finite number of tones, at different frequencies.

The output of the speed estimation method is not a time-continuous signal. In order to smooth the signal a low pass filter is applied (LPF) before processing the signal with the

DFT, as in Figure 3.23. The DFT will provide the information regarding amplitude and the phase of the harmonics of the signal, where the first harmonic is the most relevant.

The same filter LPF is applied at the input of the superimposed disturbance and to the speed estimation output. The comparison of the resulting first harmonic of the disturbance and that of the speed estimation are used to produce the frequency response plot. Similarly to the network analyzer, the measurement can be repeated two or three times per tone, and averaged prior to plotting.

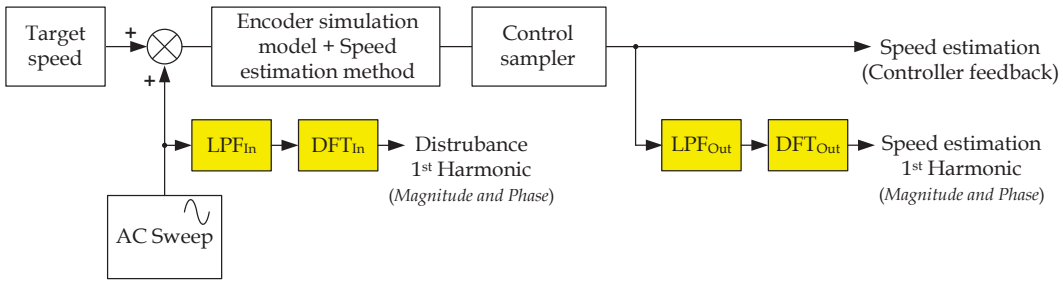

Figure 3.23 Diagram of the methodology used to obtain the frequency response of the encoder simulator, where LPF_{In} and LPF_{Out} are the same filter.

Figure 3.24 illustrates the methodology employed to validate the dynamics of the proposed simulation model in chapter 2. The results can be plotted in a linear-frequency scale as in Figure 25 (a) or a logarithmic scale, as in Figure 3.24 - (b). Note that Figure 3.24 shows the results of the phase lag and not the magnitude.

The slope of the line in Figure 3.24 can be calculated from the speed and the resolution in those cases for which the time elapsed between transitions is higher than the sample time ($T_e \gg T_s$).

$$\varphi(f) = -T_e \cdot 360^\circ \cdot f = -\frac{60 \cdot 360^\circ}{R \cdot L} \cdot f \tag{3.61}$$

The resulting interpolated line (using a linear scale) in Figure 3.24 – (a) can be represented in the logarithmic scale as in Figure 3.24 – (b). Then the impact of the encoder on the phase margin of the control can be quantified.

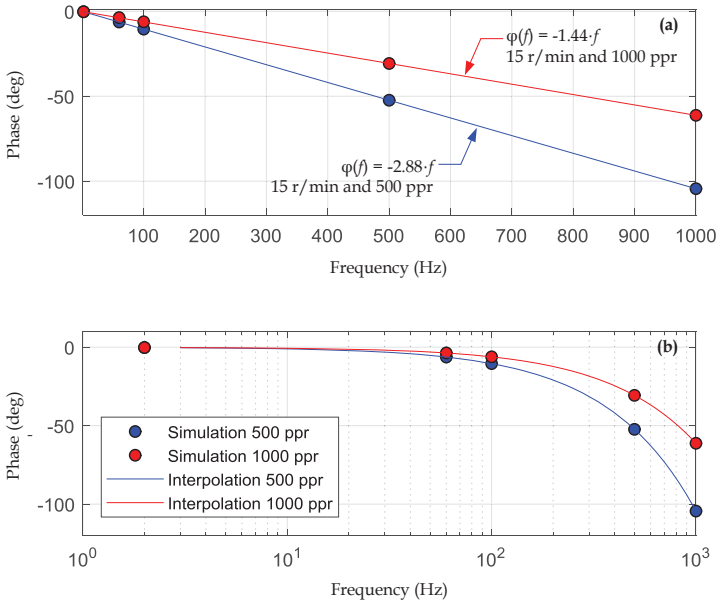

Figure 3.24 Comparison of the logarithmic representation of the time delay between the input speed and the estimated speed in a linear scale (a) and a logarithmic scale (b) for the ET method.

Figure 3.25 shows the validation of the simulation model, using the results of the simulation model and the proposed small-signal model for the PC method.

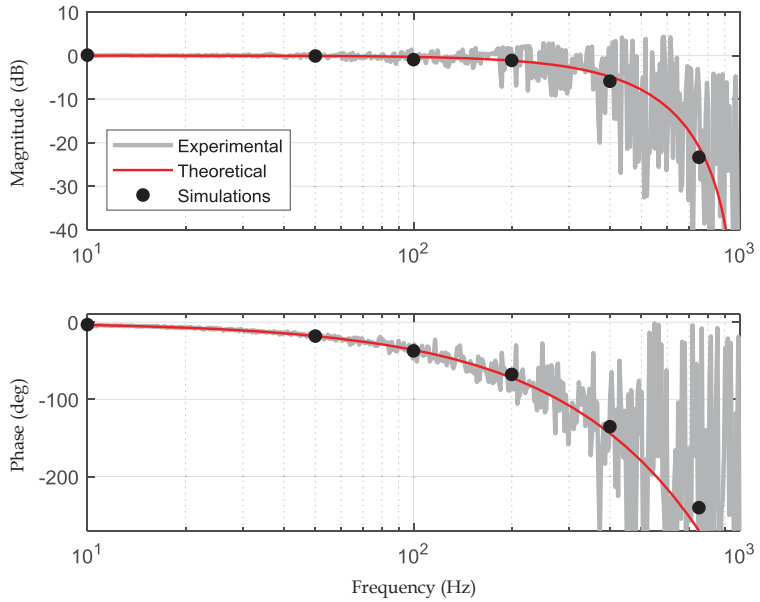

Figure 3.25 Validation of the proposed simulation model for the PC method. The evaluated speed is 3840 r/min (16 tr./T_s) with a sample time of 1 ms and the resolution of the encoder of 250 ppr.

Figure 3.26 shows the validation of the simulation model with the experimental results and the proposed small-signal model for the ET method.

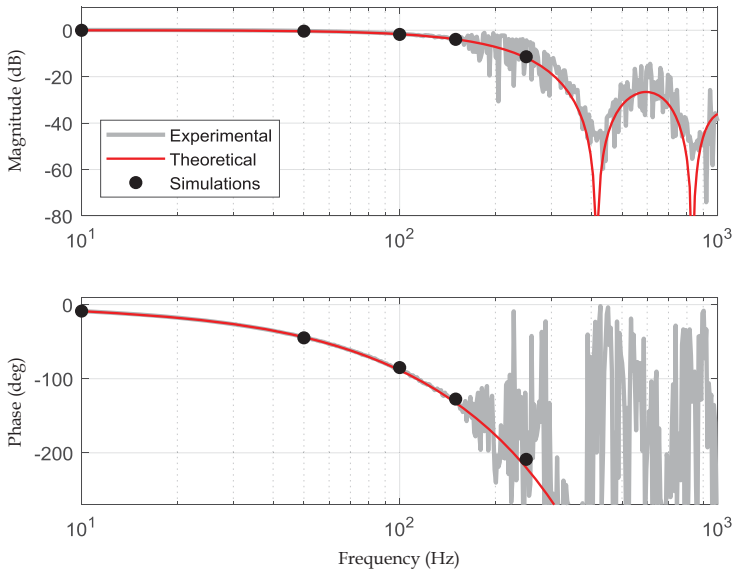

Figure 3.26 Validation of the proposed simulation model for the ET method. The evaluated speed is 100 r/min (0.41 tr./T_s) with a sample time of 0.1 ms and the resolution of the encoder of 250 ppr.

Then, the proposed simulation model can be used as a block in a more complex simulated system.

3.5.2 Validation of the Small-signal Models

The PC method is used at high speeds (>1tr./T_s). Its dynamics is determined by the control sample time T_s. Figure 3.27 shows the results of the validation.

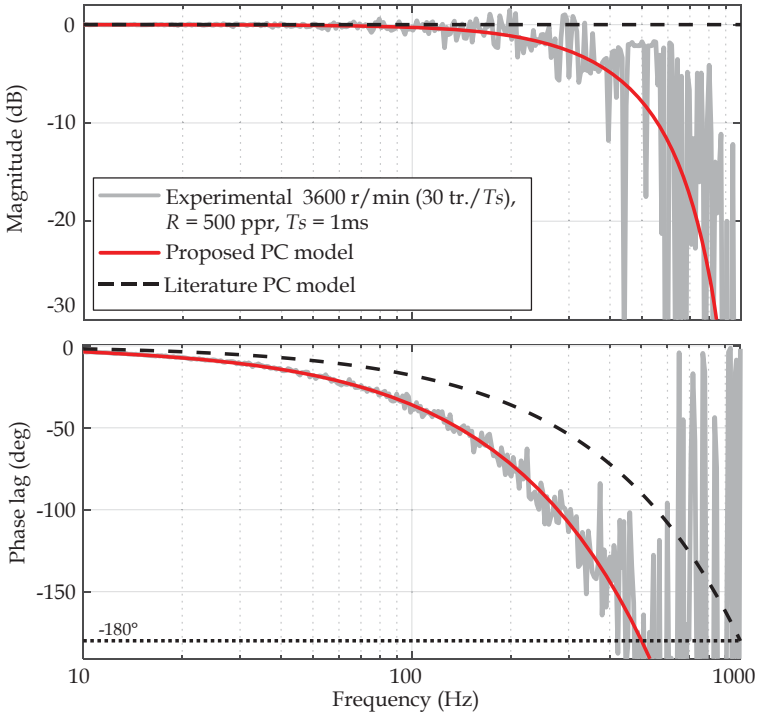

Figure 3.27 Experimental validation of the proposed small-signal model for the PC method and comparison with existing method.

The model found in the *Literature PC model* describes a delay of $T_s/2$ which is incorrect.

Experimental results show that the noise in measurement increases with the frequency. As explained at the beginning of this section, a higher performance Network Analyzer would average more than three samples to obtain a more precise measurement. In addition, as the frequency is close to the Shannon frequency aliasing appears.

In addition, as the frequency increases the system attenuates the amplitude of the injected input signal so it gets more difficult to correctly measure the output signal. A bode by part can overcome this issue. This technique consists on increasing the amplitude of the injected signal as the frequency increases to compensate for the natural attenuation of the system under study. This can be done automatically in more advanced Network Analyzers.

The result of the validation of the ET method is shown in Figure 3.28. This method is frequently used at low speed (< 1tr./T_s).

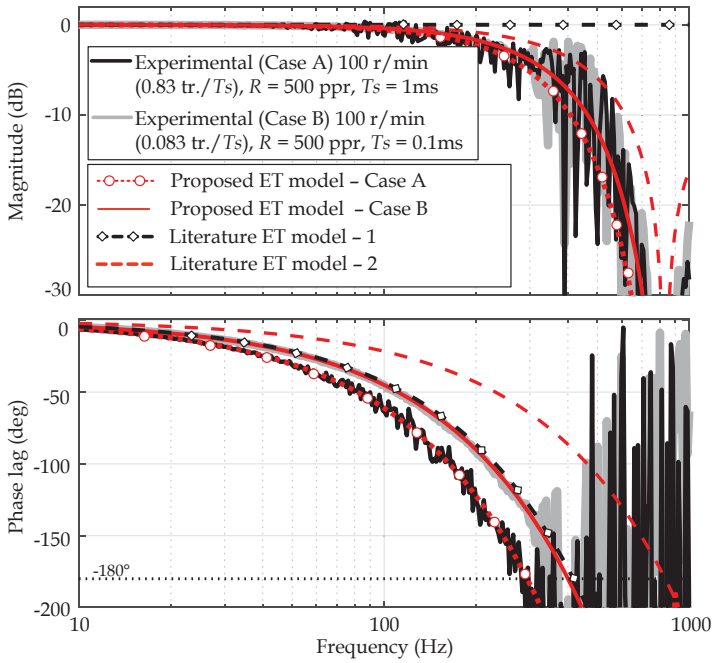

Figure 3.28 Experimental validation of the proposed small-signal model for the ET method and comparison with existing methods.

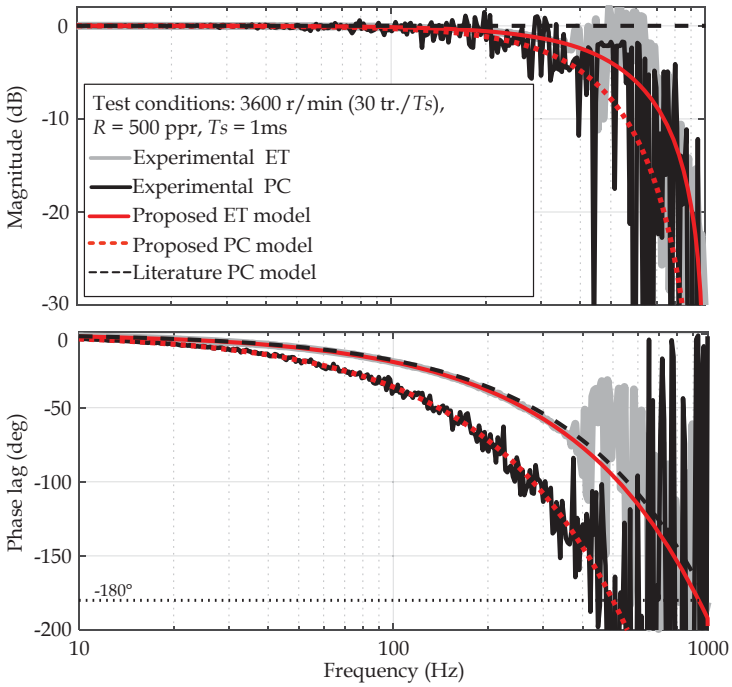

Figure 3.29 Experimental and theoretical comparison of the PC and ET methods at high speed.

Figure 3.29 shows the experimental results for the ET method at low speed, i.e. 100 r/min, at two different sampling times of 1 ms (Case A) and 0.1 ms (Case B), with normalized speed of 0.83 tr./T_s and 0.083 tr./T_s, respectively. The proposed model for the ET method is validated for all test conditions. It is also observed that the *Literature ET model – 1* has unity gain and only fits the phase lag of Case B because $T_e \gg T_s$ so the predominant phase lag is produced by the encoder signal. The *Literature ET model – 2* does not fit any of the cases.

In addition, the ET method can be used at high speed (> 1 tr./T_s). Figure 3.29 shows the experimental validation for a rated speed of 30 tr./T_s. The dynamic performance is better than that of the PC method in the same conditions. However, practical reasons, i.e. the noise of the incremental optical encoder, prevents use of ET method at high speed. Above some high speed level, the noise can destabilize the control loop.

Although the ET method could be used for medium speed, it is wiser to use a method like the CSDT. The dynamic behaviour of this method is equal to the one of the PC method as can be seen in Figure 3.30.

The main difference between the CSDT and PC methods is the quantization error. The CSDT method reduces this error by introducing the auxiliary timer and improving the accuracy of the estimation. This noise is observed in Figure 3.30.

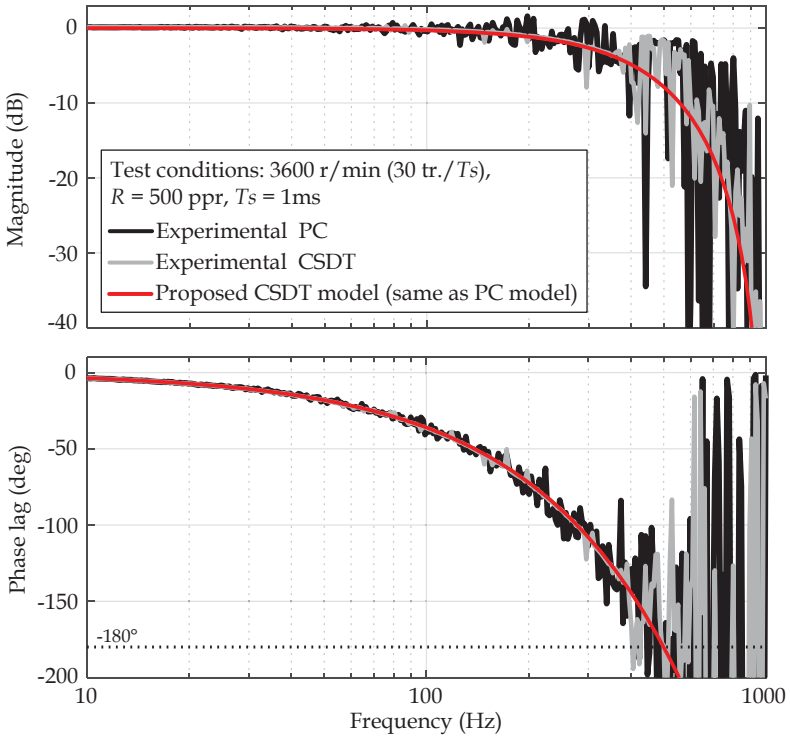

Figure 3.30 Experimental validation of the CSDT method and comparison with the PC method at high speed.

Figure 3.31 shows that the CSDT performs well at medium speeds (3 tr./T_s) while the quantization error of the PC method is excessively high. The PC does not perform well at medium speed. The dynamic model of the CSDT is also validated for this speed interval.

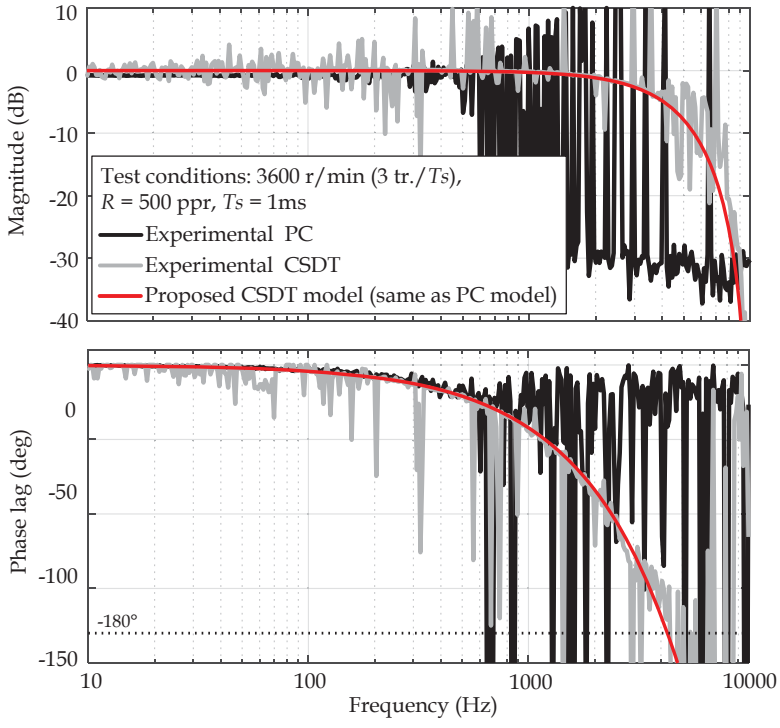

Figure 3.31 Experimental validation of the CSDT method and comparison with the PC method at medium speed.

3.6 Conclusions

In this chapter, the small-signal model of the PC, ET and CSDT method are derived and experimentally validated. It is also demonstrated that the existing literature model does not fully capture the dynamic behaviour of the studied methods. A novel experimental setup is proposed to emulate the encoder behaviour and is therefore used to validate the models.

This study covers the full speed range: the ET method for low and high speeds, the CSDT for medium and high speeds and the PC for high speeds.

It is also demonstrated that the ET method can be used at high speed, covering all speed intervals. However, practical reasons like the noise of the measurement, prevents the use of this method at high speed.

The ET method has a better dynamic performance than the PC method at high speed.

The combination of low speed and the encoder inherently produces infrequent update of the speed information, being less frequent than with smaller resolution. Many researches have focused on virtually increasing the frequency of the encoder signals by means of PLL or observers. None of the previous approaches identified or described the impact of the encoder at low speed on the phase margin of the control loop. Conversely, the small-signal models quantify such impact. This study opens the door to simpler methods of compensation of the phase margin, as will be described in chapter 5.

Chapter 4. The Improved Elapsed Time Method

In this chapter the Improved Elapsed Time (I-ET) method is presented. This is a modification of the existing well-known Elapsed Time (ET) method. The ET method is applicable at low speeds. The aim of the proposed I-ET method is to expand the applicability of the ET method to high speeds. This is particularly useful in variable speed applications because a single method can be used over the full speed range, with minor modifications for high speeds. The simultaneous use of different speed estimation methods on a single controller can be disadvantageous because the distinction between low, medium and high speed depends on each system, and the boundaries between these limits are not exact. In addition, the implementation of different speed estimation methods implies a higher consumption of microcontroller, DSP or FPGA resources. The static error of this method is analysed, as well as its dynamic performance. The I-ET method shows a good trade-off between static error and dynamic performance.

4.1 Introduction

In theory, ET could be used at high speeds. However, this method cannot be used in practice at high speeds due to measurement errors. In the next paragraphs, sources of measurement errors and methods to address them are described.

4.1.1 The Errors of the Incremental Optical Encoder

According to [11] "*the encoder error is the aggregate of quantization error, instrument error and signal processing error, including generation and transmission errors*". It is also listed in [56] and [57] that errors can be due to: disc manufacturing problems (tolerances of the slits), eccentricity of the disc due to incorrect mounting and errors due to electronic circuits. The material of the disc can be plastic, mylar, metal or glass. These surfaces are printed by means of lithographic processes. Today, the precision of those processes have small tolerance errors. A white paper from iC-Haus [58] reports that the manufacturing tolerances of the encoder disc varies approximately from 100 nm

to 1 μm. It is more likely that the errors found in the encoder measurement are produced by the electronics. The errors are found to be periodic every four transitions, in quadrature configuration, as the experimental results will demonstrate in the next sections.

Figure 4.1 shows a simplified structure of the incremental optical encoder placed on the shaft of the encoder. It also shows the relevant signals of the encoder: the signal generated by each of the photodetectors and the two squared signals and outputs of the sensor Channel A and Channel B.

The time duration of one electrical cycle is the addition of T_{On} and T_{Off} of each channel. The duty cycle of one channel is defined by the ratio T_{On} / T.

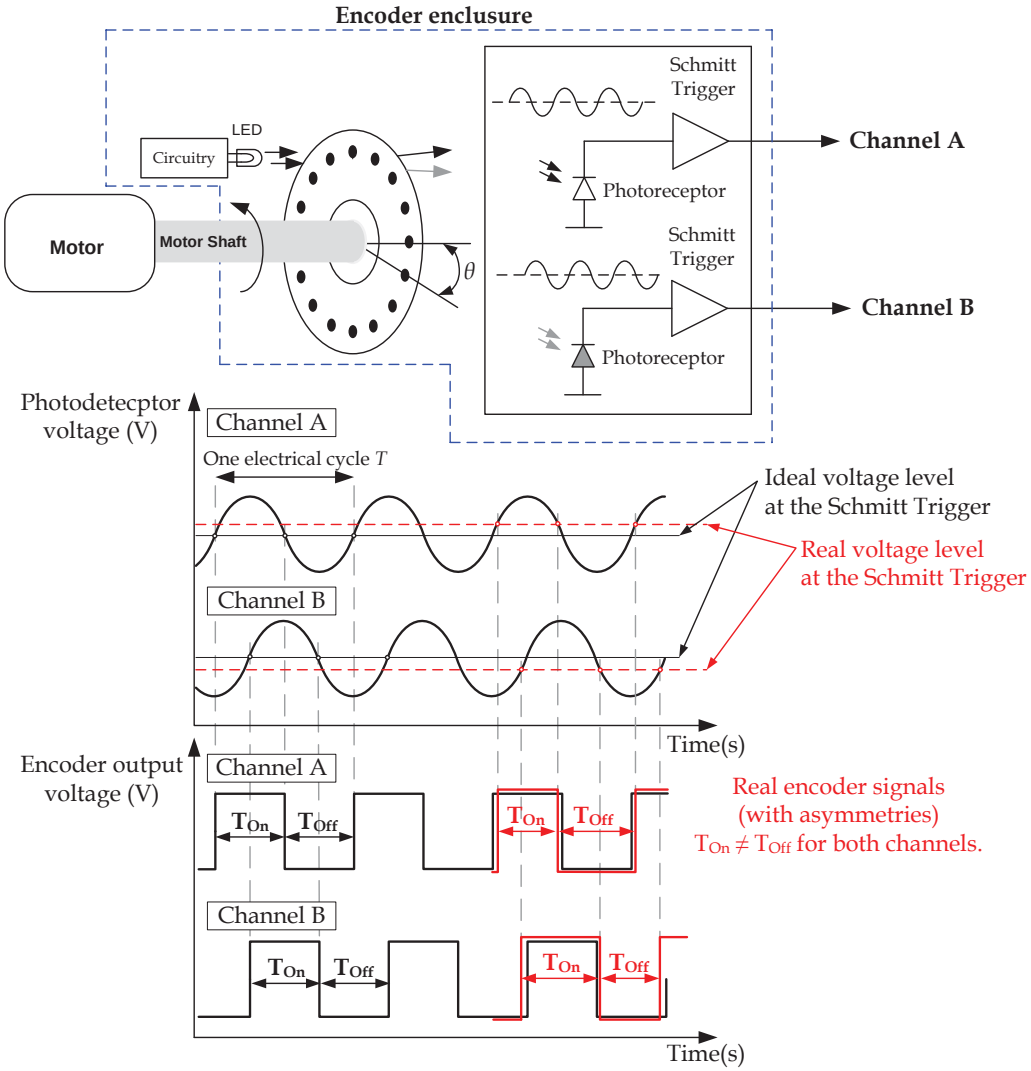

Figure 4.1 Structure of the incremental optical encoder and its main signals.

In an ideal encoder, the duty of the signal is 50%, that is $T_{On} = T_{Off}$. The duty of a real encoder is not 50% ($T_{On} \neq T_{Off}$) on each channel. Such inequality defines the asymmetry

in the signals of the encoder. This is well specified in the encoder datasheets shown in Figure 4.1.

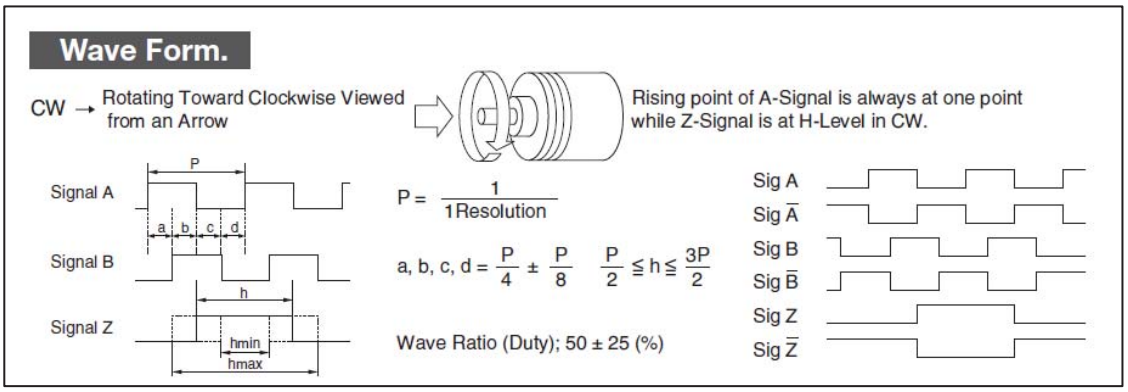

Figure 4.2 Fragment of the datasheet of the NIDEC NEMICON OVW2-10-2MC incremental optical encoder [59].

These asymmetries occur when the voltage level for the comparator in the Schmitt Trigger is not exactly equal to half of the peak to peak voltage. A case is represented in Figure 4.1. In addition, the shape of the signal of the photodetector is a distorted sinusoidal. Last but not least, the rising time of the photodetector is not equal to the falling time. The response of a photodetector's rising and falling time, is determined by drift and diffusion processes, respectively. The drift component is a relatively fast process, while the diffusion is a relatively slow movement of carriers [60]. As the speed increases and the time between transition decreases, these asymmetry errors become more relevant, particularly with the ET method. This speed estimation method is very sensitive to measurement errors. The noisy measurement degrades the performance of the controller because the control error is incorrect, and consequently the performance of the overall system is affected. This can even produce unacceptable oscillations at the output (i.e. the rotor speed).

Many research works have focused on the minimization of the measurement errors, due to asymmetries, by using dedicated hardware [61], by interpolation or by look-up-tables [62], [63], [64],[65] and [66].

Other authors propose the compensation of those asymmetry errors via the signal processing of the ET-based speed estimation. A hybrid method that combines the count of the last four encoder transitions and the auxiliary time is proposed in [67]. This method is impossible to implement on a DSP as commented in [21] because the clock frequency is of a FPGA is higher than of the DSP; this can be critical at high speed with small T_e. Alternatively, [21] proposes a speed prediction based on the least-square value

of the last *N* samples of the ET-based speed estimation. Also, in [51] the author proposed a parallel edge measurement, constant sample digital tachometer (PEM-CSDT) as an extension of the CSDT method used at high speeds. The PEM-CSDT was implemented on a FPGA and provided a significant reduction of the estimation error. The PEM-CSDT is a technique that DSP manufacturers could consider in the future when defining the encoder-peripheral capabilities of new DSP systems for motion control.

In this chapter, an improvement on of the ET method (I-ET) is introduced and analysed from the static and dynamic perspective. Consequently, the use of the ET method can be extended to the full speed range. A good trade-off between static and dynamic performance is experimentally observed.

4.2 The I-ET and the I-ET-S Speed Estimation Methods

The ET speed estimation method is based on the time duration, T_e, of the most recent completed transition.

$$\overline{n}_{ET} = \frac{1}{T_e} \cdot \frac{60}{R \cdot 4} \tag{4.1}$$

This time is measured by counting the number of cycles *m* of a high frequency clock T_{Clock}.

$$T_e = m \cdot T_{Clock} \tag{4.2}$$

The percentage error of this method, already introduced in chapter 2, is:

$$e_{ET} = \frac{1}{m-1} \cdot 100 \tag{4.3}$$

Unlike the PC or the CSDT methods, the ET does not average several encoder transitions and therefore the speed estimation is the closest estimation of the current motor speed. The averaging of pulses, inherent to the PC and the CSDT, reduces (filters) the speed error, on the other hand, this introduce a delay in the calculation.

The target of any controller is to attenuate or compensate a disturbance (acceleration) as accurately and as fast as possible. An accurate estimation of the speed through the averaging of pulses compromises the dynamic performance.

Compare motor speed of 8 tr./T_s with an ideal encoder in Figure 4.3 and a more realistic encoder in Figure 4.4.

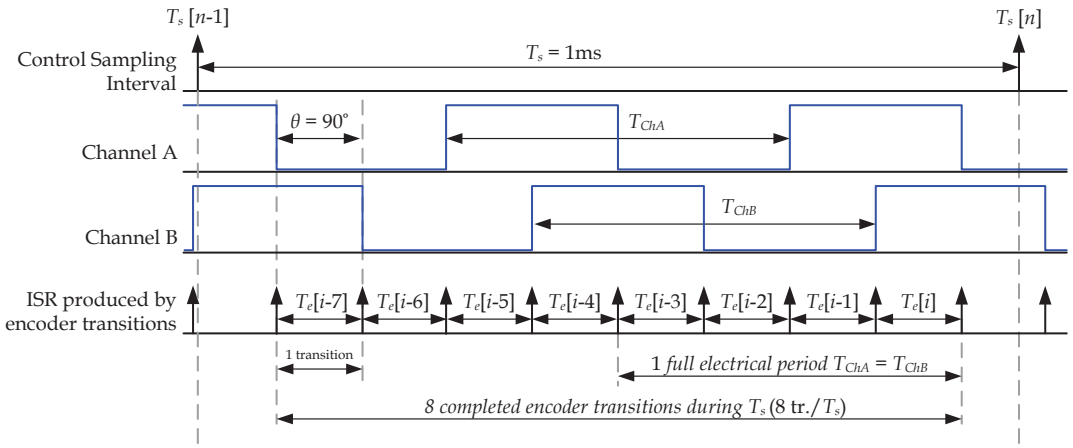

Figure 4.3 Representation of the signals of a symmetric (ideal) encoder.

In the ideal encoder in Figure 4.3:

- The full electrical period of the signal of the encoder is T_{ChA} with and ideal duty cycle of 50%
- In a quadrature configuration, the encoder transitions are shifted by 90$^{\mathrm{o}}$ electrical degrees, represented by θ.

Then, the following rules are defined for ideal encoders in quadrature configuration:

$$T_{ChA} = T_{ChB} = T_e[n] + T_e[n-1] + T_e[n-2] + T_e[n-3] \tag{4.4}$$

The equation (4.4) implies also that:

$$T_e[n] = T_e[n-1] = T_e[n-2] = T_e[n-3] = \frac{T_{ChA}}{4} = \frac{T_{ChB}}{4} \leftrightarrow \theta = 90^{\mathrm{o}} \tag{4.5}$$

In real encoders, in Figure 4.4, expression (4.4) is true but (4.5) is no longer valid. Then,

$$\theta \neq 90^{\mathrm{o}} \tag{4.6}$$

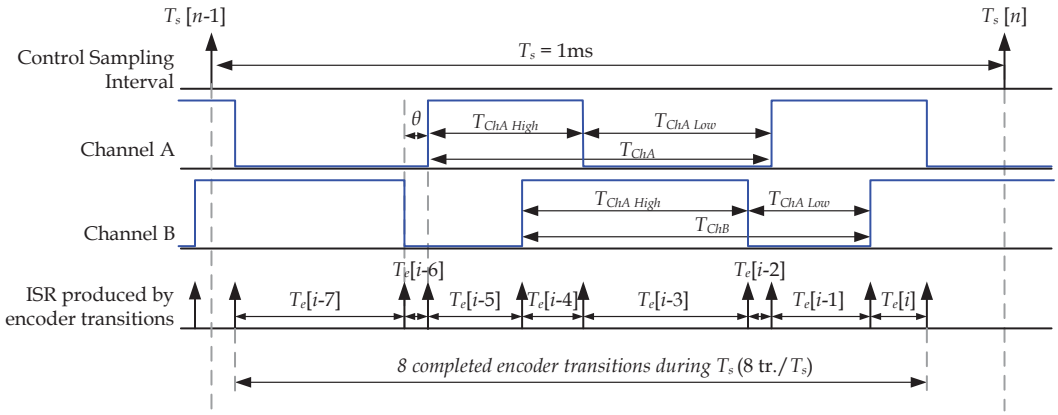

Figure 4.4 Representation of the signals of an asymmetric (real) encoder.

The asymmetries of the real encoders clearly induce estimation errors when using the ET method at high speed and in quadrature configuration. The most significant asymmetries are found to be periodic every 4 samples. Based on this, the Improved Elapsed Time (I-ET) and Improved Elapsed Time Simplified (I-ET-S) methods are proposed to cancel those asymmetries. A representation of this method is shown in Figure 4.5.

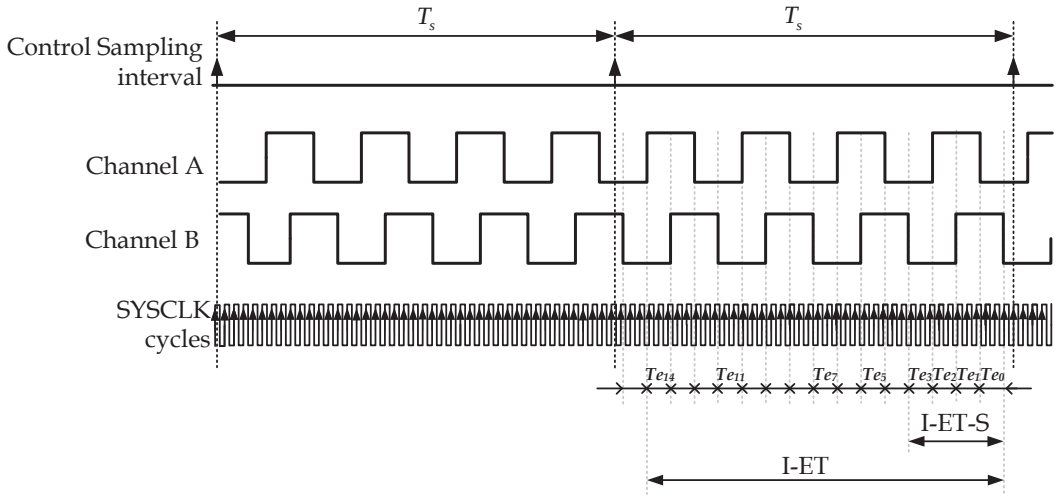

Figure 4.5 Relevant signals of the encoder for the I-ET and the I-ET-S speed estimation methods

The I-ET method consists of averaging a number of transitions, N, occurring during T_s, such that N is an entire multiple of 4.

$$\bar{n}_{I-ET} = \frac{1}{\bar{T}_e} \cdot \frac{60}{R} \tag{4.7}$$

where $\bar{T}_e$ is the average over N samples and N is an integer multiple of 4.

$$\bar{T}_e = \frac{1}{N} \cdot \sum_{i=0}^{N-1} T_e[i] \quad N = 4 \cdot k \qquad k = 1, 2, 3... \tag{4.8}$$

There is a simplified case, the I-ET-S speed estimation method, which only averages the most recent 4 transitions.

$$\bar{n}_{I-ET-S} = \frac{1}{\frac{1}{4} \cdot \sum_{i=0}^{3} T_e[i]} \cdot \frac{60}{R} \tag{4.9}$$

The minimum vector size is N = 1. For instance, for speed of 1 tr./T_s none of the proposed methods are applied. For a speed of 15 tr./T_s the I-ET-S and the I-ET speed estimation method can be applied by averaging the 4 most recent transitions or the 12 most recent transitions, respectively.

4.2.1 Small-signal Model of the I-ET and I-ET-S Methods

The small-signal model of the I-ET and the I-ET-S methods are based on the small-signal model of the ET method derived in the chapter 3.

The small signal model considers the delay introduced by the most recent encoder transition.

$$H_{ET}(s) = \underbrace{\left(\frac{1 - e^{-s \cdot T_e}}{s \cdot T_e} \right)}_{H_{MovAvg-m}(s)} \cdot \underbrace{\left(\frac{1 - e^{-s \cdot T_e}}{s \cdot T_e} \right)}_{H_{S/H-Te}(s)} \cdot \underbrace{\left(\frac{1 - e^{-s \cdot T_s}}{s \cdot T_s} \right)}_{H_{S/H-Ts}(s)} \tag{4.10}$$

The first term in (4.10) is the moving average filter due to the m-count during T_e. The second term corresponds to the inherent sample and hold effect of the encoder transition on the m-counter register, and the third term is the sample and hold of the controller. The small-signal model of the I-ET and the I-ET-S must include the effect of averaging the most recent N samples.

$$H_{I-ET}(s) = \underbrace{\left(\frac{1 - e^{-s \cdot N \cdot T_e}}{s \cdot N \cdot T_e} \right)}_{H_{MovAvg-m}(s)} \cdot \underbrace{\left(\frac{1 - e^{-s \cdot T_e}}{s \cdot T_e} \right)}_{H_{S/H-Te}(s)} \cdot \underbrace{\left(\frac{1 - e^{-s \cdot T_s}}{s \cdot T_s} \right)}_{H_{S/H-Ts}(s)} \tag{4.11}$$

N = 4 in the I-ET-S method and the small-signal model is:

$$H_{I-ET}(s) = \underbrace{\left(\frac{1-e^{-s\cdot 4\cdot T_e}}{s\cdot 4\cdot T_e}\right)}_{H_{MovAvg-m}(s)} \cdot \underbrace{\left(\frac{1-e^{-s\cdot T_e}}{s\cdot T_e}\right)}_{H_{S/H-Te}(s)} \cdot \underbrace{\left(\frac{1-e^{-s\cdot T_s}}{s\cdot T_s}\right)}_{H_{S/H-Ts}(s)} \tag{4.12}$$

Figure 4.6 plots the frequency response of equations (4.11) and (4.12). In addition, the frequency response of the ET and the PC methods are also plotted for the case that the speed is 1836 r/min (15.3 tr./T_s), the sample time is 1 ms, and the resolution is R = 500 ppr.

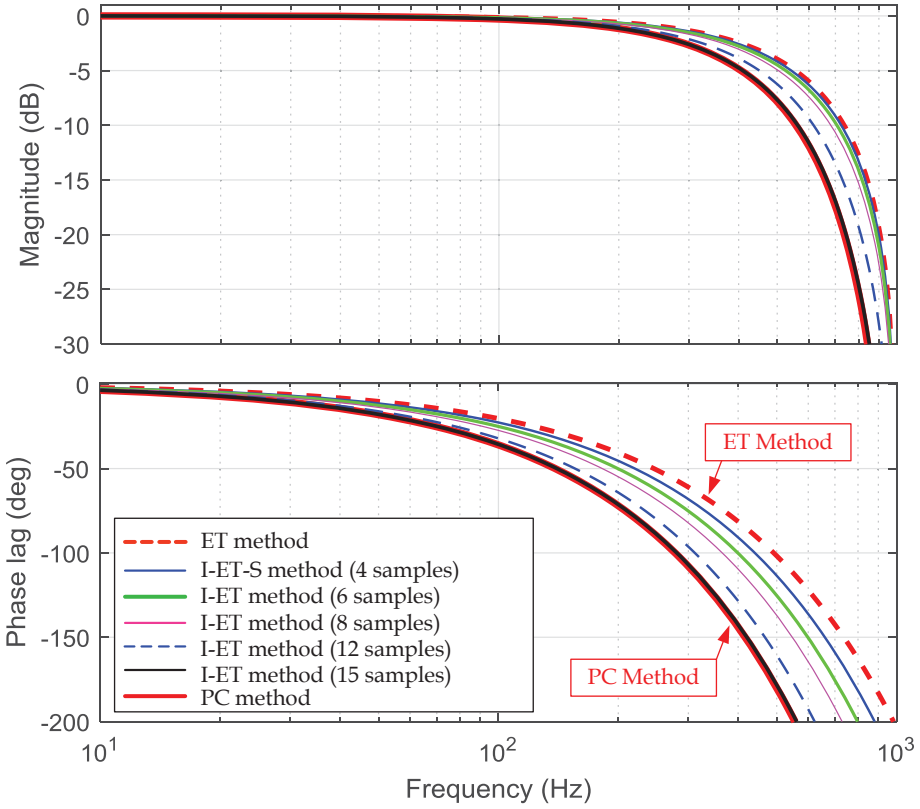

Figure 4.6 Dynamics of the proposed I-ET the I-ET-S speed estimation methods.

As expected, the I-ET and the I-ET-S methods have a smaller bandwidth than the ET method, but a better bandwidth than the PC method under the same conditions. As the number of samples N used in the averaging increases, the phase lag also increases.

For illustrative purposes, the cases of N = 6 and N = 15 are also plotted. These do not correspond to the methodology proposed in the I-ET and the I-ET-S methods, because neither are an entire multiples of 4. It can be seen, that the phase lag increases with N.

In the case of N = 15, the dynamics converge to the dynamics of the PC method because all are included in the averaging.

The dynamic response of the I-ET-S method is better than the dynamic response of the I-ET method. However, the I-ET is more effective in reducing the effect of the encoder asymmetries, because it averages more samples than the I-ET-S method.

4.3 Experimental Results of the I-ET Method and the Analysis of the Data

The following test is performed to evaluate the encoder asymmetries:

- The DC motor is connected to a dc power supply in open-loop and the speed is proportional to the voltage. The encoder used has a resolution of 1000 ppr. The DSP counts and stores the number $m[i]$, that is proportional to $T_e[i]$. The test is performed clockwise and anticlockwise.

$$T_e[i] = m[i] \cdot T_{SYSCLK} \tag{4.13}$$

The results of the test are depicted in Figure 4.7.

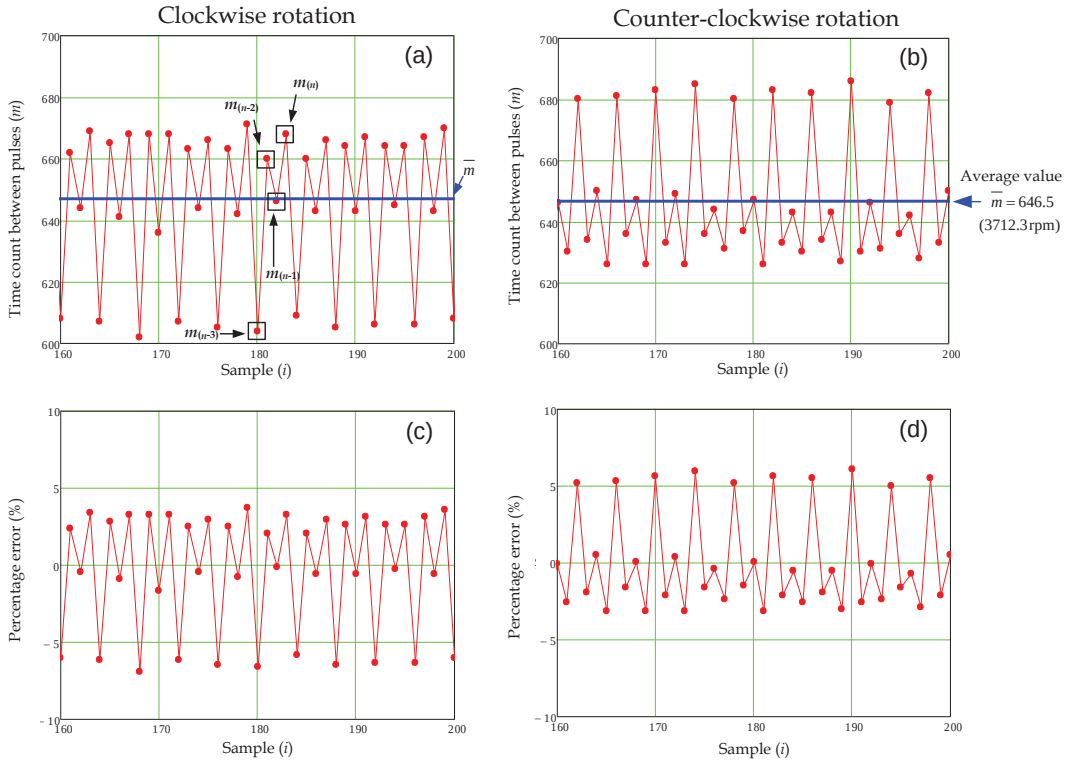

Figure 4.7 Results of the experimental test. Figure (a) shows the number of high-frequency clock "*m*" count between encoder consecutive transitions for a clockwise rotation and (b) a counter-clockwise rotation. Figures (c) and (d) show the static error of the clockwise motion and figure and the counter-clockwise motions respectively. Notice that the time between encoder transitions (T_e) and *m* are proportional as in (4.14).

A clear pattern with "M" shape is found in Figure 4.7- (a) .Similarly, a "W" pattern shape is found in Figure 4.7 - (b) as the direction of the motion is reversed. The theoretical error of the ET and I-ET methods is expressed in (4.3). The expected ideal percentage error is 0.155% (corresponding to ± 1 during the *m*-count). However, the actual value of the worst percentage error is 5%. The error in Figure 4.7 (c) and (d) is computed as:

$$e_i = \frac{m[i] - \frac{1}{N}\cdot\sum_{k=0}^{N-1} m[k]}{\frac{1}{N}\cdot\sum_{k=0}^{N-1} m[k]}\cdot 100 \tag{4.14}$$

where N is the total number of samples stored during the test. Then experimental results show that:

- The signal of the encoder, in quadrature configuration, has a well-defined pattern in clockwise and anti-clockwise rotation.
- The pattern repeats every four samples due to the quadrature configuration.
- The real error is greater than the expected theoretical error.

The set of data of the clockwise experiment can be rearranged as in Figure 4.8.

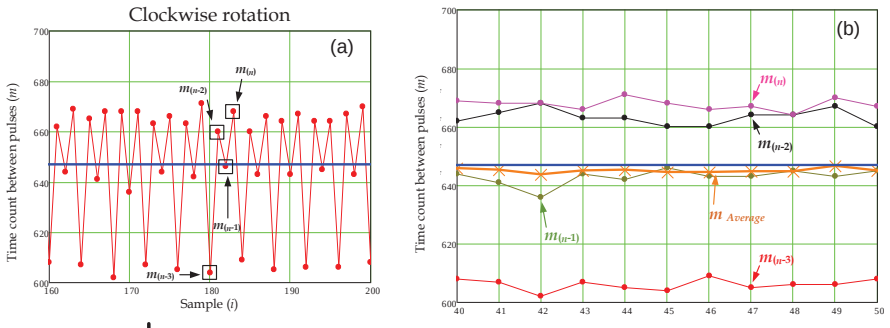

Table 1

i	m
176	605
177	663
178	642
179	671
180	604
181	660
182	646
183	668
184	609
185	660
186	643

Table 2

r	$m_{(n-3)}$	$m_{(n-2)}$	$m_{(n-1)}$	$m_{(n)}$
40	608	662	644	669
41	607	665	641	668
42	602	668	636	668
43	607	663	644	666
44	605	663	642	671
45	604	660	646	668
46	609	660	643	666
47	605	664	643	667
48	606	664	645	664
49	606	667	643	670
50	608	660	645	667

Table 3

r	$m_{Average}$
40	645.75
41	645.25
42	643.5
43	645
44	645.25
45	644.5
46	644.5
47	644.75
48	644.75
49	646.5
50	645

Figure 4.8 (a) Analysis of the results of the experimental test and (b) the plot of the reorganized data according to the pattern $m_{(n-3)}$, $m_{(n-2)}$, $m_{(n-1)}$, $m_{(n)}$.

The table in Figure 4.8 is organized as follows:

1. The row data of the DSP (stored number of *m* for each transition) are in Table 1. The index *i* organizes and sequences the samples.
2. The pattern repeats every four samples. Then data are rearranged in Table 2, with four columns as follows:
    - First column in Table 2, $m_{(n\text{-}3)}$ → terms 1-5-9-13…etc of Table 1.
    - Second column in Table 2, $m_{(n\text{-}2)}$→ terms 2-6-10-14…etc of Table 1.
    - Third column in Table 2, $m_{(n\text{-}1)}$ → terms 3-7-11-15…etc of Table 1.
    - Fourth column in Table 2, $m_{(n)}$ → terms 4-8-12-16…etc of Table 1.
3. The average of every row of Table 2 is in Table 3, with index *r*.

The data of Table 2 and Table 3 are plotted in Figure 4.8 - (b). It can be concluded that:

1. The average value of the four samples of each row of Table 2 is in the row with the same index in Table 3 (orange in Figure 4.8 - (b)). This average value $\bar{m}$ is the closest estimation to the theoretical *m* value obtained from the average measured speed (*m* = 646.847 for a speed of 3710.3 r/min).
2. The average values of every row, in Table 2, are very similar, as shown in Table 3. Then, the best estimation of the time is the average value of four consecutive samples.
3. The column of $m_{(n)}$ samples (colour pink) have a similar value, as does the values of the column $m_{(n\text{-}1)}$ (green), $m_{(n\text{-}2)}$ (black) and $m_{(n\text{-}3)}$ (red), all depicted in Figure 4.8 - (b).

This experimental result validates the foundations of proposing the I-ET-S speed estimation method based on averaging a minimum of four samples, and multiples of four in the I-ET method. The study of the periodicity of the samples is proposed to overcome the errors in the estimation due to the quadrature configuration. A procedure to use a forecasting algorithm to reduce the asymmetry error is presented in Figure 4.9.

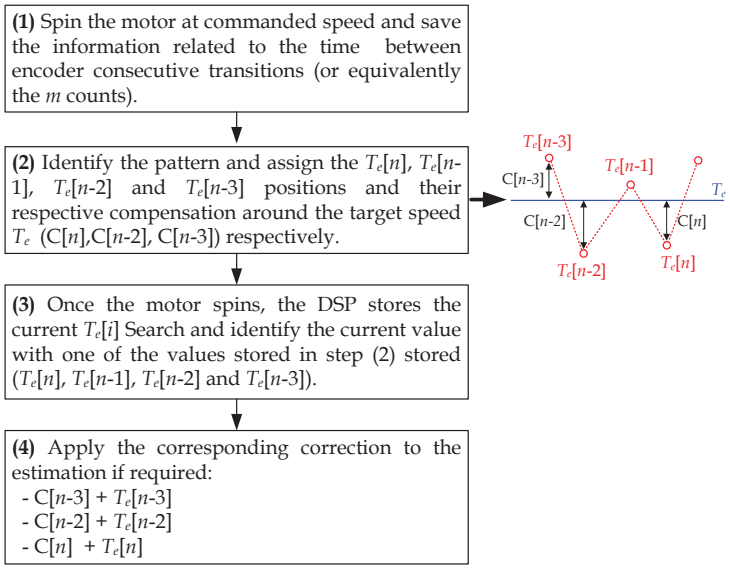

Figure 4.9 Representation of the proposed forecasting algorithm for asymmetry compensation.

By applying a forecasting technique, the ET speed estimation method can be used at high speed. Then, the resulting dynamics of the encoder and the forecasting technique will be similar to the dynamics of the ET method at high speed and quadrature configuration. Because averaging is no longer required, the delay of the forecasting ET-based method will be the same as the ET method: half of the control sample time plus half of the time duration of the most recent completed transition. The results of applying the forecasting technique offline on the stored values of Table 1 are depicted in Figure 4.10. The black dots are the resulting m_i, which is proportional to the speed, as in (4.13) and (4.1).

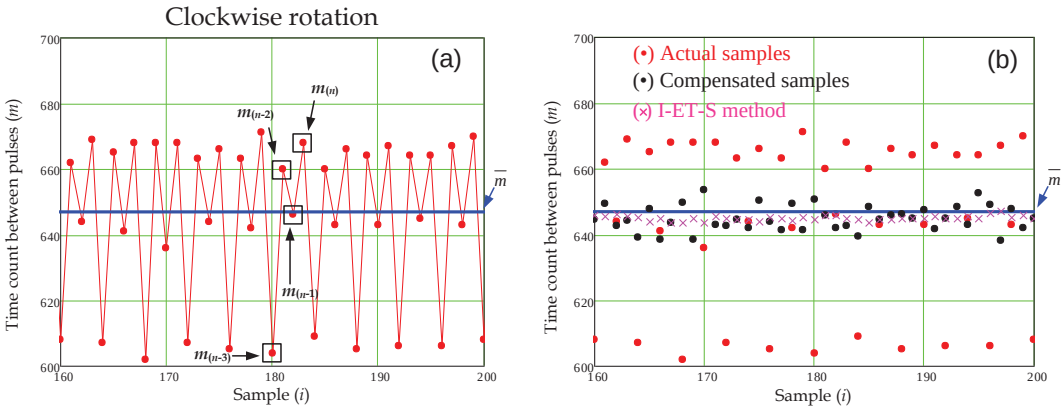

Figure 4.10 (a) Representation of $m[i]$ at the speed of 3710.3 r/min and (b) the result of the application of the forecasting technique offline. Note that the blue line represents the mathematical average value of m.

Figure 4.10 - (b) shows that once each sample is corrected by the forecasting method the resulting value (black dots) is closer to the actual average value.

The experimental results of the I-ET-S and forecasting methods are statistically analysed and compared according to the following figures of merits:

- Mean arithmetic:

$$\overline{m} = \frac{1}{N} \cdot \sum_{j=0}^{N-1} m[j] \tag{4.15}$$

- Mean deviation:

$$MD = \frac{\sum_{j=1}^{N} \left| m[j] - \overline{m} \right|}{N} \tag{4.16}$$

- Standard deviation:

$$s = \sqrt{\frac{\sum_{j=1}^{N} \left(m[j] - \overline{m} \right)^2}{N}} \tag{4.17}$$

The results of the statistical analysis are presented in Table 4.1

Table 4.1 Statistical analysis of the vector of *m* data

Samples	$\bar{m}$	MD	s
(A) - Vector of measured values (red in Figure 4.10-(a))	647.08	19.78	23.63
(B) - I-ET-S method (pink)	646.65	1.36	1.75
(C) - Forecasting method (black)	646.69	3.44	6.25

Two of the proposed methods: I-ET-S and the forecasting methods have a value close to the average of the vector of samples stored in the DSP. The row data vector (A) has the highest mean deviation and standard deviation caused by asymmetries errors. The proposed I-ET method has the smallest value of mean deviation and standard deviation. This result is consistent since the average of four consecutive samples is used to estimate the value of $\bar{m}$ over T_s, which is equivalent to an estimate of the average speed. The proposed forecasting method (C) has a *MD* and *s* higher than the I-ET-S method, but smaller than the same values corresponding to (A).

4.4 Experimental Validation of the I-ET and I-ET-S Speed Estimation Methods

In the next sections, the static error of the I-ET and the I-ET-S methods are experimentally validated.

4.4.1 Analysis and Comparison of the Static Errors of the Proposed Methods

A DC motor in open-loop conditions is used to evaluate the static performance of the proposed method. The DC motor is coupled to two encoders of different resolutions, as in Figure 4.11. Device A is a 1000 ppr encoder from US Digital and encoder B is a 500 ppr encoder of unknown brand.

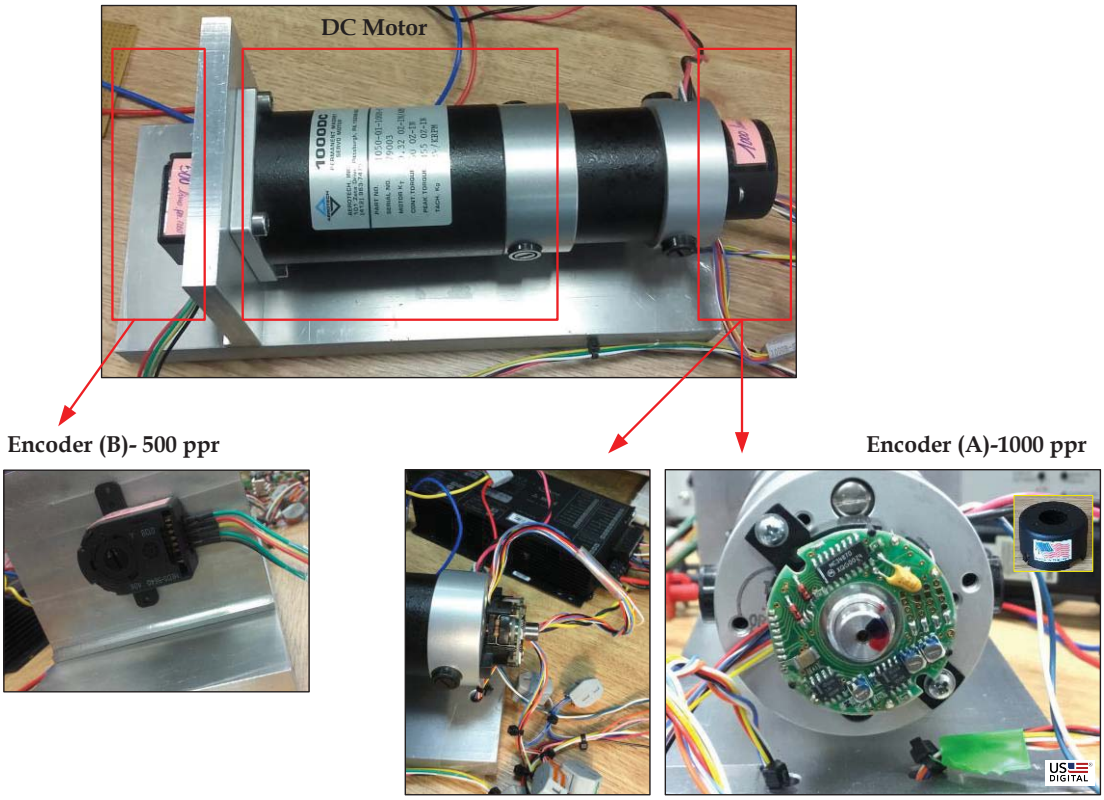

Figure 4.11 Pictures of the DC motor and the two encoders used to evaluate the performance of the proposed speed estimation methods.

The experimental set up is configured as in Figure 4.12. The DC motor from the series 1000DC of Aereotech is directly connected to the DC power supply. The output signal of each encoder is conditioned accordingly.

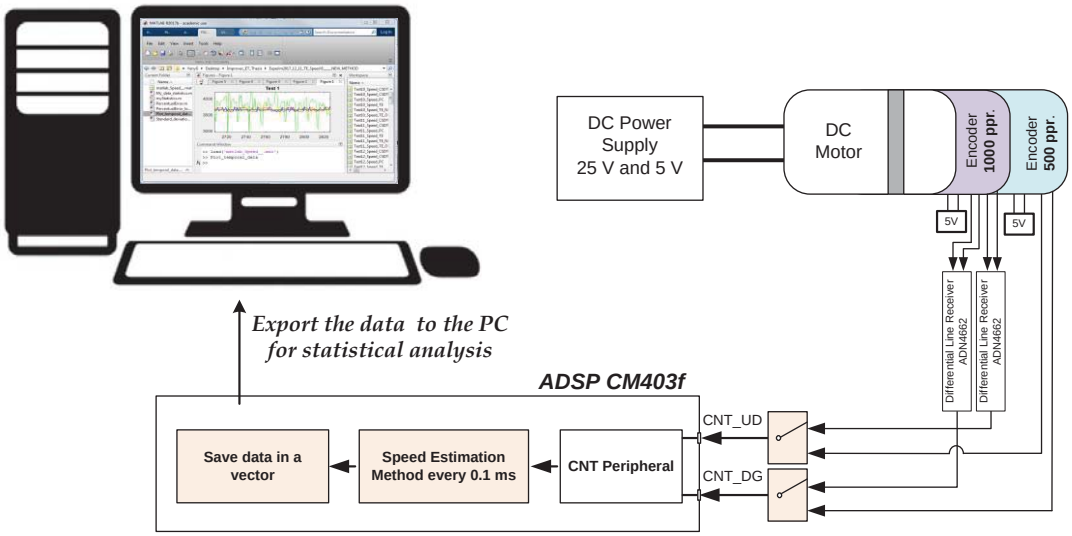

Figure 4.12 Experimental setup for the evaluation of the proposed speed estimation method.

During every test at least one encoder is connected to the DSP (CNT Peripheral). This peripheral provides information about the time elapsed between consecutive encoder transitions (TIMER_TMRn_CNT register) and the number of encoder transitions (CNT1_CNTR register) within a given sample time T_s for the ET and PC methods respectively, and also the auxiliary time required for the CSDT method. In addition, the ISR produced with encoder transitions is activated, so the T_e between consecutive encoder transitions can be stored in an auxiliary buffer and later averaged over T_s in order to estimate the speed as specified in the I-ET method. The configuration of the ISR is shown in Figure 4.13.

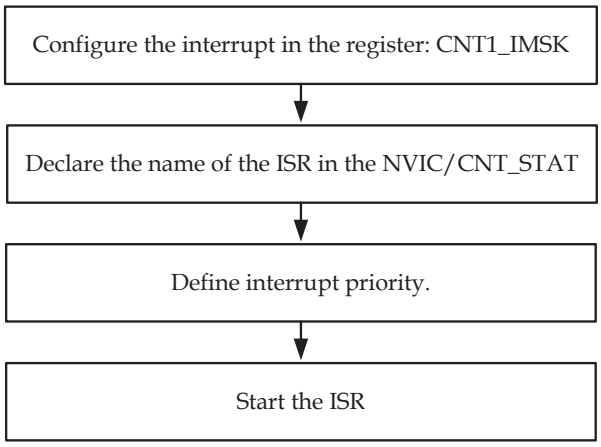

Figure 4.13 Steps to configure the ISR of the CNT peripheral.

Once the ISR is triggered by the encoder transition, the bits BIT_CNT_IMSK_UD and BIT_CNT_IMSK_DG must be cleared.

The test is performed at two speeds, with two encoders, and with and without quadrature configurations, as in Table 4.2 and Table 4.3. The tests in Table 4.2 are

performed at the speed of 3662.16 r/min and the sample time is 0.1 ms, proportional to 25V.

Table 4.2 Open-loop test for statistical analysis of the speed estimation methods at 25V.

Test numeration	Effective resolution	Normalized speed
Test 1	R = 1000 ppr · 4	24.41 tr./T_s
Test 2	R = 1000 ppr · 1	6.1 tr./T_s
Test 3	R = 500 ppr · 4	12.20 tr./T_s

The tests in Table 4.3 are performed at 5 Vdc, which produces a speed of 646.36 r/min, and the sample time is 0.1 ms.

Table 4.3 Open-loop test for statistical analysis of the speed estimation methods at 5V.

Test numeration.	Effective resolution	Normalized speed
Test 4	R = 1000 ppr · 4	4.3 tr./T_s
Test 5	R = 500 ppr · 1	0.53 tr./T_s

The PC, CSDT and ET methods are used as a base line to compare the proposed I-ET and the I-ET-S methods at high speed. At low speed the ET method is used as base line. The percentage error and the standard deviation are used to compare the methods.

- Results of Test 1 (24.41 tr./T_s).

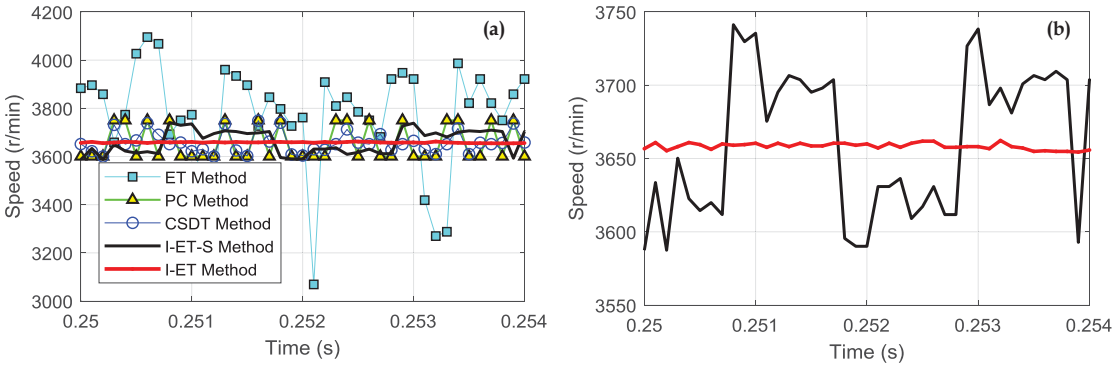

Figure 4.14 Experimental Test 1. (a) shows the comparison of the proposed methods: I-ET and I-ET-S and the previously described methods: ET, PC and CSDT methods. (b) shows details of the I-ET and I-ET-S methods.

Table 4.4 Statistical analysis of the results in Test 1.

	Mean	*e* %	MD	*s*
ET	3772.238	25.325	202.335	278.912
PC	3651.153	6.815	71.725	79.726
CSDT	3651.857	2.687	34.223	44.469
I-ET-S	3661.248	2.308	50.057	52.341
I-ET	3657.793	0.416	4.459	5.473

Figure 4.14 and Table 4.4 show that the I-ET method has the best performance of all considered methods at the nominal speed of 24.41 tr./T_s. The I-ET-S reduces the effect of the asymmetries, but not completely.

- Results of Test 2 (6.1 tr./T_s).

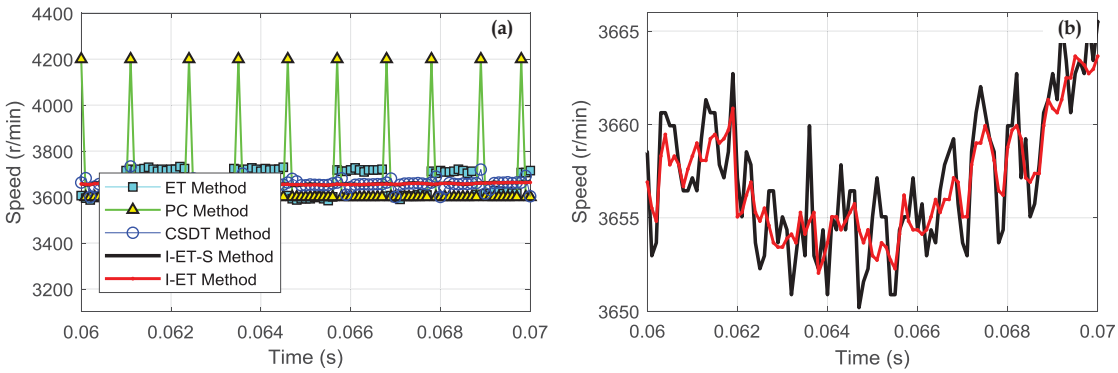

Figure 4.15 Experimental Test 2. (a) shows the comparison of the proposed methods: I-ET and I-ET-S and the previously described methods: ET, PC and CSDT methods. (b) shows details of the I-ET and I-ET-S methods.

Table 4.5 Statistical analysis of the results in Test 2.

	Mean	*e* %	MD	*s*
ET	3664.813	2.330	53.574	54.6883
PC	3659.977	14.755	107.963	180.004
CSDT	3661.169	2.9231	14.688	25.861
I-ET-S	3663.150	0.390	3.756	4.493
I-ET	3663.146	0.303	3.534	4.072

Figure 4.15 and Table 4.5 show the experimental results for the nominal speed of 6.1 tr./T_s. The I-ET and the I-ET-S have a very similar performance considering that at this speed the I-ET method is averaging only 4 samples.

- Results of Test 3 (12.20 tr./T_s).

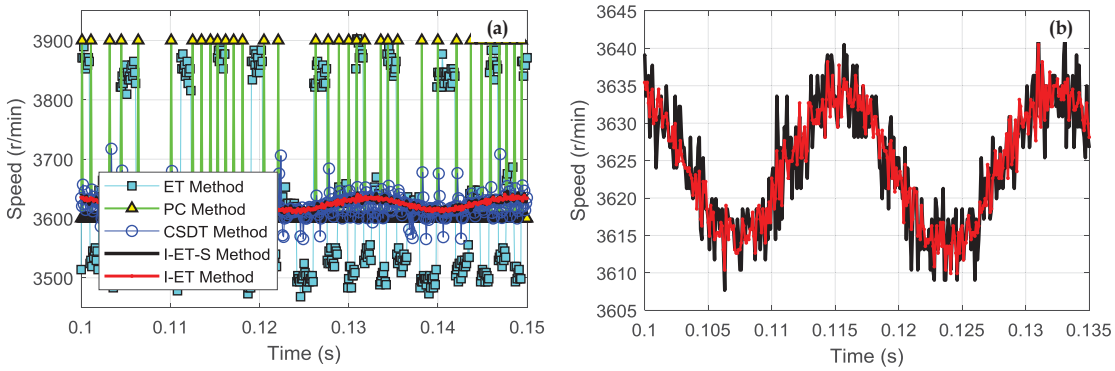

Figure 4.16 Experimental Test 3. (a) shows the comparison of the proposed methods: I-ET and I-ET-S and the previously described methods: ET, PC and CSDT methods. (b) shows details of the I-ET and I-ET-S methods.

Table 4.6 Statistical analysis of the results in Test 3.

	Mean	*e* %	MD	*s*
ET	3632.800	7.949	118.112	141.470
PC	3619.723	7.743	36.853	74.364
CSDT	3620.718	8.692	12.958	20.163
I-ET-S	3623.941	0.6478	7.014	8.222
I-ET	3623.871	0.472	6.676	7.629

Figure 4.16 and Table 4.6 for the nominal speed of 12.20 tr./T_s show that the I-ET and I-ET-S methods have a better performance in cancelling the asymmetries. The I-ET has the best performance.

- Results of Test 4 (4.3 tr./T_s).

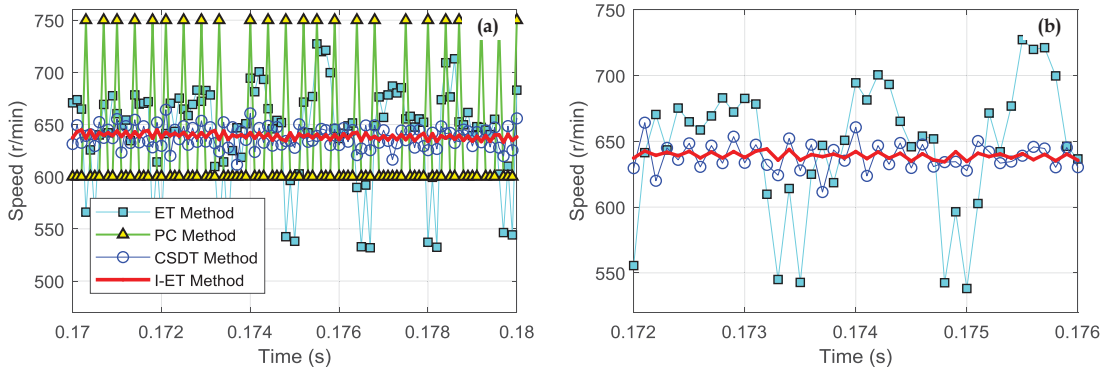

Figure 4.17 Experimental Test 4. (a) shows the comparison of the proposed method: I-ET (in this case the I-ET and the I-ET are the same because $N = 4$) and the previously described methods: ET, PC and CSDT methods. (b) shows details of the ET, the CSDT and the I-ET methods.

Table 4.7 Statistical analysis of the results in Test 4.

	Mean	*e* %	MD	*s*
ET	645.948	23.392	41.273	53.349
PC	638.408	17.479	57.147	65.480
CSDT	638.821	8.991	9.816	11.706
I-ET	639.022	1.588	3.360	4.084

Figure 4.17 and Table 4.7 show the experimental results for the speed of 4.3 tr./T_s. The I-ET reduces significantly the noise of the asymmetries.

- Results of Test 5 (0.53 tr./T_s).

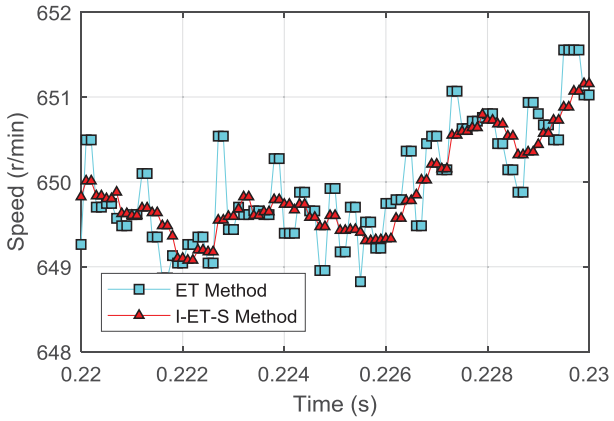

Figure 4.18 Experimental Test 5. Comparison of the performance of the ET and the I-ET methods at low speed.

Table 4.8 Statistical analysis of the results in Test 5.

	Mean	*e* %	MD	*s*
ET	650.064	0.687	1.262	1.617
I-ET-S	650.067	0.586	1.172	1.531

Figure 4.18 and Table 4.8 show results of the test at the nominal speed of 0.53 tr./T_s for didactic purposes and the I-ET method is compared to the classical ET speed estimation method. As can be seen, the precision of the estimation improves as four samples are averaged at low speed for the I-ET method. However, as shown earlier in section 4.2.1, this penalizes the dynamic performance of the speed estimation as a consequence of averaging several transitions.

Figure 4.19 shows an experimental comparison of the speed estimation under study at medium and high speed in a quadrature configuration based on the percentage error (4.14). In this condition the asymmetries errors are particularly critical.

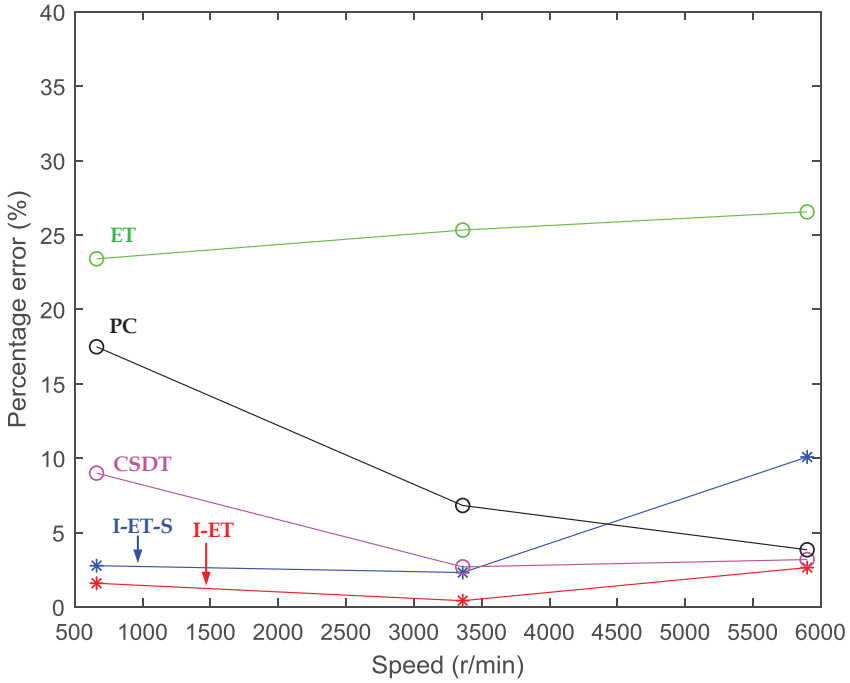

Figure 4.19 Comparison of the different speed estimation methods under analysis at the speeds of 660 r/min (4.4 tr./T_s), 3660 r/min (24.4 tr./T_s) and 5900 r/min (39.33 tr./T_s) using an encoder with effective resolution of 4000 ppr (quadrature configuration) and a sample time of 0.1 ms.

As can be seen the ET, the CSDT and the PC methods have a higher error than the proposed two methods. At medium speed, 660 r/min (4.4 tr./T_s) the I-ET-S must be equal to the I-ET since both methods average 4 samples. However, a difference of 1.2 % is noticed between these two methods. As the speed increases to 3660 r/min (24.4 tr/T_s) and 5900 r/mn (39.33 tr./T_s) the performance of the I-ET improves because this method averages the maximum number of samples that is an integer multiple of 4 (N = 36)

4.5 Conclusions

A new I-ET speed estimation method is proposed, which has lower or equal static error to the classical ET method, the classical PC method or the CSDT method, over the full speed range, particularly in quadrature configuration.

The Improved Elapsed Time (I-ET) is designed for the minimization of the negative effect of the encoder asymmetries, which is crucial at high speed. Its basis lies on the averaging of four consecutive encoder signals (time elapsed between encoder transitions). As the speed increases the number of samples used in the averaging increases in a factor of integer multiples of four. From this method the other two extensions are derived:

- The Improved Elapsed Time Simplified (I-ET-S) which consists of an estimate the speed based on the average of T_e the last four transitions. This is the most basic configuration of the I-ET (buffer size 4).
- The forecasting method, which proposes to identify and quantify the asymmetries at a given speed.

The methods I-ET and I-ET-S are also analyzed from the dynamic perspective already introduced in chapter 3. The three methods are evaluated in open-loop configuration at different speeds and using two different encoders.

From the theoretical study and validations, it can be concluded that:

I. **The forecasting method**: This is based on the last encoder transition value with compensated error. This is recommended for high bandwidth applications. This method should be evaluated experimentally online.
II. **The I-ET-S method**: This averages the last 4 samples, which has lower error and more phase lag than the forecasting method in I.
III. **Average values** from the maximum possible number samples (multiple of 4), has a very low error but introduces a phase lag.

The new I-ET method maximizes the effective encoder resolution with a low error at low, medium and high speeds, increasing effective bandwidth of encoders. This method is particularly useful in variable speed applications.

The proposed method is easy to implement. There is no need for additional DSP hardware resources such as timers, DAC, ADC, other peripheral devices, etc.

In the next chapter, the performance of the I-ET speed estimation method is evaluated and compared to other existing methods in a closed-loop configuration.

Chapter 5. Practical Case Study

This chapter describes practical cases of the concepts developed in this thesis. This section is divided in two parts that group the two major contributions of this thesis:

- Part I. A practical case study of the use of the small-signal model developed in chapter 3 to study the stability of the motor at low, speed with a low resolution encoder, and secondly to use the same small-signal model to propose a compensation technique (a lead compensator).
- Part II. The implementation of the I-ET method proposed in chapter 4 within a speed motion control loop.

The performance of the system in both cases is evaluated at different speeds by means of speed step test responses.

5.1 Description of the Workbench

The test workbench is mainly composed of:

- The DC motor from Aerotech with inertia $J = 3.8 \cdot 10^{-5}$ Kg·m^2, viscous friction $B = 3.1 \cdot 10^{-3}$ N · m / (rad / s), armature inductance La = 2.0 mH, and armature resistance Ra = 0.9 Ω.
- A linear driver, the four quadrant inverter, SCA-SS-70-10.
- A 30 A power supply.
- Two incremental optical encoders coupled on each side of the motor shaft with resolutions 500 ppr and 1000 ppr. A 1000 ppr encoder from US Digital was initially used for the I-ET method test. This sensor was later replaced by another encoder of the same resolution from NEMICON.
- A tachometer integrated with the motor.
- A digital controller ADSP CM403f from Analog Devices.
- And the additional circuitry used to condition the sensor signals.

A schematic of the workbench is depicted in Figure 5.1 and a picture is found in Figure 5.2. This figure shows all the possible configurations of the setup. Not all of the configured sensors and devices and other components are used simultaneously.

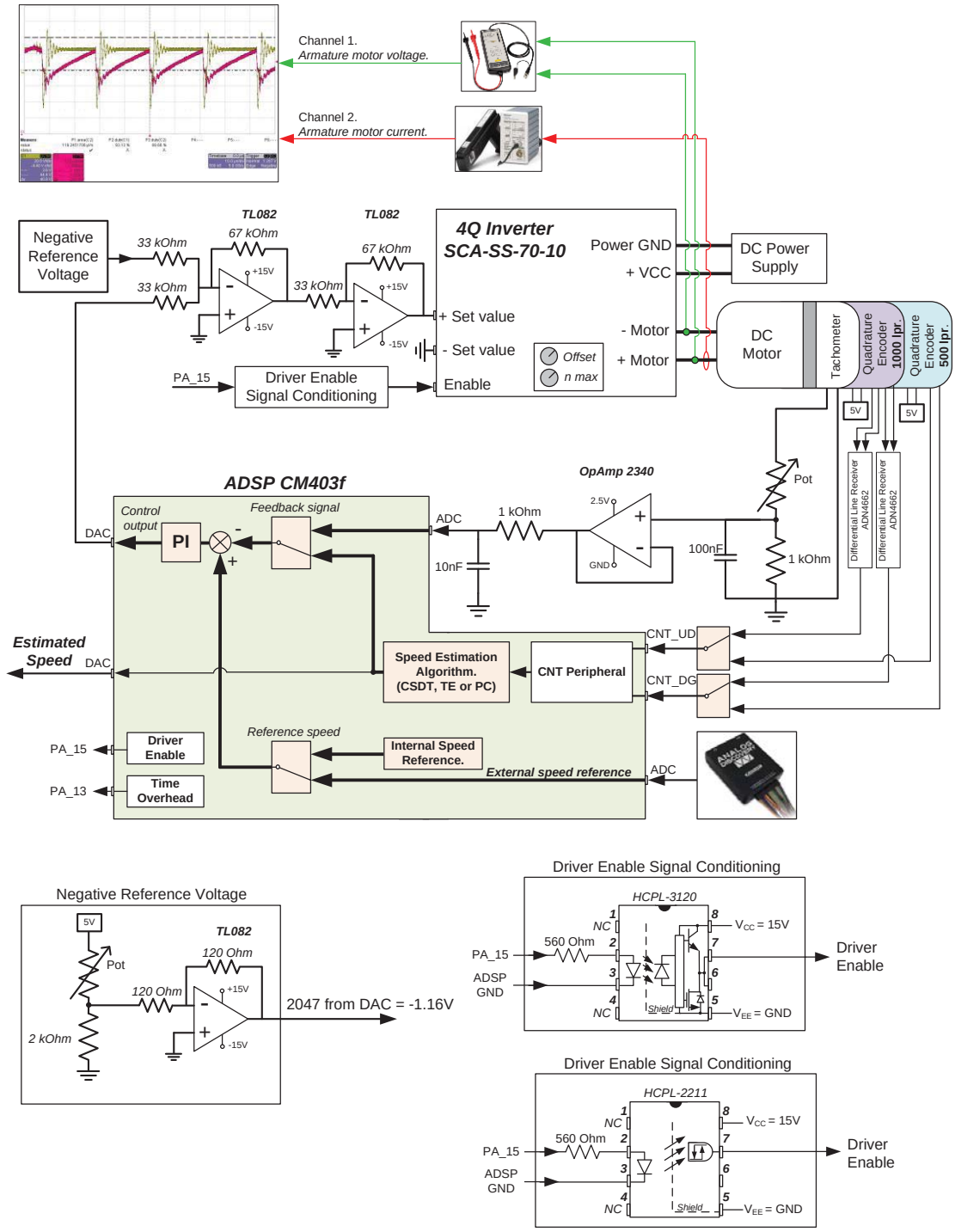

Figure 5.1 Diagram of the workbench.

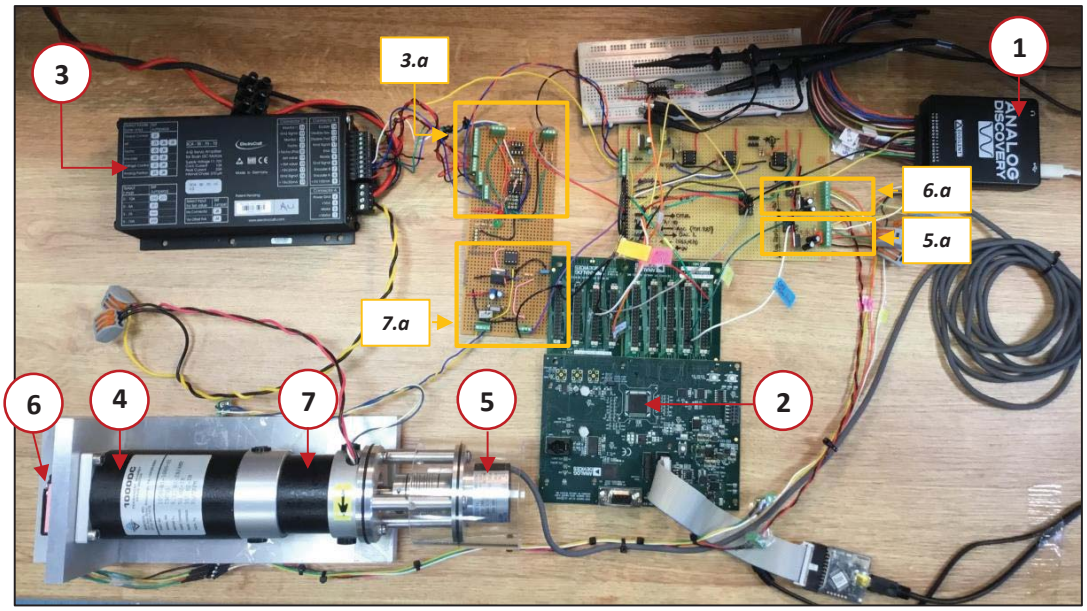

Figure 5.2 (1) - Analog Discovery. It is used as external speed reference and as a network analyzer from Digilent. (2) - ADSP CM403F (Cortex M4) Analog Devices. It performs the digital control (3)-The motor driver SCA-SS-70-10 from ElectroCraft (4)-The Brushed DC Motor from Aerotech. (5)-Incremental optical encoder (1000ppr) from NIDEC NEMICON. (6)-Incremental optical encoder (500ppr) unknown brand. (7) Tachometer. *(3.a), (5.a), (6.a) and (7.a) are signal conditioning for the Driver, encoders and tachometer.*

The configuration of the CNT peripheral, the implementation of the different speed estimation methods and the control loop on the ADSP were described in chapter 2.

5.2 Part I. Implementation of a Digital Lead Compensator for Motor Control

For the study of the impact of the encoder dynamics on a real system, the open-loop transfer function $T(j\omega)$ of the system was measured using the Analog Discover using its configuration as Network Analyzer, as depicted in Figure 5.3.

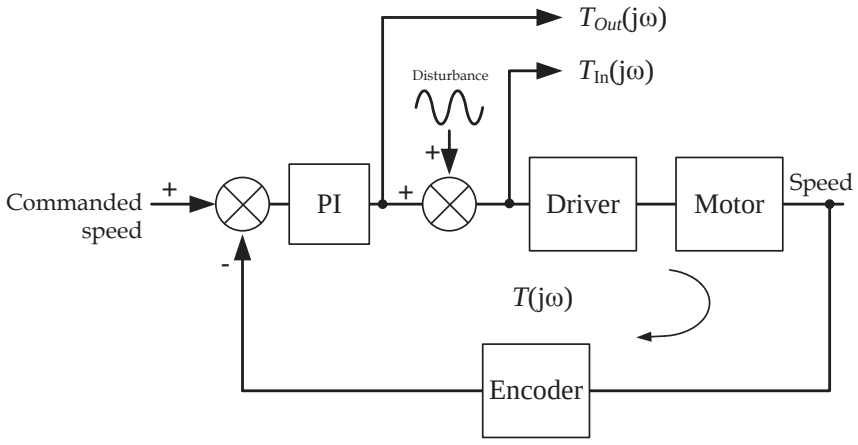

Figure 5.3 Open-loop measurement $T(j\omega)$ of the speed control loop.

The open-loop transfer function is measured actually in a closed-loop configuration because the controller has an integral part. The integral part increases uncontrolled over time in open-loop leading to an incorrect measurement of the dynamics. Instead, $T(j\omega)$ must be measured by virtually opening the control loop and introducing a small-signal disturbance.

This measurement is performed at a speed for which the dynamics of the encoder can be considered as unity gain, as will be demonstrated later. This result will be next used to predict and quantify the impact of the sensor at much lower speed, and finally to implement a lead compensator.

The frequency response of the open-loop is used to analyse the stability of the system according to the gain margin (GM) and phase margin (PM) criteria [68], where the PM is the most critical parameter in this case. The configuration for the gain-loop measurement is shown in Figure 5.4

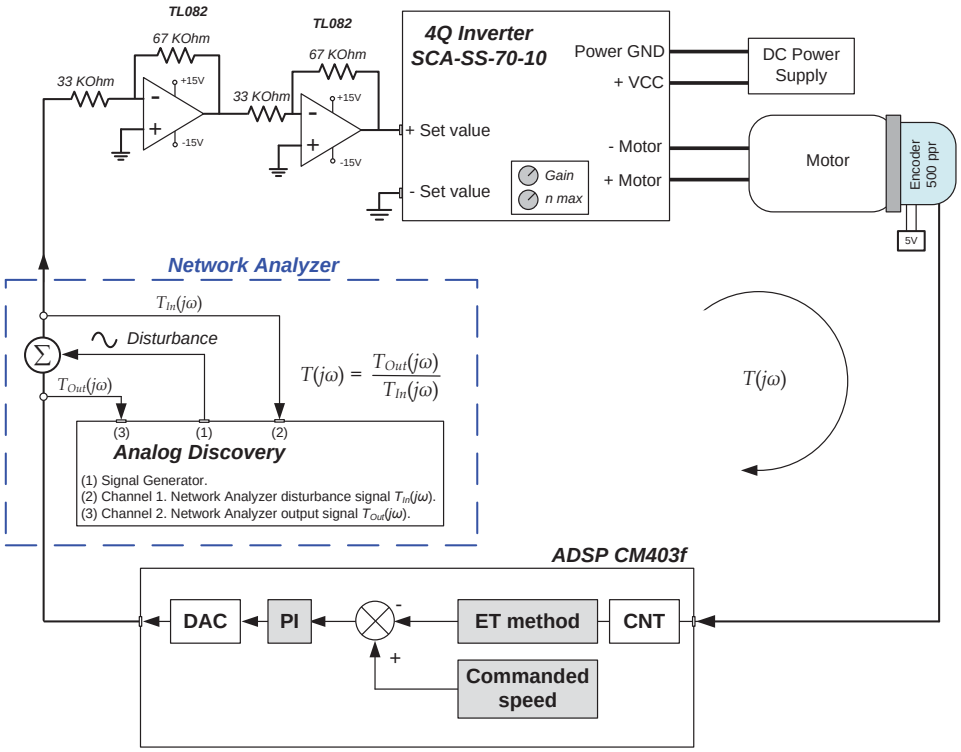

Figure 5.4 Configuration of the system for the open-loop frequency response measurement.

A PI compensator is used to regulate speed. The PI has been tuned aiming to illustrate the impact of the encoder dynamics at low speed, as well as the usefulness of the proposed model to predict stability issues. Specifically, the gains of the PI controller are adjusted based on the frequency response of the plant within the speed loop, in a way that the system is stable at 500 r/min (where the impact of the encoder dynamics is

negligible) but unstable at 15 r/min (where the impact of the encoder dynamics is significant in the phase).

5.2.1 Characterization of the Motor System at Low Speed and Stability Analysis

The open-loop of the system is measured at the speed of 500 r/min with the two different resolution encoders, and results are depicted in Figure 5.5.

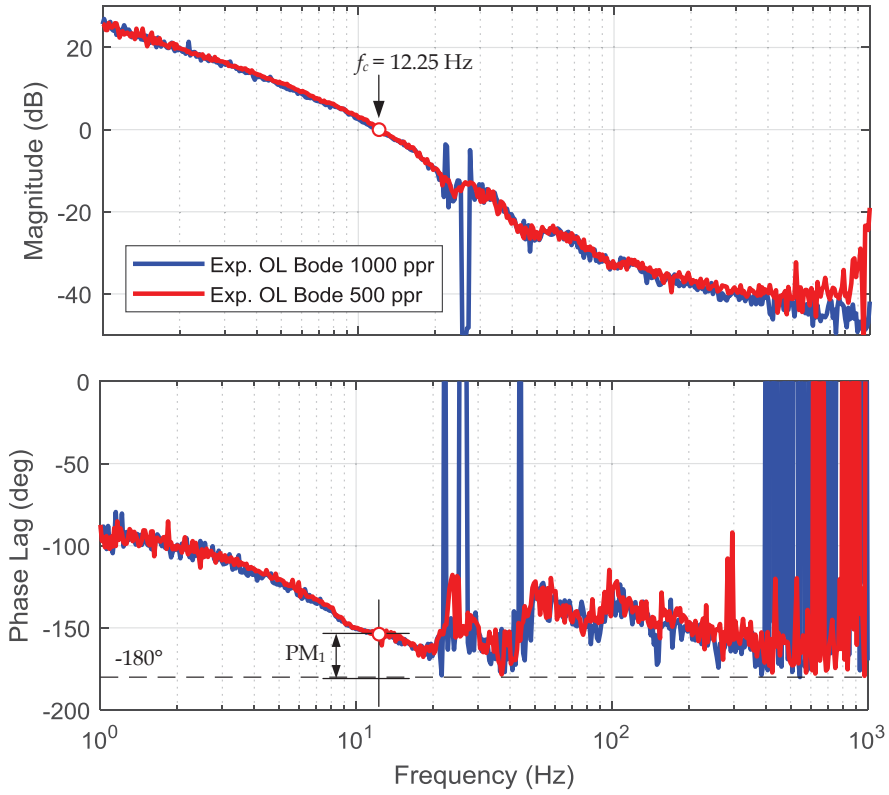

Figure 5.5 Experimental gain-loop.

These experimental results are only valid up to 20 Hz. Beyond this value the results are affected by the device resolution and the signal processing method (the Analog Discovery only averages three full periods). However, results could be improved by first using a more precise measurement device and secondly by measuring the Bode by parts. The Bode by parts method consists of measuring the transfer function for a small frequency interval. The amplitude of the disturbing signal changes for each frequency interval in a way that compensates the system attenuation at the specific frequency interval.

As can be seen in both cases, the resultant phase margin at the crossover frequency (f_c = 12.25 Hz) is similar, with a phase margin PM_1 = 28.43°. The noise at higher frequencies is due to the finite resolution of the digital acquisition device of the Analog Discovery

unit and the attenuation of the signal is due to the reduction of gain of the motor system, as observed in the magnitude plot of Figure 5.5.

For any reasonable encoder resolution, the dynamics are similar in both tests. This occurs because at the chosen operating speed (500 r/min) and around the crossover frequency the dynamics of the encoder can be considered unity gain due to the high bandwidth. The bandwidth of the incremental optical encoder at low speed (< 1 tr./T_s) in conjunction with the ET method depends of the speed of operation and the resolution, as demonstrated in chapter 3. Figure 5.6 shows the impact of two sensors (of different resolutions) on the open-loop.

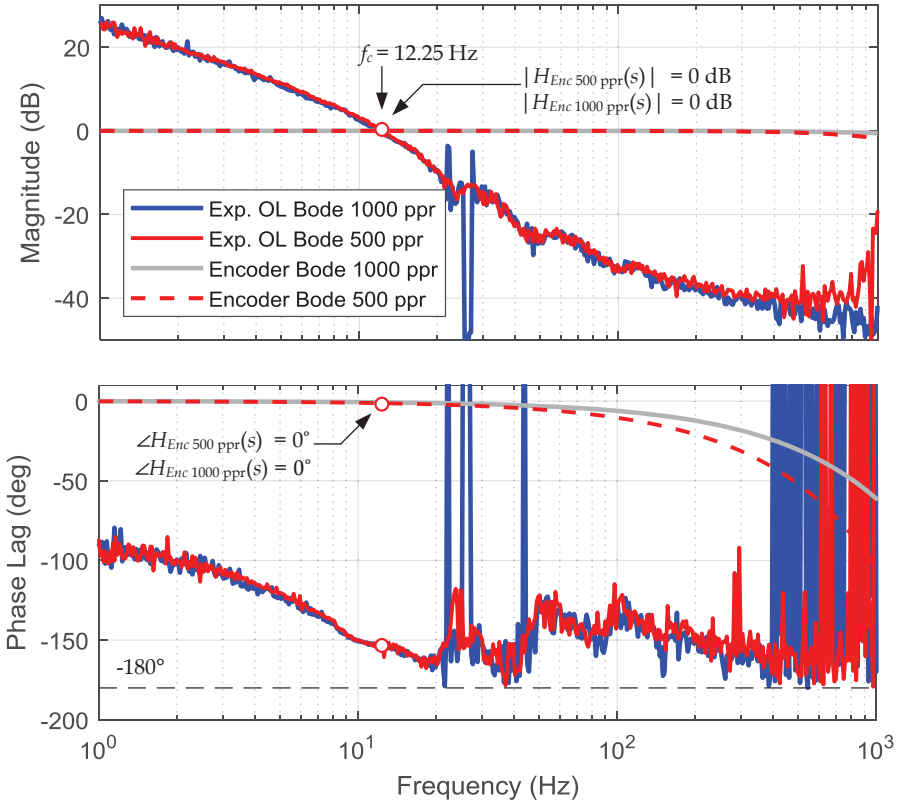

Figure 5.6 Impact of the encoders of different resolution on the open-loop.

The frequency response of the encoders has been plotted using the expression developed in chapter 3. The encoders do not affect the dynamics of the motor system at 500 r/min in either case.

The closed-loop system can be generically represented as in Figure 5.7 - (a). However, at this speed and with the given encoder resolution it can be simplified to Figure 5.7 – (b). This explains why the dynamics of the encoder have not been sufficiently studied previously. The stability performance of the motor downgrades as the speed reduces. The manufacturers of encoders recommend the use of an encoder of higher resolution in

the feedback to overcome this issue. Nevertheless, this implies an increase of the cost of the motor system. A sufficiently high encoder resolution will imply that the dynamics of the sensor will provide the bandwidth to close the loop properly.

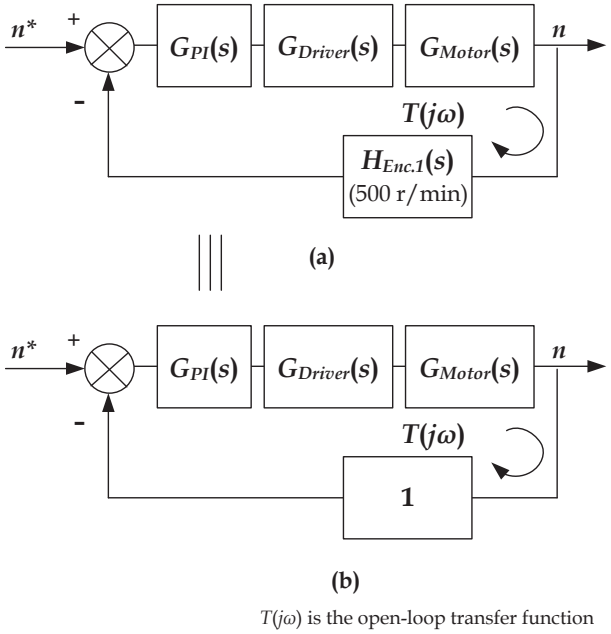

Figure 5.7 Block diagram of the motor system (a) considering the theoretical impact of the encoder and (b) considering the effective impact of the device at the speed of 500 r/min.

The motor system is stable at the speed of 500 r/min. The performance is still good at a lower speed of approximately 200 r/min. The deterioration of the performance occurs suddenly given the non-linear nature of the sensor. The following hypothesis is stated:

- The control-loop of the system is composed of different components depicted in Figure 5.7-(a). As the speed decreases, only the dynamics of the encoder block placed in the feedback network varies, the rest of the blocks remain invariant.
- The invariance of the other blocks is checked by replacing the sensor in the feedback network by a tachometer.
- At a speed of 15 r/min the performance of the motor system with a low resolution encoder is not adequate. However, the performance of the same motor system at the same speed is adequate with a tachometer.

It is concluded that the difference in the performance is caused by the encoder in the feedback network. However, given the limitation of the acquisition system dealing with very small signals, this hypothesis cannot be directly verified with an open-loop measurement. The developed small-signal model for the ET method and the encoder

can be used instead to predict the deterioration of the motor performance. The prediction is later validated by means of a speed step response test in the time domain.

To predict the phase margin of the motor system at the speed of 15 r/min with an encoder of 500 ppr in the feedback network, the polynomial corresponding to the experimental open-loop measurement must be obtained by fitting the coefficients of a theoretical polynomial with the experimental results:

$$T_{fitting}(s) = \frac{1.2 \cdot 10^4 \cdot s + 7.5 \cdot 10^5}{2 \cdot s^3 + 2 \cdot 10^2 \cdot s^2 + 5 \cdot 10^3 \cdot s} \tag{5.1}$$

This fitted polynomial is validated with the experimental results shown in Figure 5.8.

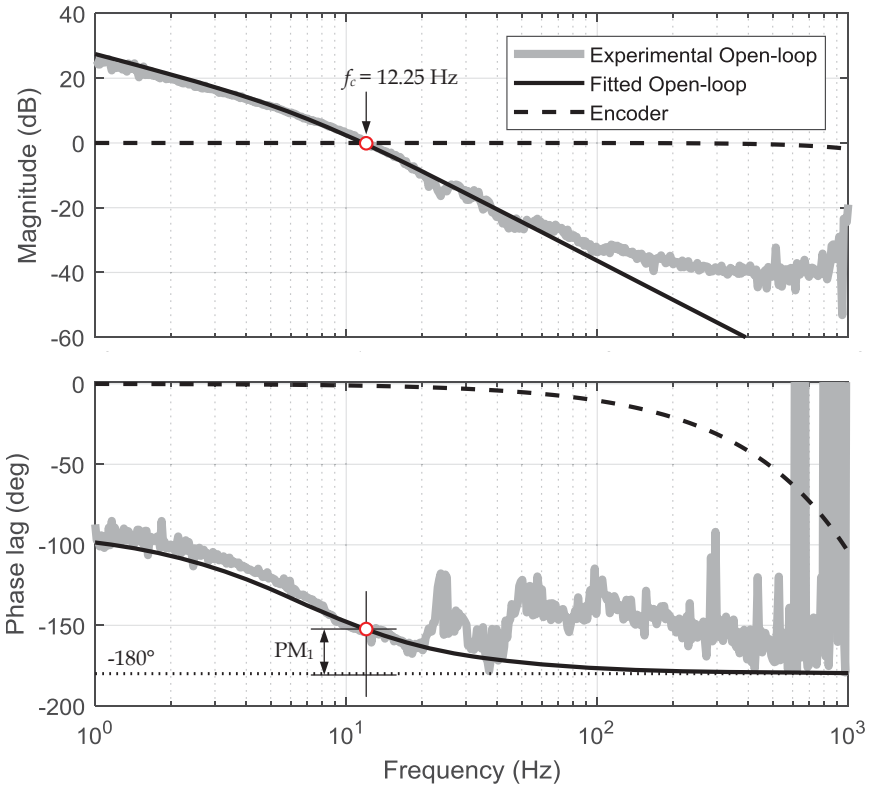

Figure 5.8 Fitting of the experimental results.

The experimental results are valid up to 20 Hz. Beyond this value the results are noisy and are out of the bandwidth of the system under study. The diagram of the system at low speed is depicted in Figure 5.9.

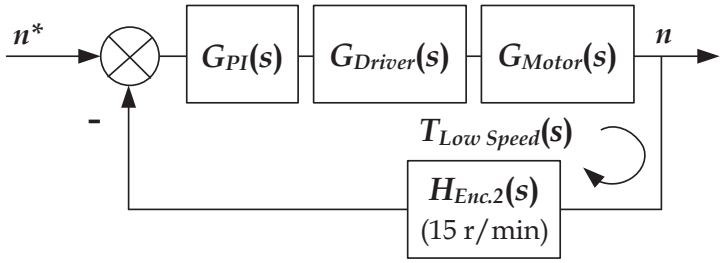

Figure 5.9 Block diagram of the motor system at very low speed (0.0125 tr./T_s).

The stability of the motor system at low speed is obtained from the experimental gain-loop (5.1) and the small-signal model of the ET method developed in chapter 3 ($H_{Enc.2}(s)$).

$$T_{fitting}(s) = G_{PI}(s) \cdot G_{Driver}(s) \cdot G_{Motor}(s) \tag{5.2}$$

$$T_{Low}(s) = T_{fitting}(s) \cdot H_{Enc.2}(s) \tag{5.3}$$

The representation of (5.3) in the frequency domain is depicted in Figure 5.10.

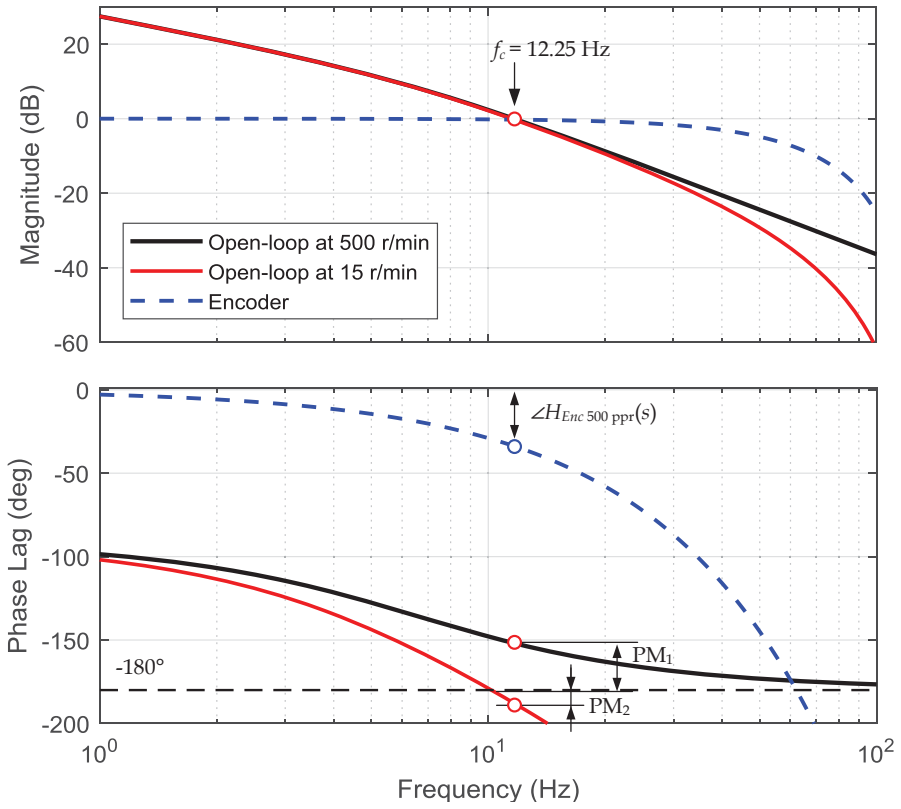

Figure 5.10 Gain-loop diagram of the motor system at very low speed (15 r/min) with a low resolution encoder (500 ppr)

The phase margin, PM_2, of the predicted motor system open-loop at the speed of 15 r/min is -8.54°. This negative value anticipates a poor performance of the system at such speed.

5.2.2 Evaluation of the Performance of the System at Low Speed

The stability of the system is studied in the time domain by means of the speed step response from a stable speed of 300 r/min (0.25 tr./T_s) to the very low speed of 15 r/min (0.0125 tr./T_s) using the ET method. The amplitude of the speed ripple is 1.76 % of the average speed (300 r/min), as in Figure 5.11.

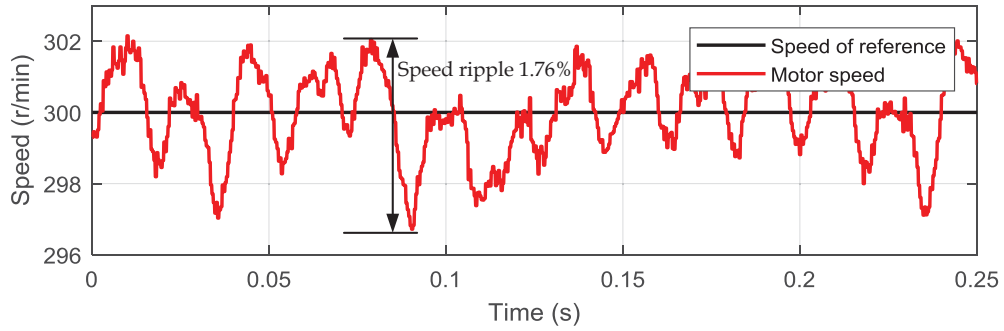

Figure 5.11 Details of the performance of the DC motor at 300 r/min with R = 500 ppr.

This test is performed in two different conditions:

- With knowledge of the sign of the rotation. This is the case if both channels of the encoders are used in quadrature configuration and the direction of the rotation is detected by the phase shift of the two channels.
- Without knowledge of the sign of the rotation. This is the case if the encoder has a single channel.

The sign of the rotation indicates the direction of the rotation: clock-wise or counter-clockwise. During variations of the target speed, the motor could rotate in the opposite direction during a short period of time because of the inertia. This change in the rotation is indicated with the sign of the estimated speed and is corrected by the controller. However, if the direction of the rotation is not detected (if only one channel is used) the controller, that operates only based on the information of the absolute value of the speed, does not correct the change in the direction of the rotation. Even more, if the absolute value of the speed is different from the target speed the controller attempts to correct the speed deviation, but this in fact reinforces the incorrect behaviour leading finally to motor control instability.

Figure 5.12 shows the experimental response of the motor system when a single encoder channel is available, so the direction is unknown. In this condition, the response of the motor system to the speed step is to jump to the maximum speed, which is conditioned by the maximum value of the power supply and the maximum speed of the

motor. However, in the experimental results depicted in Figure 5.12 the change in the direction of the rotation, after the reduction of the commanded speed, is not noticed.

In real applications with an incremental encoder of a single channel, this situation can damage the motor system. Therefore, precautions must be taken to avoid this type of motor response.

Figure 5.13 shows the response of the motor to the speed step test with an encoder of two channels in quadrature configuration. In this case the configuration of the encoder allows the detection of the direction of the rotation. In this case the reduced phase margin (PM_2) produces an oscillation around the target speed of 15 r/min.

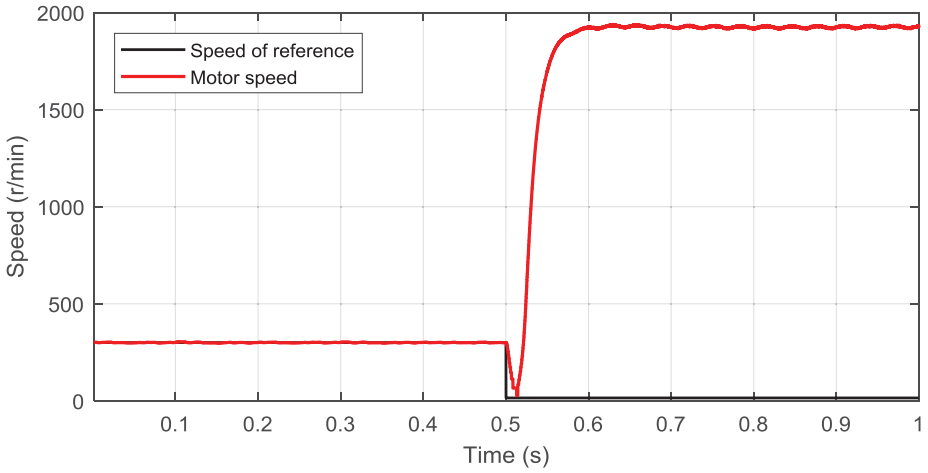

Figure 5.12 Motor response to the speed step test with an encoder in the feedback network without knowledge of the sign of the rotation (experimental results). Notice that the motor rotates backwards although the depicted results have a positive sign. In this case the encoder has a single channel and provides information about the absolute value of the speed only.

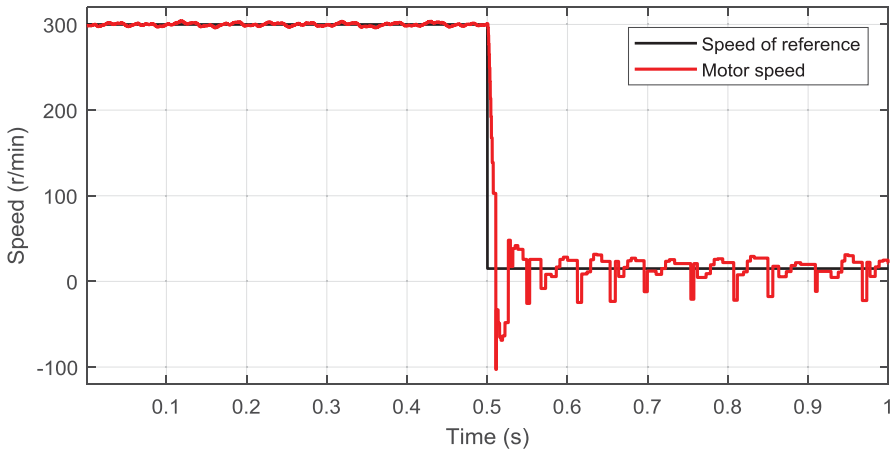

Figure 5.13 Motor response to the speed step test using an encoder in the feedback network with knowledge of the sign of the rotation (experimental results).

In either case: the use of a single channel or the quadrature configuration of the encoder, the reduced PM_2 = -8.54° provokes an incorrect performance of the motor.

5.2.3 The Lead Compensator

The solution proposed in this thesis to recover the performance of the motor consists of boosting the phase that is reduced by the low resolution encoder at the low speed. This can be done by means of a classical lead compensator [68] placed in the feedback network, as in Figure 5.14. $T_{compensated}(s)$ is referred to hereinafter as the open-loop transfer function with compensator.

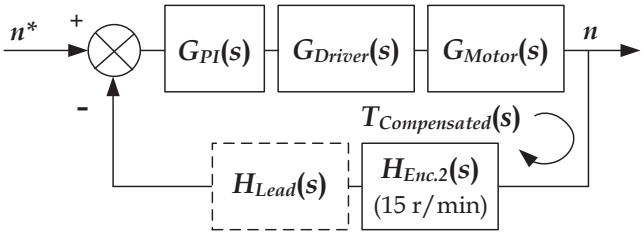

Figure 5.14 Propose lead compensator.

This compensator cancels mathematically the negative impact of the incremental optical encoder on the phase margin.

$$T_{Low}(s) = T_{fitting}(s) \cdot H_{Enc.2}(s) \cdot H_{Lead}(s) \tag{5.4}$$

The transfer function of the lead compensator is:

$$H_{Lead}(s) = \frac{1+\frac{s \cdot T_{Speed}}{\alpha}}{1+\frac{s \cdot T_{Speed}}{\beta}} = \frac{\frac{T_{Speed}}{\alpha}}{\frac{T_{Speed}}{\beta}} \cdot \frac{\frac{\alpha}{T_{Speed}}+s}{\frac{\beta}{T_{Speed}}+s} = \frac{\beta}{\alpha} \cdot \frac{\frac{\alpha}{T_{Speed}}+s}{\frac{\beta}{T_{Speed}}+s} \tag{5.5}$$

The values of α and β determine the distance between the phase lead and the phase lag. The term T_{Speed} defines the frequency and the amount of phase lead applied to this frequency. This term is related to the commanded speed. Consequently, parameters of the lead compensator adapt online to provide the required compensation to the specific operating point. Figure 5.15 shows the bode plot of the lead compensator.

$$T_{Speed} = \frac{1}{n* \cdot \frac{R}{60}} \tag{5.6}$$

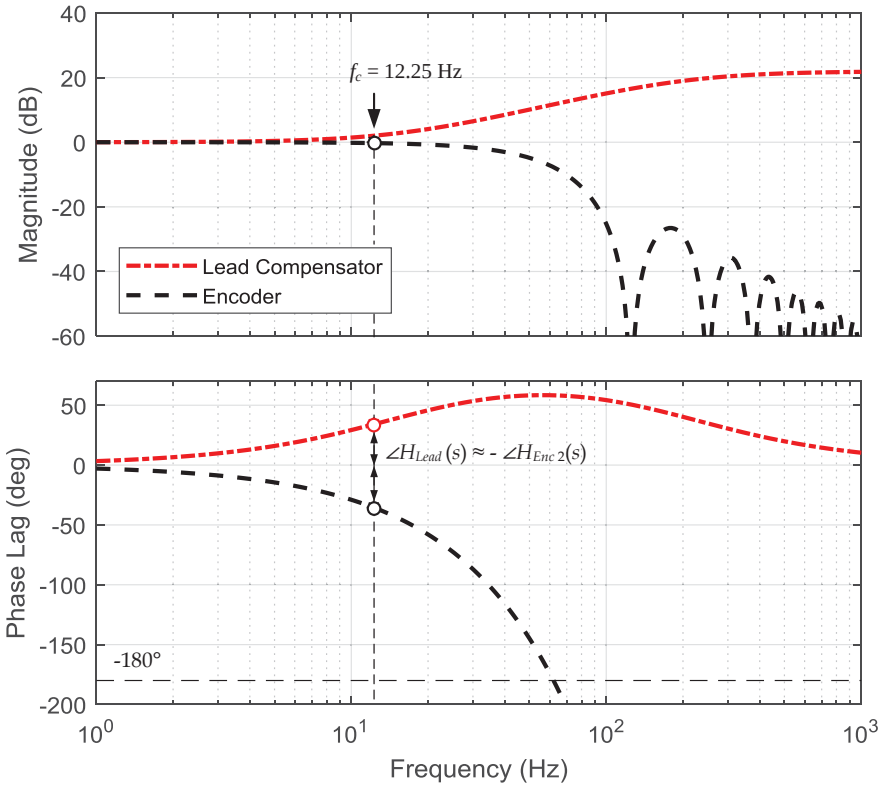

Figure 5.15 Transfer function of the lead compensator.

Figure 5.15 shows the transfer function of an encoder of resolution 500 ppr at a speed of 15 r/min, and the corresponding lead compensator with α = 0.8 and β = 10. These values are selected to provide the required compensation at the crossover frequency (f_c). It must be considered that the lead compensator should not significantly impact on the gain of the feedback sensor over the frequency range of interest; otherwise, the noise will be amplified and the closed-loop performance will be compromised when occurs, the gain has been lifted by 10 dB (in this case). In consequence, α and β should be selected to guarantee that the maximum injection of phase occurs beyond f_c.

As can be observed, the amount of phase compensation $\angle H_{Lead}(s)$ is almost equal to the delay introduced by the encoder $\angle H_{Enc.2}(s)$ at the crossover frequency. As for the increment of gain introduced by the compensator, it is attenuated by the gain-loop at that speed.

The lead compensator must be discretized before being implemented in the ADSP. For this purpose, (5.5) is redefined as a function of the terms: *kk*, *c* and *p*.

$$H_{Lead}(s)=\frac{\beta}{\alpha}\cdot\frac{\frac{\alpha}{T_{Speed}}+s}{\frac{\beta}{T_{Speed}}+s}=kk\cdot\frac{c+s}{p+s}\quad\begin{cases}kk=\dfrac{\beta}{\alpha}\\ c=\dfrac{\alpha}{T_{Speed}}\\ p=\dfrac{\beta}{T_{Speed}}\end{cases}\tag{5.7}$$

The process of discretization starts with:

$$Hd(z)=\frac{z-1}{z}\cdot Z\left\{\frac{H_{Lead}(s)}{s}\right\}\tag{5.8}$$

The discretization procedure of the lead compensator is in Annex A. The final discrete expression of the lead compensator is:

$$\begin{aligned}&Hd(z)=\frac{kk\cdot z+b}{(z-a)}\\ &\text{where}: b=\frac{kk\cdot\alpha}{\beta}\cdot(1-a)-kk;\ a=e^{-\frac{\beta}{T_{Speed}}\cdot T};\ kk=\frac{\beta}{\alpha}\end{aligned}\tag{5.9}$$

Notice that the constants *kk*, *b* and *a* depends on α , β and T_{Speed} as in (5.6). Coefficients α , β are fixed for this application; in all speed ranges, only T_{Speed} varies with the commanded speed. The term *T* is the discrete sampling time.

5.2.4 Simulation of the Lead Compensator

The performance of the lead compensator was simulated as depicted in Figure 5.16.

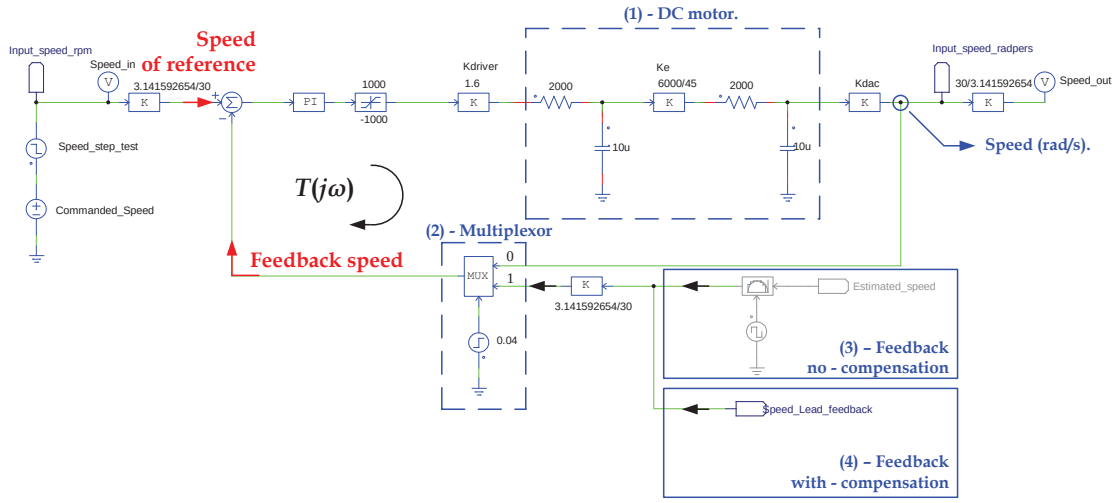

Figure 5.16 Main parts of the simulated motor system in PSIM. The simulation time step is $1.6\cdot10^{-6}$ s. Notice that for feedback purposes either block 3 or block 4 is used.

The diagram of Figure 5.16 simulates the dynamics of the motor and the motor control under study. The overall open-loop transfer function $T(j\omega) = T_{fitting}(s)$ as in (5.1). There are four main blocks.

1. **The first block** corresponds to the DC motor. The motor is mathematically represented by a second-order system of two poles, which in this case is simulated by means of two low-pass filters.

2. **The second block** is a multiplexor. Initially, the system starts the simulation using the ideal feedback (multiplexor output is connected to input 0). After 0.04 s, the control switches to the feedback coming from the speed estimation based on the signal of the incremental optical encoder (multiplexor output is connected to input 1). As can be seen in Figure 5.16.

   During the start-up, the motor has to overcome the friction and it takes several seconds to start the rotation ($t_{start\text{-}up}$). Hence, the encoder does not provide any feedback during this start-up time interval. However, $t_{start\text{-}up} > T_s$ (Figure 5.17) and the integral part of the controller increases sufficiently to destabilize the system. This problem is also found experimentally in the DC motor system at low speed.

   As a protection, the output of the PI is limited to – 1000 and 1000 in the simulation.

3. **The third block** corresponds to the encoder and the implementation of the Elapsed Time speed estimation method as depicted in Figure 5.18. The implementation of the ET method is already explained in chapter 2. This block does not include lead compensation unlike the fourth block.

Blocks three and four are used in different types of simulations, the grey colour in Figure 5.16 indicates that this block is not in use. Block three is used for a non-compensated simulation and block four is used in a compensated simulation.

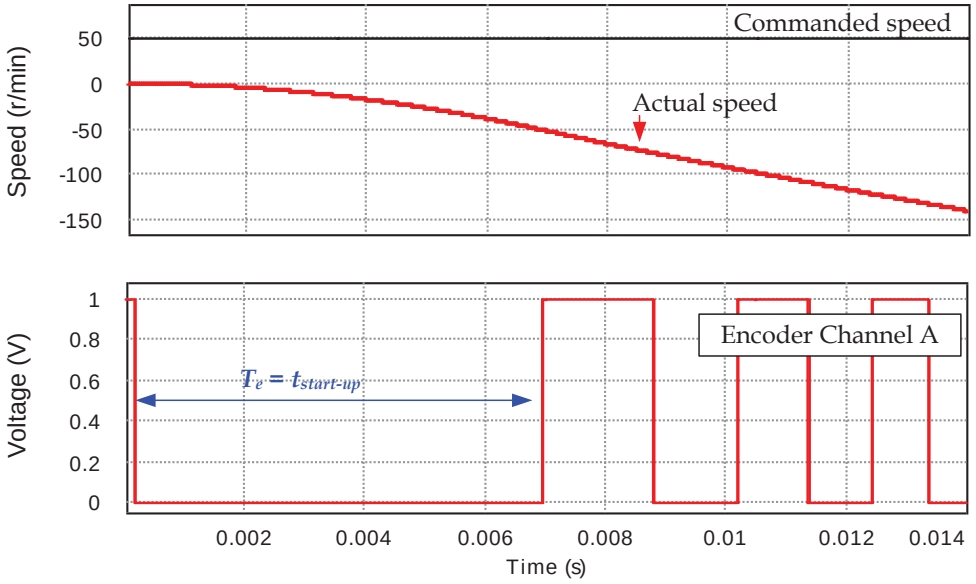

Figure 5.17 Details of the encoder and speed estimation during the motor start-up.

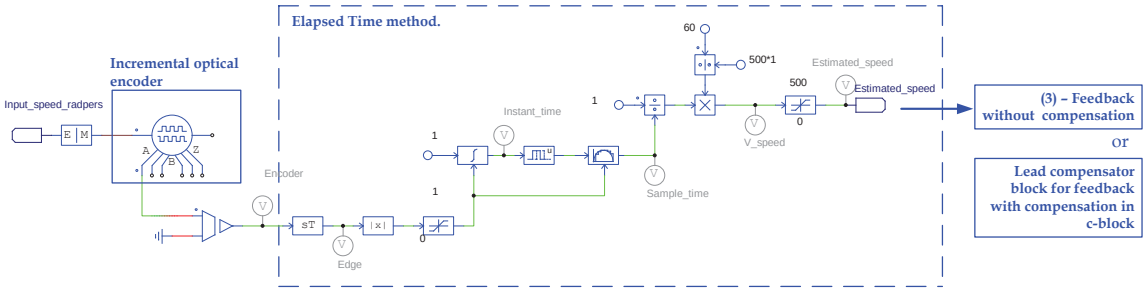

Figure 5.18 Encoder signal generation and ET speed estimation.

4. **The fourth block** is the controller and the lead compensation. The effect of the discrete control sample time, T_s = 0.1 ms, is already included in the corresponding c-block. The digital lead compensator and the controller implemented in the c-block, as in Figure 5.19.

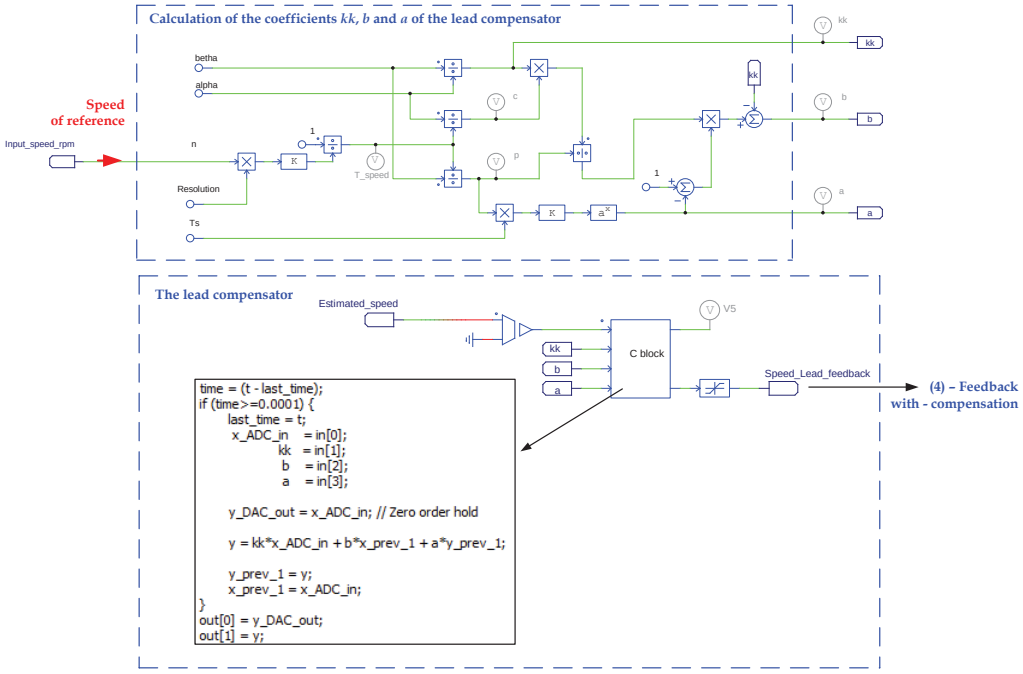

Figure 5.19 Lead compensation block. The coefficients *kk*, *b* and *a* depend of the speed reference value (signal named *Input_speed_rpm*) which is proportional to T_e.

A more general diagram of the system configuration for the speed step response test is depicted in Figure 5.20.

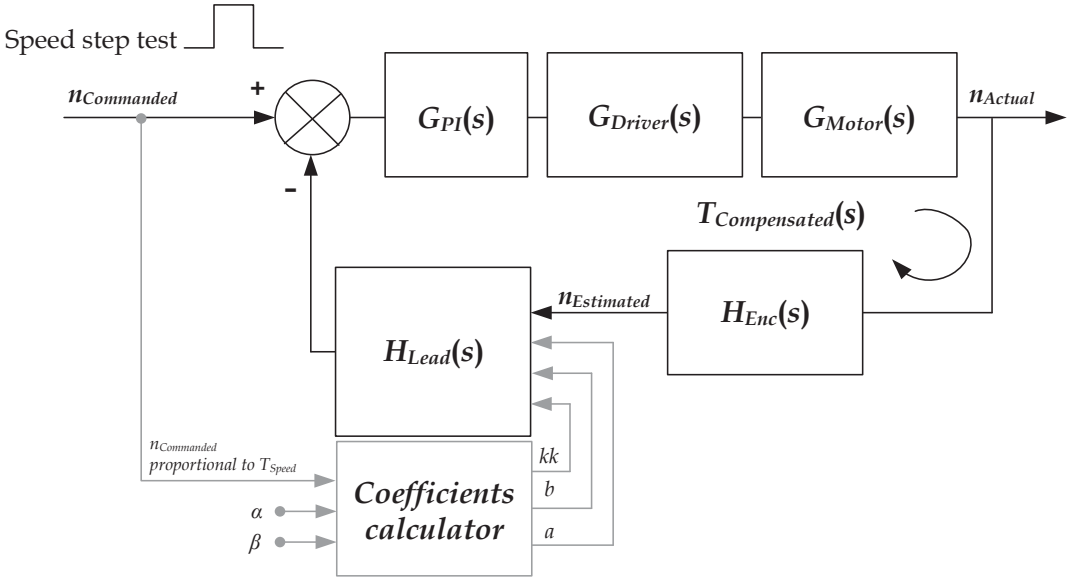

Figure 5.20 Block diagram of the compensated system. The coefficient calculator box has the mathematical operations to obtain the coefficients *kk*, *a* and *b* as in (5.9).

The coefficients of the lead compensator ($H_{Lead}(s)$), as defined in equation (5.9), are *kk*, *a* and *b*. Those values depend of the fixed terms α and β and the commanded speed $n_{Commanded}$ (which is proportional to T_{Speed} that is equal to T_e). The term T_{Speed} adjusts the amount of lead compensation to the specific f_c that varies when the commanded speed is modified.

The coefficients (*kk*, *b* and *a*) adapt to the specific commanded speed when it varies, providing the phase compensation for the lag introduced by the encoder at that specific speed. The input of the lead compensator is the estimated speed and the output is the compensated estimated speed that is subtracted to the commanded speed.

Figure 5.21–(b) shows the response of the simulated motor system considering a quadrature encoder and Figure 5.21-(c) is the response of the system when using a single channel encoder.

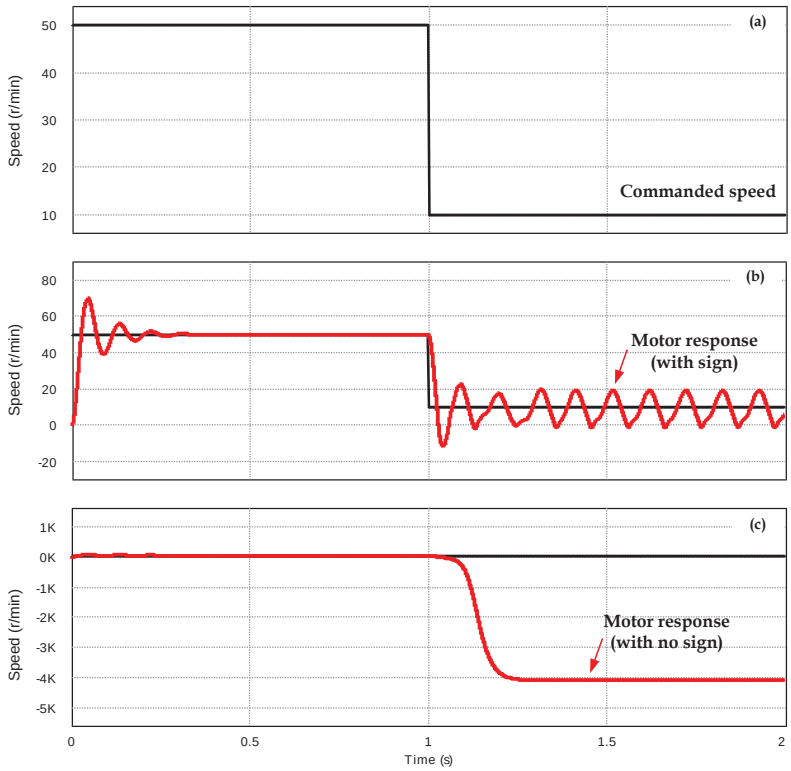

Figure 5.21 Simulation results of (a) speed reference step test, (b) response of the motor with knowledge of the sign of the rotation and (c) without knowledge of the sign of the rotation. In both cases (b) and (c) the system is not compensated.

The motor, simulated in Figure 5.21-(b), with the encoder in quadrature configuration (knowledge of the rotation direction) oscillates around the target speed. This simulation corresponds with the experimental results observed in Figure 5.13 previously shown. Also, the simulation in Figure 5.21-(c) shows the motor behaviour when a single channel of the encoder is used for the feedback. This result matches with the experimental results shown in Figure 5.12.

These incorrect performances (destabilization and oscillations around target speed) are caused by a significant reduction of the phase margin of the control loop because of the impact of the dynamic of the encoder at low speed, especially with low resolution

encoders. The phase margin reduction due to the sensor can be quantified by using the small-signal model for the ET method discussed in chapter 3. Section 5.2.1 details the procedure to use the small-signal model and also presents the way to overcome the phase margin reduction and consequent deterioration of the motor performance.

Figure 5.22 shows a reduction of the phase margin from PM_3 to PM_2 as the speed reduces from 500 r/min to 15 r/min, with a resolution of 500 ppr. The reduced PM_2 provokes a deterioration of the performance. However, a lead compensator with coefficients $\alpha = 0.8$, $\beta = 10$ and $T_{Speed} = 8$ ms boost the phase margin to PM_3 recovering the system stability ($PM_3 = 25.5°$).

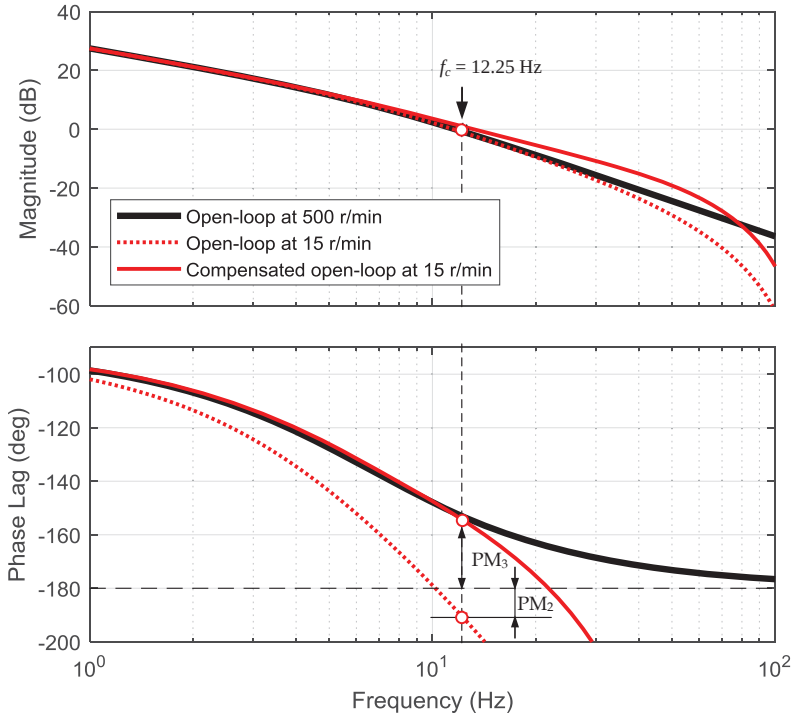

Figure 5.22 Bode plot of the open-loop compensated system.

The stability of the compensated system is also tested in simulation by introducing increasing and decreasing speed step tests with increments of 20 r/min starting at the speed of 13 r/min (0.011 tr./T_s). Note that this speed is chosen for didactic purposes.

Figure 5.23 shows first the response of the uncompensated system. The system oscillates at the speed of 13 r/min because of the reduced phase margin. The phase margin increases as the speed increases and the performance of the motor improves.

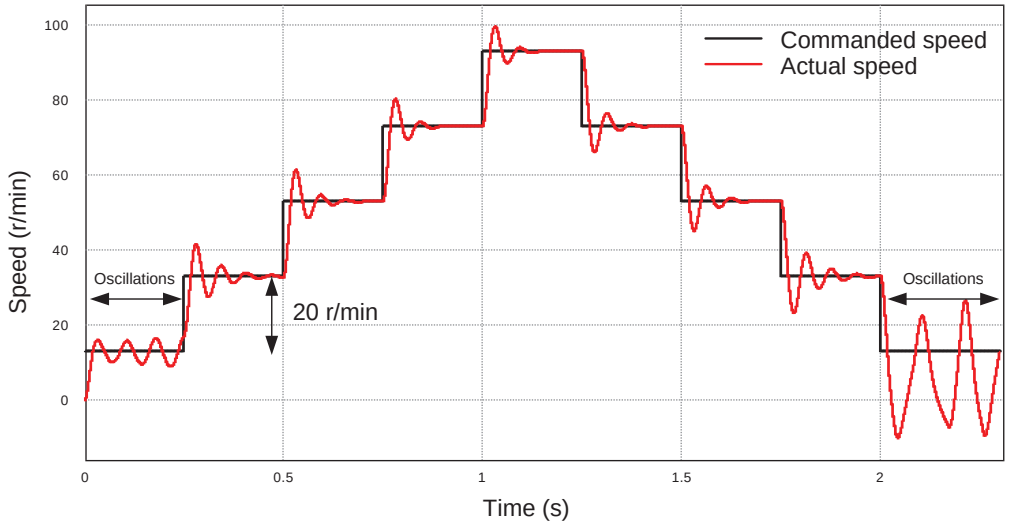

Figure 5.23 Simulation of the speed step test response of the uncompensated system.

Figure 5.24 shows the simulation that corresponds to the compensated system. The system recovers the correct performance at the speed of 13 r/min. As the speed increases, the bandwidth of the encoder and the lead compensator increases as well. However, the overall and predominant dynamics is delimited by the bandwidth of the closed DC motor system.

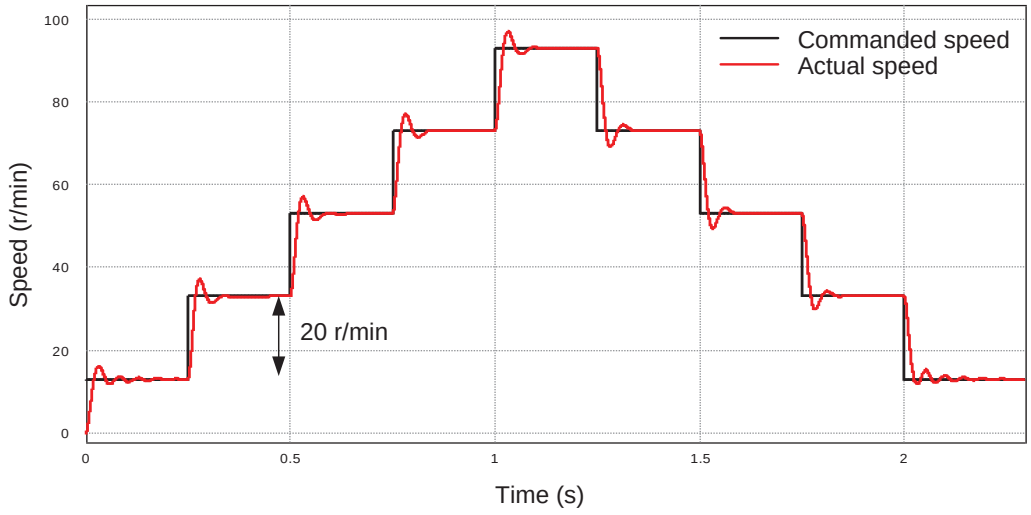

Figure 5.24 Simulation of the speed step test response of the compensated system with adaptive lead compensator.

Figure 5.25 shows the response of the system for a fixed *kk*, *a* and *b* parameters. The lead compensator is fixed to $T_{Speed} = 60 / (13 \text{ r/min} \cdot 500 \text{ ppr})$ in this simulation. As can be seen, the oscillation at that speed of 13 r/min disappears. As the commanded speed increases the lead compensator, together with the PI regulator, overdamps the response of the DC closed-loop system.

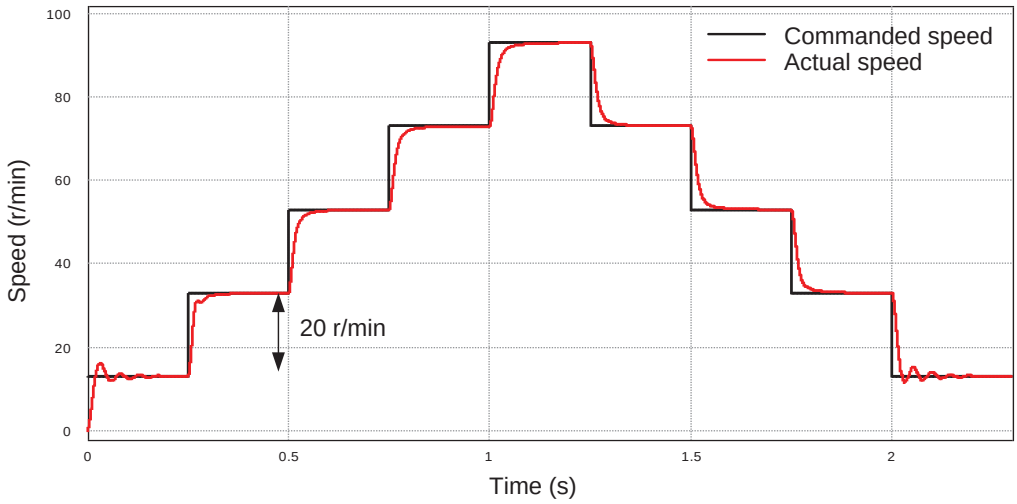

Figure 5.25 Simulation of the speed step test response of the compensated system where the lead compensator is fixed to 13 r/min.

5.2.5 Experimental Validation of the Lead Compensator

The discrete lead compensator proposed in (5.9) and simulated with a c-block in PSIM (see Figure 5.19). It is also implemented in the ADSP that controls the motor. The experimental results are depicted in Figure 5.26.

Figure 5.26 - (a) shows the results of the estimated speed after the speed step test are stored in the memory of the ADSP and later exported to the PC. Figure 5.26 - (b) shows the details at the speed of interest, 15 r/min.

It is experimentally validated that the lead compensator recovers the system performance previously degraded by the encoder phase lag.

Then, it can be concluded that the encoder degrades the performance of the motor system as the speed reduces because of the phase lag. This is quantified with the developed small-signal model. It was shown that this phase lag can be compensated if the phase margin of the open-loop system is boosted. The phase-margin can be increased with a lead compensator. However, other techniques, not explored in this thesis, can be valid as well. A Type III compensator [69] could be compared or combined with the lead compensator, a feedforward technique [70] and [71] or a gain scheduler control scheme [72] could be used to improve the transient performance over all speed range.

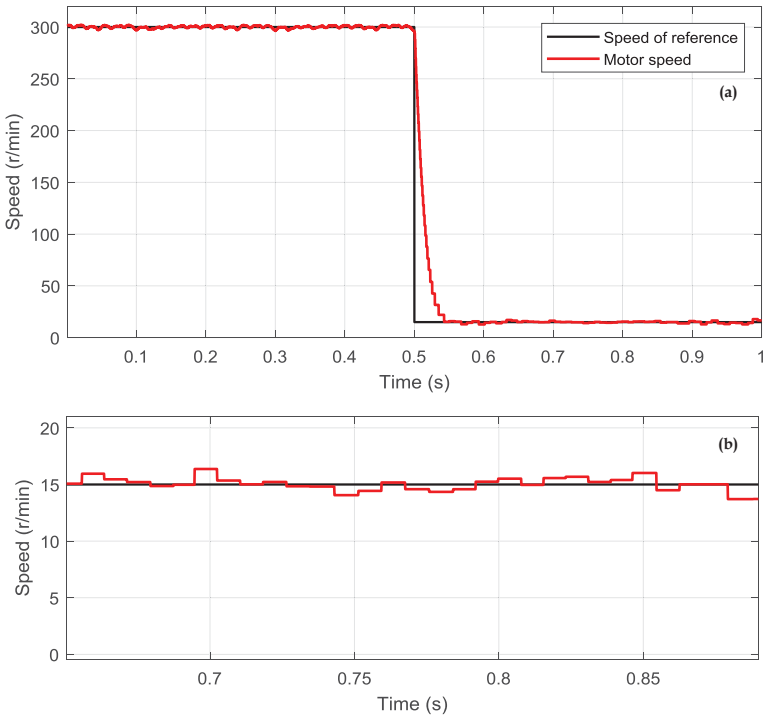

Figure 5.26 (a) Actual motor response to speed step test. Data of the speed estimation stored in the ADSP and later exported to the PC. (b) Details of the performance at low speed 15 r/min.

5.3 Part II. Experimental validation of the I-ET and I-ET-S Methods in Closed-Loop

In this section, the performance of the I-ET and the I-ET-S methods are compared with other baseline speed estimation methods that are: the PC, the ET and the CDST methods. The performance of each method is evaluated as the capability of tracking different speed profiles (sinusoidal, triangular and square) in a closed-loop configuration. For this purpose, the speed of reference of the control loop in commanded by the Analog Discovery unit connected to the ADSP as in Figure 5.27.

An encoder of 1000 ppr in quadrature configuration is used for the test. The maximum speed is 2300 r/min, which corresponds to 153 tr./T_s, with a sample time of 1 ms. The minimum evaluated speed is 240 r/min, corresponding to 16 tr./T_s. As indicated in Figure 5.27, the estimated speed is transformed into an analog voltage by the DAC of the ADSP. The first channel of the scope CH1 (yellow) represents the commanded speed and the second channel of the scope CH2 (blue) represents the estimated speed according to the chosen method.

The aim of Part II is to test the performance of the proposed I-ET and the I-ET-S methods in closed-loop conditions and to compare them with base line methods: the

CPSD, the PC and the ET methods. These two speed estimation methods are analysed theoretically and in open-loop conditions in chapter 4. Experimental results for a sinusoidal speed profile are depicted in Figure 5.28.

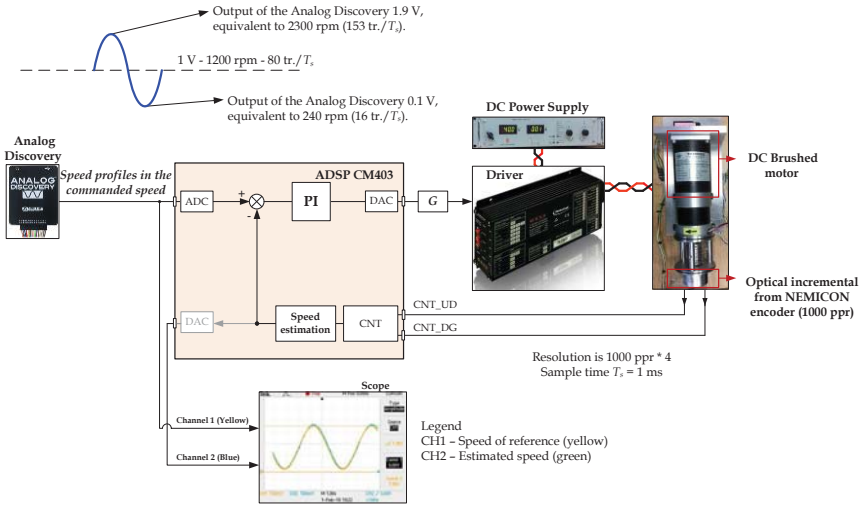

Figure 5.27 Experimental setup for the evaluation of the different speed estimation methods: the CSDT, the PC, the ET, the I-ET and the I-ET-S methods.

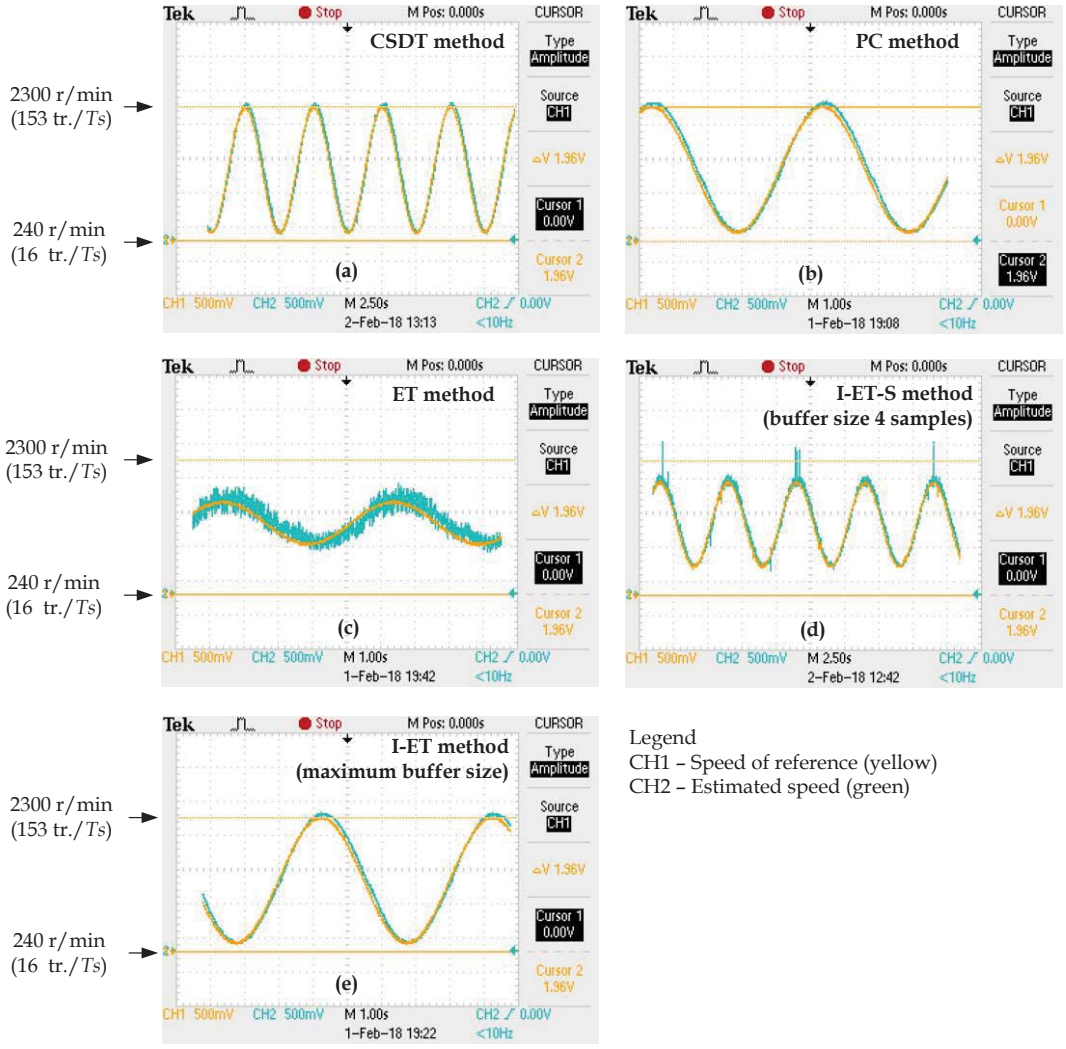

Figure 5.28 Experimental results of the methods tracking a sinusoidal speed profile.

In Figure 5.28 the base line CSDT (a) and PC (b) methods can operate in all speed range under study (from 16 tr./T_s to 153 tr./T_s). However, the ET (c) method shows a significant amount of noise because of the real encoder asymmetries. The noise causes the ET method to be inoperable at higher speed. The I-ET-S in (d) reduces the noise but not enough for the system to operate between 16 tr./T_s to 153 tr./T_s. Finally, (e) shows that the I-ET method can perform at all speed range as the CSDT and the PC methods.

Figure 5.29 shows the test for a triangular speed profile.

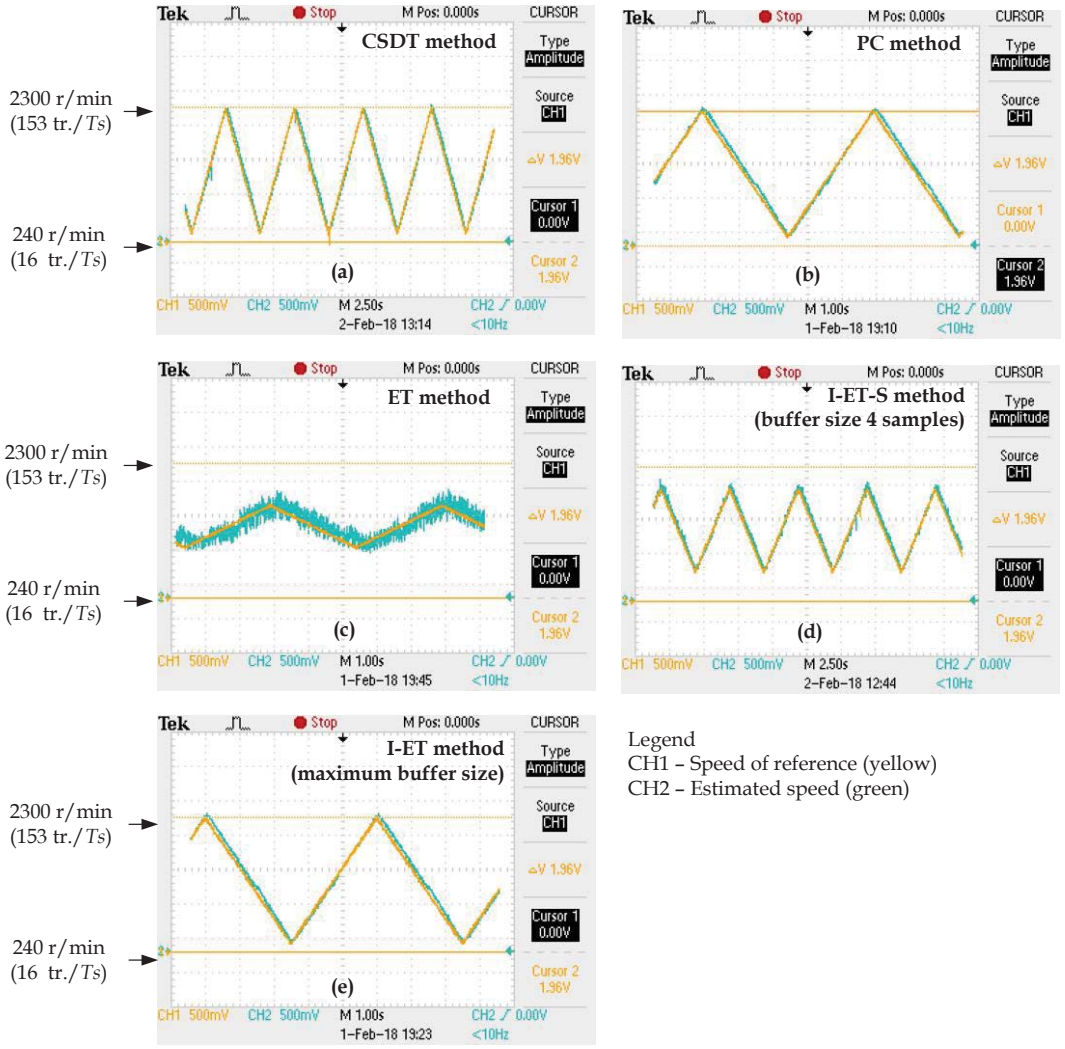

Figure 5.29 Experimental results of the methods tracking a triangular speed profile.

Figure 5.29 show that the CDST (a) and the PC (b) methods perform correctly in closed-loop for a triangular speed profile. Similarly, the ET method (c) presents excessive noise; and the I-ET-S method reduces the noise but not enough, as in Figure 5.28 (c) and (d). The I-ET speed estimation method in Figure 5.29 (e) has a good performance in closed-loop when tracking a triangular speed profile.

Figure 5.30 shows the results the different methods tracking a square signal.

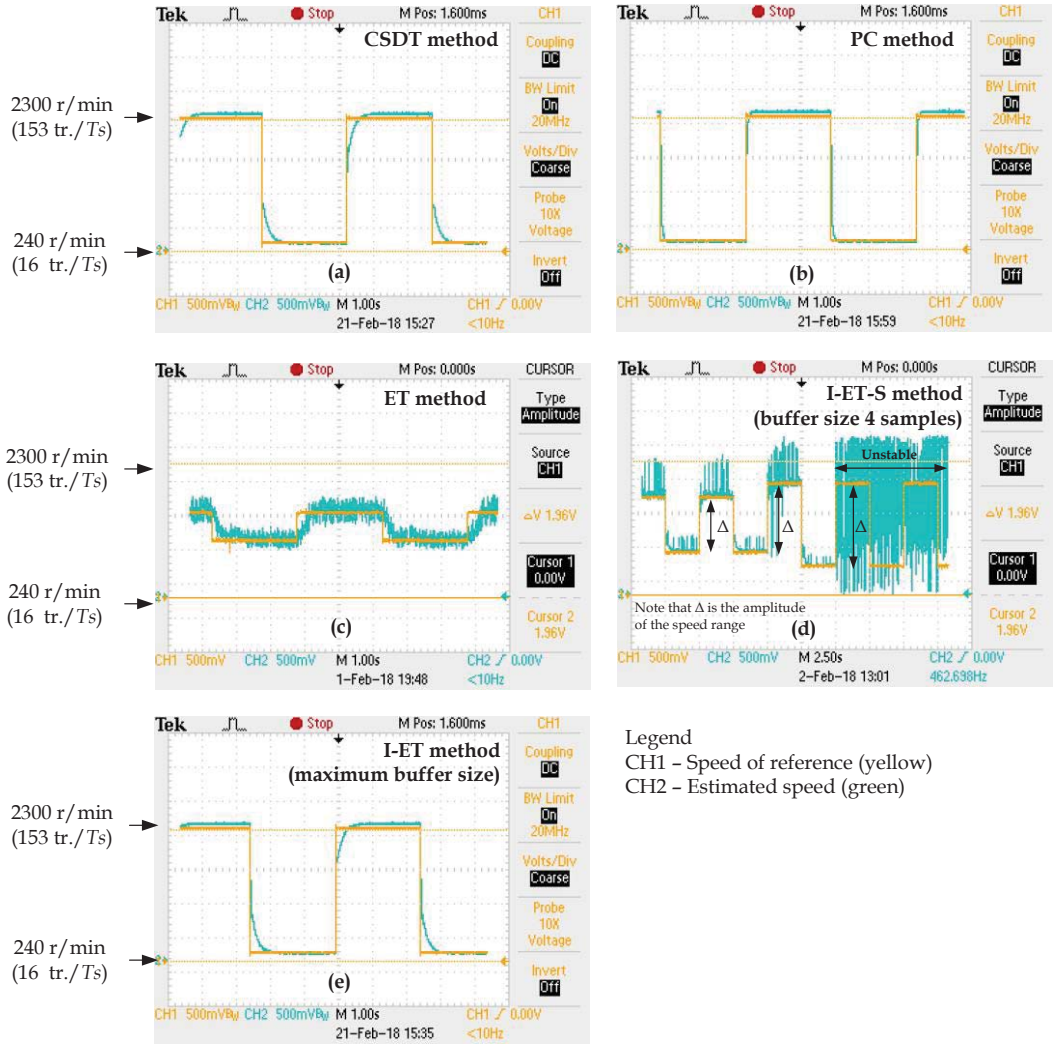

Figure 5.30 Experimental results of the methods tracking a square speed profile.

Figure 5.30 shows that the CSDT (a), the PC (b) and the I-ET (c) methods can track correctly a square speed profile in closed-loop, unlike the ET method (c) because of the noise and the I-ET despite the noise reduction.

In addition, Figure 5.30 (d) shows that the I-ET-S method cancels the noise; nevertheless, as the amplitude of the signal to track (that is proportional the speed range to track) increases, this noise cancelation is not sufficient producing the destabilization of the motor system.

Regarding the dynamic performance of the CSDT, the PC and the I-ET method cannot be compared based on the results of this test because the PI of the control loop of each method was tuned with different constants to achieve a good response individually. This topic is covered in chapters 3 and chapter 4 and more experimental testing, in the closed-loop, is required to thoroughly compare these methods.

5.4 Conclusions

Throughout this chapter, the practical application of the developed contents in this thesis has been demonstrated with a physical workbench and through standard tests. It has been demonstrated that:

- The developed small-signal models of the encoders and the speed estimation methods can be used to first predict quantitatively the impact of the sensor on the control loop. Moreover, the model can be used to design a compensation technique to overcome the negative impact of a low resolution encoder at low speed in an inexpensive manner.
- Secondly, it is shown that the reported asymmetries of the incremental optical encoder can be compensated by averaging samples multiple of four samples. This extends the use of the well-known ET method to high speed. This result is particularly useful in variable speed applications. The static error of the I-ET method is comparable to other methods like the CSDT and the PC methods.

Chapter 6. Conclusions

6.1 Conclusions and Summary of Original Contributions

This thesis arises from an industrial problem formulated by the enterprise supervisor from Analog Devices that partially sponsored the work.

- *Poor motor performance is observed at low speed when a low resolution encoder is employed in the feedback network.*

The research to find the cause of this problem led to the following major contributions of this thesis.

1- Small signal modelling of optical incremental encoders in conjunction with the used speed estimation method. The speed estimation methods covered in this thesis include Elapse Time (ET), Pulse Count (PC) and Constant Sampled-Time Digital Tachometer (CSDT).

2- Improvements of the Elapse Time method (I-ET) to extend its use at high speeds (with more than one encoder transition per sample time) in quadrature configuration. This method can be particularly convenient for variable speed applications.

Additional contributions:

3- A method and experimental setup used to evaluate experimentally the dynamic response of an encoder, including the speed estimation method, based on the use of Voltage Controlled Oscillators (VCO).

4- Utilization of lead compensators to compensate for the phase lag of encoders at low speeds predicted by the developed small-signal model. This is particularly useful in motion control at low speed.

The conclusions associated to those contributions are described below.

6.1.1 Small-signal Modelling

The incremental optical encoder is a nonlinear sensor. In order to develop a model, small-signal perturbations are superimposed on a certain operating point. This method is typically applied to develop dynamic models of power supplies.

The mathematical models demonstrate that the encoder introduces a phase lag in the speed estimation signal used in the feedback network of the motor control. At low speed, the ET method is typically used. The dynamics of the sensor operating with this method depend on the resolution and the speed. As these two parameters decrease the phase lag increases and the phase margin of the control loop is reduced; leading to the deterioration of the motor system performance.

At high speeds PC and CSDT are typically used. In both cases, the dynamic response depends on the control sample time.

It is worth making the following observation: the developed small-signal model shows that two signals, with different frequencies, drift from each other. The delay between the two signals varies uniformly (t_d) and can be modelled by a pure delay $e^{-s \cdot td}$, with no impact on the magnitude. This difference of frequency in two signals is found, for instance, between the encoder signal and the high frequency clock of the CNT peripheral. This was validated experimentally in chapter three.

The proposed experimental setup described in chapter three is used for the emulation of the encoder behaviour. The setup is based on a VCO and is the pillar of the theory behind the small-signal models developed in this thesis. It allowed the validation of the small-signal model without the models being affected by the motor and the motor drive dynamics.

The usefulness of the developed small-signal model for low speed has been demonstrated in chapter 5 through a practical case. As an example, it has been shown that low resolution encoders (500 ppr) can limit the dynamic performance of the system below 100 rpm. At 15 rpm, the encoder imposed a phase lag of -36.97° at 12.25 Hz.

The small-signal model has been used to predict such reduction of phase margin and to support a control design. In order to alleviate the observed phase lag due to the encoder, a digital lead compensator is proposed. This is an inexpensive method to recover the system performance. The coefficients of the lead compensator can be adapted

instantaneously to the commanded speed, providing the correct compensation for different commanded speed. Some work has to be done in this matter to explore alternative solutions in order to be able to compare different methods and to choose the optimum compensator.

6.1.2 The Improved Elapsed Time (I-ET) Method for High Speed

The small-signal models were developed and validated for high, medium and low speeds for the PC, ET and CSDT methods. The ET method exhibits the best dynamic behaviour. The small-signal model of the ET is valid for all speed intervals. However, in practice, this method is not effective particularly in quadrature configuration mode. This is the second dilemma that directed to the second major contribution also derived from an industrial problem:

- *The ET method has the best dynamic performance of all methods as demonstrated in chapter 3. However, it cannot be used in quadrature configuration because the real encoder asymmetries, which implies that the natural resolution of the encoder cannot be electrically increased in a factor of four. Additionally, a lower resolution implies a lower bandwidth of the sensor. Furthermore, the quadrature configuration is paramount for the detection of the rotation during transients, as demonstrated in chapter 5.*

It was found that such degraded performance of the ET method at high speed, in quadrature configuration, is caused by the asymmetries of the signals in the two channels. This problem is described in the technical specification of the encoder manufacturer.

The asymmetries are periodic over four consecutives samples (a full electrical period of each channel). It is also reported that the asymmetries are produced by tolerances in the associated electronics. The asymmetries result in noise superimposed on the average value of the speed.

In order to address this limitation, in this thesis an extension of the ET method in quadrature configuration is proposed. Instead of using the last transition for speed estimation within a control sampling interval, the average of the time elapsed in the last N transitions is proposed, where N is a multiple of four. This method is named I-ET.

The I-ET method has been derived from the observation that the noise pattern caused by asymmetries is repeated every four transitions with the conventional ET method. Therefore, by using four transitions for averaging, or an integer multiple of four transitions, the impact of the asymmetries is mitigated.

The small-signal model of the I-ET method has been developed. It is observed that the phase lag increases as N increases. The phase lag is also related to the number of transitions used for estimation in proportion to the total number of transitions within a control sampling period.

The I-ET method has been implemented on the ADSP and evaluated experimentally on the workbench. Its performance was evaluated considering the capability of the method when tracking different speed profiles in closed-loop configuration. The method has been also compared with the PC, CSDT and ET methods which were the baseline methods. The experimental results demonstrate that the I-ET significantly reduces the error due to the asymmetries and its performance is similar to the performance of the PC and CSDT method at high speed in terms of static error.

This result is particularly relevant for variable speed applications since the combination of multiple speed estimation techniques is no longer required. In addition, the ET method can be used in quadrature configuration as the I-ET method, maximizing the effective encoder resolution, enabling the system to detect the sign of the rotation (clock or anticlockwise).

The main benefit of the proposed method is that it enables the use of the same speed estimation method for low, medium and high speed. Just the factor N needs to be adjusted. Today, in typical applications different methods are used for low, medium and high speeds.

The limitation of the proposed I-ET method found by the author is related to the implementation of the method. The vector of size N, containing the row data ($T_e[i]$), is simultaneously manipulated by the interrupt service routine associated (ISR) to the encoder transitions (with frequency $1/T_e$) and the controller (with frequency $1/T_s$). The number of stored samples, N, is averaged at each control sample instant. Precautions must be taken to avoid unexpected modifications of the vector by the ISR while the average of samples is being performed.

6.2 Future Work

The proposed future work is:

1. Extend the small-signal model to other sensors like magnetic encoders. The new sensor may have different and specific problems like magnetic pick-up in magnetic sensor that should be included in the new model.
2. Apply the developed small-signal model to a motor drive employing Field Oriented Control.
3. Evaluate the performance of the lead compensator with a load step test.
4. Implement compensation techniques alternative to the proposed lead compensator.
5. Determine the optimal value of the parameters α and β of the lead compensator.
6. Quantify the impact of the noise content in the speed estimated by the I-ET method in the harmonic content of the inner current control loop. Compare this to other estimation methods. Evaluate and correlate this harmonic content to the motor noise and overheating.
7. The implementation of the forecasting method proposed in chapter 4. This method is based on the identification of the asymmetries over four encoder transition in quadrature mode and the compensation of those values different from the expected average value. This method can potentially give a good compromise between a dynamic performance and static error.

Annex A. The discretization of the lead compensator

The lead compensator is redefined as a function of the terms: *kk*, *c* and *p*.

$$H(s)=\frac{\beta}{\alpha}\cdot\frac{\frac{\alpha}{T_{Speed}}+s}{\frac{\beta}{T_{Speed}}+s}=kk\cdot\frac{c+s}{p+s}\quad\begin{cases}kk=\dfrac{\beta}{\alpha}\\ c=\dfrac{\alpha}{T_{Speed}}\\ p=\dfrac{\beta}{T_{Speed}}\end{cases}\tag{1}$$

The process of discretization starts with:

$$Hd(z)=\frac{z-1}{z}\cdot Z\left\{\frac{H(s)}{s}\right\}\tag{2}$$

First, the expression (2) is transformed to the time domain.

$$\begin{aligned}L^{-1}\left\{\frac{kk\cdot\dfrac{s+c}{s+p}}{s}\right\}&=L^{-1}\left\{kk\cdot\frac{s+c}{s\cdot(s+p)}\right\}=kk\cdot L^{-1}\left\{\frac{s+c}{s\cdot(s+p)}\right\}\\&=kk\cdot L^{-1}\left\{\frac{s}{s\cdot(s+p)}+\frac{s}{s\cdot(s+p)}\right\}\\&=kk\cdot L^{-1}\left\{\frac{c}{s\cdot(s+p)}\right\}+kk\cdot L^{-1}\left\{\frac{1}{s+p}\right\}\\&=kk\cdot c\cdot L^{-1}\left\{\frac{1}{s\cdot(s+p)}\right\}+kk\cdot e^{-p\cdot t}\end{aligned}\tag{3}$$

$$L^{-1}\left\{\frac{1}{s\cdot(s+p)}\right\} \Rightarrow \frac{1}{s\cdot(s+p)}=\frac{A}{s}+\frac{B}{s+p} \quad \begin{cases} s=0 \\ s=-p \end{cases}$$

$$\frac{1}{s\cdot(s+p)}=\frac{A\cdot(s+p)+B\cdot s}{s\cdot(s+p)}$$

$$1=A\cdot(s+p)+B\cdot s \tag{4}$$

$$if\ s=0 \Rightarrow 1=A\cdot(0+p) \Rightarrow A=\frac{1}{p}$$

$$if\ s=-p \Rightarrow 1=B\cdot(-p) \Rightarrow B=-\frac{1}{p}$$

$$L^{-1}\left\{\frac{1}{s\cdot(s+p)}\right\}=L^{-1}\left\{\frac{1/p}{s}+\frac{-1/p}{s+p}\right\}=\frac{1}{p}\cdot L^{-1}\left\{\frac{1}{s}\right\}-\frac{1}{p}\cdot L^{-1}\left\{\frac{1}{s+p}\right\}$$

$$=\frac{1}{p}\cdot L^{-1}\left\{\frac{1}{s}\right\}-\frac{1}{p}\cdot L^{-1}\left\{\frac{1}{s-(-p)}\right\}=\frac{1}{p}\cdot 1-\frac{1}{p}\cdot e^{-p\cdot t} \tag{5}$$

$$L^{-1}\left\{\frac{kk\cdot\frac{s+c}{s+p}}{s}\right\}=kk\cdot c\cdot\left(\frac{1}{p}-\frac{1}{p}\cdot e^{-p\cdot t}\right)+kk\cdot e^{-p\cdot t}=\frac{kk\cdot c}{p}\cdot\left(1-e^{-p\cdot t}\right)+kk\cdot e^{-p\cdot t} \tag{6}$$

The next step is to transform the expression (6) into the discrete time domain.

$$H(t)=\frac{kk\cdot c}{p}\cdot\left(1-e^{-p\cdot t}\right)+kk\cdot e^{-p\cdot t} \xrightarrow{t=kT} H(kT)=\frac{kk\cdot c}{p}\cdot\left(1-e^{-p\cdot kT}\right)+kk\cdot e^{-p\cdot kT} \tag{7}$$

followed by the discretization of (7)

$$Z\{H(kT)\}=Z\left\{\frac{kk\cdot c}{p}\cdot\left(1-e^{-p\cdot kT}\right)+kk\cdot e^{-p\cdot kT}\right\}$$

$$=Z\left\{\frac{kk\cdot c}{p}\cdot\left(1-e^{-p\cdot kT}\right)+kk\cdot e^{-p\cdot kT}\right\}$$

$$=Z\left\{\frac{kk\cdot c}{p}\cdot\left(1-e^{-p\cdot kT}\right)\right\}+Z\left\{kk\cdot e^{-p\cdot kT}\right\} \tag{8}$$

$$=\frac{kk\cdot c}{p}\cdot Z\left\{1-e^{-p\cdot kT}\right\}+kk\cdot Z\left\{e^{-p\cdot kT}\right\}$$

$$=\frac{kk\cdot c}{p}\cdot\frac{\left(1-e^{-pT}\right)\cdot z}{\left(z-e^{-pT}\right)\cdot(z-1)}+kk\cdot\frac{z}{\left(z-e^{-pT}\right)}$$

$$H(z)=\frac{kk\cdot c}{p}\cdot\frac{\left(1-e^{-pT}\right)\cdot z}{\left(z-e^{-pT}\right)\cdot(z-1)}+kk\cdot\frac{z}{\left(z-e^{-pT}\right)}$$
$$=\frac{\frac{kk\cdot c}{p}\cdot\left(1-e^{-pT}\right)\cdot z+kk\cdot z\cdot(z-1)}{\left(z-e^{-pT}\right)\cdot(z-1)} \tag{9}$$

The discrete expression of the lead compensator is derived from the expression defined in (9).

$$Hd(z)=\frac{z-1}{z}\cdot H(z)=\frac{\left[\frac{kk\cdot c}{p}\cdot\left(1-e^{-pT}\right)+kk\cdot(z-1)\right]\cdot z}{\left(z-e^{-pT}\right)\cdot(z-1)}\cdot\frac{z-1}{z}$$
$$=\frac{\frac{kk\cdot c}{p}\cdot\left(1-e^{-pT}\right)+kk\cdot(z-1)}{\left(z-e^{-pT}\right)} \tag{10}$$

$$Hd(z)=\frac{\frac{kk\cdot c}{p}\cdot\left(1-e^{-pT}\right)+kk\cdot(z-1)}{\left(z-e^{-pT}\right)}\Rightarrow \text{Replace } a=e^{-pT}$$
$$=\frac{\frac{kk\cdot c}{p}\cdot(1-a)+kk\cdot(z-1)}{(z-a)}$$
$$=\frac{kk\cdot z+\left[\frac{kk\cdot c}{p}\cdot(1-a)-kk\right]}{(z-a)} \tag{11}$$

$$Hd(z)=\frac{kk\cdot z+\left[\frac{kk\cdot c}{p}\cdot(1-a)-kk\right]}{(z-a)}\Rightarrow \text{Define } b=\frac{kk\cdot c}{p}\cdot(1-a)-kk$$
$$Hd(z)=\frac{kk\cdot z+b}{(z-a)} \tag{12}$$

Finally, the expression of the lead compensator is:

$$Hd(z)=\frac{kk\cdot z+b}{(z-a)}$$
$$\text{where: } b=\frac{kk\cdot\alpha}{\beta}\cdot(1-a)-kk;\ a=e^{-\frac{\beta}{T_{Speed}}\cdot T};\ kk=\frac{\beta}{\alpha} \tag{13}$$

Bibliography

[1] Energy Technology Network., “Energy efficiency roadmap for electroc motor and motros systems.,” Nov. 2015.

[2] P. Waide and C. U. Brunner, “Energy-Efficiency Policy Opportunities for Electric Motor-Driven Systems,” International Energy Agency, 2011.

[3] H. Mikami, K. Ide, Y. Shimizu, S. Masaharu, and H. Seki, “Historical Evolution of Motor Technology,” Vol. 60, 2011.

[4] D. W. Novotny, T. A. Lipo, and T. M. Jahns, *Introduction to Electric Machines and Drives*. Madison Wisconsin: Wisconsin Power Electronics Research Center. University of Wisconsin - Madison, 2009.

[5] D. W. Novotny and T. A. Lipo, *Vector Control and Dynamics of AC Drives*. Oxford: Oxford University Press, 1996.

[6] I. Takahashi and T. Noguchi, “A New Quick-Response and High-Efficiency Control Strategy of an Induction Motor,” *IEEE Trans. Ind. Appl.*, vol. IA-22, no. 5, pp. 820–827, Sep. 1986.

[7] D. Casadei, F. Profumo, G. Serra, and A. Tani, “FOC and DTC: two viable schemes for induction motors torque control,” *IEEE Trans. Power Electron.*, vol. 17, no. 5, pp. 779–787, Sep. 2002.

[8] “Importance of Mounting Tolerances for Modular Encoders,” *HEIDENHAIN*. .

[9] C. Gonzalez, “What’s the Difference Between Absolute and Incremental Encoders?,” *Machine Design*, 26-Oct-2017. [Online]. Available: https://www.machinedesign.com/motion-control/what-s-difference-between-absolute-and-incremental-encoders. [Accessed: 05-Sep-2018].

[10] M. Zhao and J. Lin, “Health Assessment of Rotating Machinery Using a Rotary Encoder,” *IEEE Trans. Ind. Electron.*, vol. 65, no. 3, pp. 2548–2556, Mar. 2018.

[11] Electro-Craft Corporation, *DC Motors. Speed Controls. Servosystems.* 1980.

[12] K. Saito, K. Kamiyama, T. Ohmae, and T. Matsuda, “A microprocessor-controlled speed regulator with instantaneous speed estimation for motor drives,” *IEEE Trans. Ind. Electron.*, vol. 35, no. 1, pp. 95–99, Feb. 1988.

[13] C. Xia, B. Ji, and Y. Yan, “Smooth Speed Control for Low-Speed High-Torque Permanent-Magnet Synchronous Motor Using Proportional-Integral-Resonant Controller,” *IEEE Trans. Ind. Electron.*, vol. 62, no. 4, pp. 2123–2134, Apr. 2015.

[14] J. Lara, J. Xu, and A. Chandra, “Effects of Rotor Position Error in the Performance of Field-Oriented-Controlled PMSM Drives for Electric Vehicle Traction Applications,” *IEEE Trans. Ind. Electron.*, vol. 63, no. 8, pp. 4738–4751, Aug. 2016.

[15] P. J. Roche, J. M. D. Murphy, and M. G. Egan, “Reduction of quantisation noise in position servosystems,” in *and Automation Proceedings of the 1992 International Conference on Industrial Electronics, Control, Instrumentation*, 1992, pp. 464–469 vol.1.

[16] R. Raja, T. Sebastian, M. Wang, A. Gebregergis, and M. S. Islam, “Effect of Position Sensor Error on the Performance of Permanent Magnet Machine Drives,” *IEEE Trans. Ind. Appl.*, vol. 53, no. 6, pp. 5518–5526, Nov. 2017.

[17] R. Iskakov, A. Albu-Schaeffer, M. Schedl, G. Hirzinger, and V. Lopota, “Influence of sensor quantization on the control performance of robotics actuators,” in *2007 IEEE/RSJ International Conference on Intelligent Robots and Systems*, 2007, pp. 1085–1092.

[18] V. Kisner, E. Lenz, A. Wahrburg, K. D. Listmann, and U. Konigorski, “Harmonic approximation of velocity oscillations in electrical drives,” in *2016 IEEE Conference on Control Applications (CCA)*, 2016, pp. 1137–1142.

[19] S.-M. Yang and S.-J. Ke, “Performance evaluation of a velocity observer for accurate velocity estimation of servo motor drives,” *IEEE Trans. Ind. Appl.*, vol. 36, no. 1, pp. 98–104, Jan. 2000.

[20] L. Kovudhikulrungsri and T. Koseki, “Precise Speed Estimation From a Low-Resolution Encoder by Dual-Sampling-Rate Observer,” *IEEEASME Trans. Mechatron.*, vol. 11, no. 6, pp. 661–670, Dec. 2006.

[21] A. Anuchin, V. Astakhova, D. Shpak, A. Zharkov, and F. Briz, “Optimized method for speed estimation using incremental encoder,” in *2017 International Symposium on Power Electronics (Ee)*, 2017, pp. 1–5.

[22] “Motion Control Theory,” Kimberly-Clark GNW & HC Electrical Forum.

[23] N. Willemsen, “Estimating Rotational Speed with a Phase-Locked Loop,” KTH Electrical Engineering, Sweden, 2008.

[24] N. Chaudhuri, S. Ghosh, and A. M. Ghosh, “Wide-Range Precision Speed Measurement with Adaptive Optimization Using a Microcomputer,” *IEEE Trans. Ind. Electron.*, vol. IE-30, no. 4, pp. 369–373, Nov. 1983.

[25] T. Ohmae, T. Matsuda, K. Kamiyama, and M. Tachikawa, “A Microprocessor-Controlled High-Accuracy Wide-Range Speed Regulator for Motor Drives,” *IEEE Trans. Ind. Electron.*, vol. IE-29, no. 3, pp. 207–211, Aug. 1982.

[26] R. C. Kavanagh, “Improved digital tachometer with reduced sensitivity to sensor nonideality,” *IEEE Trans. Ind. Electron.*, vol. 47, no. 4, pp. 890–897, Aug. 2000.

[27] R. H. Brown, S. C. Schneider, and M. G. Mulligan, “Analysis of algorithms for velocity estimation from discrete position versus time data,” *IEEE Trans. Ind. Electron.*, vol. 39, no. 1, pp. 11–19, Feb. 1992.

[28] R. C. Kavanagh, “An enhanced constant sample-time digital tachometer through oversampling,” *Trans Inst Meas Control*, vol. 26, no. 2, pp. 83–98, Apr. 2004.

[29] W. H. Chen, J. Yang, L. Guo, and S. Li, “Disturbance-Observer-Based Control and Related Methods--An Overview,” *IEEE Trans. Ind. Electron.*, vol. 63, no. 2, pp. 1083–1095, Feb. 2016.

[30] R. E. Kalman and R. S. Bucy, “New Results in Linear Filtering and Prediction Theory,” *J. Basic Eng.*, vol. 83, no. 1, pp. 95–108, Mar. 1961.

[31] D. Luenberger, “An introduction to observers,” *IEEE Trans. Autom. Control*, vol. 16, no. 6, pp. 596–602, Dec. 1971.

[32] H.-W. Kim and S.-K. Sul, “A new motor speed estimator using Kalman filter in low-speed range,” *IEEE Trans. Ind. Electron.*, vol. 43, no. 4, pp. 498–504, Aug. 1996.

[33] R. D. Lorenz and K. V. Patten, “High resolution velocity estimation for all digital, AC servo drives,” in *Conference Record of the 1988 IEEE Industry Applications Society Annual Meeting*, 1988, pp. 363–368 vol.1.

[34] D. Tian, H. Shen, and M. Dai, “Improving the Rapidity of Nonlinear Tracking Differentiator via Feedforward,” *IEEE Trans. Ind. Electron.*, vol. 61, no. 7, pp. 3736–3743, Jul. 2014.

[35] J. Kim and B. K. Kim, “Development of Precise Encoder Edge-Based State Estimation for Motors,” *IEEE Trans. Ind. Electron.*, vol. 63, no. 6, pp. 3648–3655, Jun. 2016.

[36] T.-J. Kweon and D.-S. Hyun, “High-performance speed control of electric machine using low-precision shaft encoder,” *IEEE Trans. Power Electron.*, vol. 14, no. 5, pp. 838–849, Sep. 1999.

[37] T. Shi, Z. Wang, and C. Xia, “Speed Measurement Error Suppression for PMSM Control System Using Self-Adaption Kalman Observer,” *IEEE Trans. Ind. Electron.*, vol. 62, no. 5, pp. 2753–2763, May 2015.

[38] S. Jeon, “State estimation based on kinematic models considering characteristics of sensors,” in *Proceedings of the 2010 American Control Conference*, 2010, pp. 640–645.

[39] A. Suzumura, Y. Fujimoto, T. Murakami, and R. Oboe, “A General Framework for Designing SISO-Based Motion Controller With Multiple Sensor Feedback,” *IEEE Trans. Ind. Electron.*, vol. 63, no. 12, pp. 7607–7620, Dec. 2016.

[40] S. A. A. Rizvi, M. Faisal, H. Aftab, S. Ahmed, and A. Y. Memon, “A robust observer and controller design for a DC motor with a low-resolution encoder,” in *The 27th Chinese Control and Decision Conference (2015 CCDC)*, 2015, pp. 3038–3043.

[41] R. Bonert, “Digital Tachometer with Fast Dynamic Response Implemented by a Microprocessor,” *IEEE Trans. Ind. Appl.*, vol. IA-19, no. 6, pp. 1052–1056, Nov. 1983.

[42] L. Bascetta, G. Magnani, P. Rocco, and A. M. Zanchettin, “Performance Limitations in Field-Oriented Control for Asynchronous Machines With Low Resolution Position Sensing,” *IEEE Trans. Control Syst. Technol.*, vol. 18, no. 3, pp. 559–573, May 2010.

[43] M. Maaref, A. Rezazadeh, and H. Shokouhandeh, “An implementable speed measurement method in order to eliminate quantization error while using rotary incremental encoders.,” *J. Basic Appl. Sci. Res.*, vol. 3, no. 9, pp. 7–19, 2013.

[44] Heidenhain Corp., “Motion Control Design: Top 5 Challenges (and Opportunities),” *MCMA - Motion Control Online*. [Online]. Available: https://www.motioncontrolonline.org/content-detail.cfm/Motion-Control-Tech-Papers/Motion-Control-Design-The-Top-5-Challenges-and-Opportunities/content_id/2206. [Accessed: 19-Sep-2018].

[45] “Top Tips Specifiying an Incremental Encoder,” *Machine Design*. [Online]. Available: https://www.machinedesign.com/motion-control/6-tips-specifying-incremental-encoder. [Accessed: 05-Sep-2018].

[46] G. A. Woolvet, *Transducers in Digital Systems*. 1977.

[47] “Fundamentals of the Electronics Counters,” Agillent Technologies, U.S.A, 1997.

[48] “ADSP-CM40x Mixed-Signal Control Processor with ARM Cortex-M4 Hardware Reference,0.2 ed.,” Analog Devices, 2013.

[49] L. Bascetta, G. Magnani, and P. Rocco, “Velocity Estimation: Assessing the Performance of Non-Model-Based Techniques,” *IEEE Trans. Control Syst. Technol.*, vol. 17, no. 2, pp. 424–433, Mar. 2009.

[50] H. Zhu and T. Sugie, “Velocity Estimation of Motion Systems Based on Low-Resolution Encoders,” *J. Dyn. Syst. Meas. Control*, vol. 135, no. 1, pp. 011006-011006–8, Oct. 2012.

[51] R. C. Kavanagh, “Improved Analysis and Design Techniques for Digital Tachometry,” University College Cork, Cork.

[52] L. Corradini, D. Maksimović, P. Mattavelli, and R. Zane, *Digital control of high-frequency switched-mode power converters*, 1st ed. New Jersey: John Wiley & Sons, Inc., 2015.

[53] R. C. Kavanagh and J. M. D. Murphy, “The effects of quantization noise and sensor nonideality on digital differentiator-based rate measurement,” *IEEE Trans. Instrum. Meas.*, vol. 47, no. 6, pp. 1457–1463, Dec. 1998.

[54] “The Analog Discovery 2: A portable USB laboratory for everyone.” .

[55] T. Emura and L. Wang, “A high-resolution interpolator for incremental encoders based on the quadrature PLL method,” *IEEE Trans. Ind. Electron.*, vol. 47, no. 1, pp. 84–90, Feb. 2000.

[56] R. Merry, R. van de Molengraft, and M. Steinbuch, “Error modeling and improved position estimation for optical incremental encoders by means of time stamping,” in *2007 American Control Conference*, 2007, pp. 3570–3575.

[57] L. M. Sanchez-Brea and T. Morlanes, “Metrological errors in optical encoders,” *Meas. Sci. Technol.*, vol. 19, no. 11, p. 115104, 2008.

[58] “Absolute Encoder Design: Magnetic or Optical?,” iC-Haus, White Paper.

[59] “Technical Specifications. Incremental encoder-Shaft type. Economical Model (OVW-2 model),” NEMICON.

[60] A. O. Goushcha and B. Tabbert, “On response time of semiconductor photodiodes,” *Opt. Eng.*, vol. 56(9), Sep. 2017.

[61] J. N. Lygouras, K. A. Lalakos, and P. G. Ysalides, “High-performance position detection and velocity adaptive measurement for closed-loop position control,” *IEEE Trans. Instrum. Meas.*, vol. 47, no. 4, pp. 978–985, Aug. 1998.

[62] M. Wang, Y.-S. Kung, Y.-M. Tu, and T.-T. Lin, “Novel interpolation method for quadrature encoder square signals,” in *2009 IEEE International Symposium on Industrial Electronics*, 2009, pp. 333–338.

[63] N. Hagiwara, Y. Suzuki, and H. Murase, “A method of improving the resolution and accuracy of rotary encoders using a code compensation technique,” *IEEE Trans. Instrum. Meas.*, vol. 41, no. 1, pp. 98–101, Feb. 1992.

[64] N. C. Cheung, “An innovative method to increase the resolution of optical encoders in motion servo systems,” in *Proceedings of the IEEE 1999 International Conference on Power Electronics and Drive Systems. PEDS’99 (Cat. No.99TH8475)*, 1999, vol. 2, pp. 797–802 vol.2.

[65] K. K. Tan, H. X. Zhou, and T. H. Lee, “New interpolation method for quadrature encoder signals,” *IEEE Trans. Instrum. Meas.*, vol. 51, no. 5, pp. 1073–1079, Oct. 2002.

[66] K. K. Tan and K.-Z. Tang, “Adaptive online correction and interpolation of quadrature encoder signals using radial basis functions,” *IEEE Trans. Control Syst. Technol.*, vol. 13, no. 3, pp. 370–377, May 2005.

[67] J. N. Lygouras, T. P. Pachidis, K. N. Tarchanidis, and V. S. Kodogiannis, “Adaptive High-Performance Velocity Evaluation Based on a High-Resolution Time-to-Digital Converter,” *IEEE Trans. Instrum. Meas.*, vol. 57, no. 9, pp. 2035–2043, Sep. 2008.

[68] K. Ogata, *Modern control engineering*, 4. ed., international ed. Upper Saddle River, NJ: Prentice Hall [u.a.], 2002.

[69] H. D. Venable, “The K factor: a new mathematical tool for stability analysis and synthesis.”, *PowerCon Proc.*, Mar. 1983.

[70] M. Iwasaki and N. Matusi, “Robust speed control of IM with torque feedforward control,” *IEEE Trans. Ind. Electron.*, vol. 40, no. 6, pp. 553–560, Dec. 1993.

[71] J. Talla, V. Q. Leu, V. Šmídl, and Z. Peroutka, “Adaptive Speed Control of Induction Motor Drive With Inaccurate Model,” *IEEE Trans. Ind. Electron.*, vol. 65, no. 11, pp. 8532–8542, Nov. 2018.

[72] M. R. Matausek, B. I. Jeftenic, D. M. Miljkovic, and M. Z. Bebic, “Gain scheduling control of DC motor drive with field weakening,” *IEEE Trans. Ind. Electron.*, vol. 43, no. 1, pp. 153–162, Feb. 1996. .